ORNL
MASTER COPY

ORNL-3507
UC-34 -- Physics
TID-4500 (24th ed.)

CALCULATIONS OF THERMAL-NEUTRON FLUX DISTRIBUTIONS IN CONCRETE-WALLED DUCTS USING AN ALBEDO MODEL WITH MONTE CARLO TECHNIQUES

V. R. Cain

OAK RIDGE NATIONAL LABORATORY
operated by
UNION CARBIDE CORPORATION
for the
U.S. ATOMIC ENERGY COMMISSION

Printed in USA. Price: $2.75 Available from the
Office of Technical Services
U. S. Department of Commerce
Washington 25, D. C.

LEGAL NOTICE

This report was prepared as an account of Government sponsored work. Neither the United States, nor the Commission, nor any person acting on behalf of the Commission:

A. Makes any warranty or representation, expressed or implied, with respect to the accuracy, completeness, or usefulness of the information contained in this report, or that the use of any information, apparatus, method, or process disclosed in this report may not infringe privately owned rights; or

B. Assumes any liabilities with respect to the use of, or for damages resulting from the use of any information, apparatus, method, or process disclosed in this report.

As used in the above, "person acting on behalf of the Commission" includes any employee or contractor of the Commission, or employee of such contractor, to the extent that such employee or contractor of the Commission, or employee of such contractor prepares, disseminates, or provides access to, any information pursuant to his employment or contract with the Commission, or his employment with such contractor.

ORNL-3507

Contract No. W-7405-eng-26

Neutron Physics Division

CALCULATIONS OF THERMAL-NEUTRON FLUX DISTRIBUTIONS IN CONCRETE-WALLED DUCTS USING AN ALBEDO MODEL WITH MONTE CARLO TECHNIQUES*

V. R. Cain

*Work performed under Order No. DASA-EO-800-63.

Date Issued

JAN 21 1964

Submitted as a thesis to the Graduate Council of the University of Tennessee in partial fulfillment of the requirements for the degree of Master of Science.

OAK RIDGE NATIONAL LABORATORY
Oak Ridge, Tennessee
Operated by
UNION CARBIDE CORPORATION
for the
U. S. ATOMIC ENERGY COMMISSION

ABSTRACT

When radiation shields are penetrated by ducts, the gamma rays resulting from the radiative capture of low-energy neutrons in the duct walls can be principal contributors to the total dose along the duct. In order to calculate the effect of these capture gamma rays, the distribution of low-energy neutrons in the ducts must be known. This report presents calculations of low-energy neutron distributions in concrete-walled ducts by a method in which an albedo model and a Monte Carlo technique were used. One series of calculations was performed for straight ducts so that comparisons could be made with the Simon-Clifford analytic approximation. Another series was for three-legged rectangular ducts similar to those used in a Tower Shielding Facility experiment. When an albedo similar to that to be expected for a pure thermal-neutron source was used, the results agreed very closely with the TSF data. A digital computer code was written to perform the calculations.

TABLE OF CONTENTS

CHAPTER		PAGE
I.	INTRODUCTION	1
II.	THE ALBEDO—RANDOM WALK MODEL	7
	Mathematical Model	8
	Applicability to the Physical Case	14
III.	STRAIGHT DUCTS	18
	Calculations for Cylindrical Ducts	19
	Calculations for Rectangular Ducts	26
	Comparisons with an Analytic Approximation	41
IV.	DUCTS WITH BENDS	58
	Calculations	58
	Comparisons with Experimental Data	76
V.	SUMMARY, CONCLUSIONS, RECOMMENDATIONS	82
	Summary	82
	Conclusions	83
	Recommendations	84
	BIBLIOGRAPHY	89
	APPENDICES	
	A. The Albedo Monte Carlo Machine Program	93
	B. Identification of Important Symbols Used in Machine Programs	132
	C. Descriptions of the Geometry Subroutines and Inputs	137

CHAPTER PAGE

D. Individual Subroutine Checks 151

E. Calculations of Uncollided Flux and Current in Straight Ducts 162

F. Calculations of the Thermal-Neutron Albedo 168

G. Derivation of Statistical Formulae 172

LIST OF FIGURES

FIGURE PAGE

1. Total Neutron Flux Calculated for 0.5-ft-diam cylindrical Duct Using an Isotropic Albedo of 0.80 (10,000 Histories)... 20
2. Total Neutron Flux Calculated for 0.5-ft-diam Cylindrical Duct Using a Cosine Albedo of 0.8 (4000 Histories)..... 21
3. Scattered Neutron Flux Calculated for 1-ft-diam Cylindrical Duct Using an Isotropic Albedo of 0.12 (10,000 Histories)... 22
4. Scattered Neutron Flux Calculated for 1-ft-diam Cylindrical Duct Using a Cosine Albedo of 0.12 (10,000 Histories)..... 23
5. Scattered Neutron Flux Calculated for 1-ft-diam Cylindrical Duct Using an Isotropic Albedo of 0.8 (4000 Histories)..... 24
6. Scattered Neutron Flux Calculated for 1-ft-diam Cylindrical Duct Using a Cosine Albedo of 0.8 (10,000 Histories)..... 25
7. Total Neutron Flux Calculated for 1.382-ft-diam Cylindrical Duct Using an Isotropic Albedo of 0.8 (10,000 Histories).... 27
8. Total Neutron Flux Calculated for 1.382-ft-diam Cylindrical Duct Using a Cosine Albedo of 0.8 (10,000 Histories)..... 28
9. Total Neutron Flux Calculated for 1.9544-ft-diam Cylindrical Duct Using an Isotropic Albedo of 0.8 (10,000 Histories).... 29
10. Total Neutron Flux Calculated for 1.9544-ft-diam Cylindrical Duct Using a Cosine Albedo of 0.8 (10,000 Histories)..... 30

FIGURE PAGE

11. Total Neutron Flux Calculated for 6-ft-diam Cylindrical Duct Using an Isotropic Albedo of 0.8 (4000 Histories)..... 31

12. Total Neutron Flux Calculated for 6-ft-diam Cylindrical Duct Using a Cosine Albedo of 0.8 (1000 Histories)..... 32

13. Total Neutron Flux Calculated for 6-ft-diam Cylindrical Duct Using a Cosine^2 Albedo of 0.8 (4000 Histories)..... 33

14. Total Neutron Flux Calculated for 3 by 0.5 ft Rectangular Duct Using an Isotropic Albedo of 0.12 (4000 Histories)..... 34

15. Total Neutron Flux Calculated for 3 by 0.5 ft Rectangular Duct Using a Cosine Albedo of 0.12 (4000 Histories)..... 35

16. Total Neutron Flux Calculated for 3 by 0.5 ft Rectangular Duct Using an Isotropic Albedo of 0.4 (4000 Histories)..... 36

17. Total Neutron Flux Calculated for 3 by 0.5 ft Rectangular Duct Using a Cosine Albedo of 0.4 (4000 Histories)..... 37

18. Total Neutron Flux Calculated for 3 by 0.5 ft Rectangular Duct Using an Isotropic Albedo of 0.8 (4000 Histories)..... 38

19. Total Neutron Flux Calculated for 3 by 0.5 ft Rectangular Duct Using a Cosine Albedo of 0.8 (4000 Histories)..... 39

20. Total Neutron Flux Calculated for 3 by 0.5 ft Rectangular Duct Using a Cosine^2 Albedo of 0.8 (4000 Histories)..... 40

21. Total Neutron Flux Calculated for 3 by 1 ft Rectangular Duct Using a Cosine Albedo of 0.8 (4000 Histories)..... 42

FIGURE PAGE

22. Total Neutron Flux Calculated for 3 by 1 ft Rectangular Duct Using a Cosine Albedo of 0.8 (4000 Histories)..... 43

23. Total Neutron Flux Calculated for 3 by 1 ft Rectangular Duct Using a Cosine^2 Albedo of 0.8 (4000 Histories)..... 44

24. Total Neutron Flux Calculated for 3 by 6 ft Rectangular Duct Using an Isotropic Albedo of 0.8 (4000 Histories)..... 45

25. Total Neutron Flux Calculated for 3 by 6 ft Rectangular Duct Using a Cosine Albedo of 0.8 (4000 Histories)..... 46

26. Total Neutron Flux Calculated for 3 by 6 ft Rectangular Duct Using a Cosine^2 Albedo of 0.8 (4000 Histories)..... 47

27. Scattered Neutron Flux in a 1-ft-diam Cylindrical Duct: Comparison of Calculations Using Isotropic and Cosine Albedoes of 0.12 With an Analytic Approximation..... 50

28. Scattered Neutron Flux in a 1-ft-diam Cylindrical Duct: Comparison of Calculations Using Isotropic and Cosine Albedoes of 0.8 With an Analytic Approximation..... 51

29. Total Neutron Flux Using an Isotropic Albedo of 0.8: Comparison of Calculations for a 1.38198-ft-diam Cylindrical Duct, a 3 by 0.5-ft Rectangular Duct, and an Analytic Approximation..... 53

30. Total Neutron Flux Using an Isotropic Albedo of 0.8: Comparison of Calculations for a 1.95441-ft-diam Cylindrical Duct, a 3 by 1-ft Rectangular Duct, and an Analytic Approximation... 54

FIGURE PAGE

31. Total Neutron Flux Using a Cosine Albedo of 0.8: Comparison of Calculations for a 1.38198-ft-diam Cylindrical Duct, a 3 by 0.5 ft Rectangular Duct, and an Analytic Approximation... 56

32. Total Neutron Flux Using a Cosine Albedo of 0.8: Comparison of Calculations for a 1.95441-ft-diam Cylindrical Duct, a 3 by 1-ft Rectangular Duct, and an Analytic Approximation..... 57

33. Cross Section of x-y Plane Showing Detector Locations and Numbers for Three-legged Duct Geometry and Room Plus Two-Legged Duct Geometry..... 59

34. Total Neutron Flux Calculated for Three-Legged 3 by 1 ft Rectangular Duct Using a Cosine Albedo of 0.24 (4000 Histories)..... 61

35. Total Neutron Flux Calculated for Three-Legged 3 by 1 ft Rectangular Duct Using an Isotropic Albedo of 0.8 (4000 Histories)..... 62

36. Total Neutron Flux Calculated for Three-Legged 3 by 1 ft Rectangular Duct Using a Cosine Albedo of 0.80 (4000 Histories). 63

37. Total Neutron Flux Calculated for Three-Legged 3 by 6 ft Rectangular Duct Using a Cosine Albedo of 0.12 (10,000 Histories)..... 64

38. Total Neutron Flux Calculated for Three-Legged 3 by 6 ft Rectangular Duct Using a Cosine Albedo of 0.24 (10,000 Histories)..... 65

FIGURE PAGE

39. Total Neutron Flux Calculated for Three-Legged 3 by 6 ft Rectangular Duct Using a Cosine Albedo of 0.7 (4000 Histories).. 66

40. Total Neutron Flux Calculated for Three-Legged 3 by 6 ft Rectangular Duct Using a Cosine Albedo of 0.8 (4000 Histories).. 67

41. Total Neutron Flux Calculated for Three-Legged 3 by 6 ft Rectangular Duct Using a Cosine Albedo of 0.9 (4000 Histories).. 68

42. Total Neutron Flux Calculated for Three-Legged 3 by 6 ft Rectangular Duct Using a Cosine Albedo of 0.8 (1000 Histories).. 69

43. Total Neutron Flux Calculated for Three-Legged 3 by 6 ft Rectangular Duct Using a Cosine Albedo of 0.8 (1000 Histories). Calculation based on statistical estimation..... 70

44. Total Neutron Flux Calculated for Three-Legged 3 by 8 ft Rectangular Duct Using an Isotropic Albedo of 0.8 (4000 Histories)..... 72

45. Total Neutron Flux Calculated for Three-Legged 3 by 8 ft Rectangular Duct Using a Cosine Albedo of 0.8 (4000 Histories).. 73

46. Total Neutron Flux Calculated for Room (6 x 7.5 x 7.5 ft) and Two-Legged Duct (3 by 6 ft) Configuration (Shown in Fig. 33) Using a Cosine Albedo of 0.80 (4000 Histories). See text for explanation of geometrical configuration..... 74

47. Total Neutron Flux Calculated for Room (8 by 7.5 by 7.5 ft) and Two-Legged Duct (3 by 8 ft) Configuration (Shown in Fig. 33) Using a Cosine Albedo of 0.80 (4000 Histories). See text for explanation of geometrical configuration..... 75

FIGURE PAGE

48. Bunker-Tunnel Configuration Used in TSF Experiment..... 77

49. Fast-Neutron and Gamma-Ray Dose Rates and Thermal-Neutron Fluxes Along Center Line of Interconnecting Tunnel for No Front Shield and 20-in. Top Shield..... 78

50. Fast-Neutron and Gamma-Ray Dose Rates and Thermal-Neutron Fluxes Along Center Line of Interconnecting Tunnel for 20-in. Front Shield and No Top Shield..... 79

51. Comparison of Calculations Using a Cosine Albedo of 0.8 with Thermal-Neutron Flux Measurements Along a Three-Legged Duct.. 81

52. Comparison of Calculations of Flux Distribution in a 3 by 1-ft Duct Using a Cosine Albedo of 0.80..... 85

53. Block Diagram of Albedo Monte Carlo Machine Program..... 94

54. Zone Configuration of Three-Legged Duct Geometry..... 142

55. Block Configuration of Zones 7, 8, and 9 of Three-Legged Duct Geometry..... 143

CHAPTER I

INTRODUCTION

The general problem of protection against nuclear weapons is quite complex, with the effects to be considered falling naturally into three categories: (1) blast effects, including those due to blast waves and thermal radiations, (2) the effects of delayed radiations (fallout), and (3) the effects of initial nuclear radiations, defined as those radiations emitted within one minute after detonation. The blast effects are similar to those encountered with conventional weapons except in degree; therefore, design procedures which take into account nuclear weapon blast protection are similar to those used for conventional weapon blast protection. The effects of fallout and initial radiations are, of course, unique to nuclear weapons and are of concern in regions where no damage from blast exists. For example, unprotected persons hundreds of miles from the point of detonation may receive lethal doses from fallout radiation. Because of this, fallout radiation has received a great deal of attention in the past few years, the major effort consisting in a series of moments-method calculations performed by Spencer at the National Bureau of Standards.[1] Spencer's results have been reformulated in such

---

[1] L. V. Spencer, Structure Shielding Against Fallout Radiation from Nuclear Weapons, National Bureau of Standards Monograph 42 (1962).

a way that routine calculational procedures[2,3] for designing structures to shield against fallout radiation are now available.

The effects of initial nuclear radiations, on the other hand, have only recently received attention. This is largely due to the fact that initial radiations are important only for rather special cases. If, for example, the possible combinations of weapon size, altitude and distance of detonation, and characteristics of the protective structures (or lack of a structure) are considered, it will be found that for only a limited number of combinations are the initial radiations a significant problem. This is because as the weapon size increases, the blast damage area increases more rapidly than the area covered by high initial radiation levels.[4] Consequently, initial radiations are significant only for small weapons or for high blast levels around large weapons. Since there appears to be little incentive for a prospective enemy to use small weapons either against the general public (because large area coverage would be required) or against hardened military installations (because high blast levels would be needed), a primary area of concern, insofar as initial radiation dose protection is concerned, is for large weapons

---

[2] Design and Review of Structures for Protection from Fallout Gamma Radiation, Office of Civil Defense (Rev. Oct. 1, 1961).

[3] Fallout Shelter Surveys: Guide for Architects and Engineers, Department of Defense, Office of Civil Defense NP-10-2 (May, 1960).

[4] S. Glasstone (ed.), The Effects of Nuclear Weapons, Department of the Army Pamphlet No. 39-3 (April, 1962).

and heavily shielded structures, such as missile bases or military command posts.

An investigation of the effectiveness of such structures in attenuating initial weapons radiation was recently initiated at Oak Ridge National Laboratory (ORNL). The program consists of measurements of radiation intensities inside basically simple geometric shapes and correlation with corresponding calculations, the overall purpose being to develop experimentally verified calculational techniques which will yield "handbook"-type design data for initial radiation protection. Although, in general, simple structures of the type used are amenable to rather straightforward radiation attenuation calculations, a major difficulty arises as a result of various penetrations through the main shield, such as air passages, conduits, and entranceways. Such penetrations, or ducts, allow "streaming" of radiation through the shield and also increase the production of secondary radiations within the shield. Both of these components are difficult to calculate.

The ORNL experiments have shown that fast-neutron dose rates inside complex duct configurations fall off rapidly as the duct is traversed (see Figs. 49 and 50 in Chapter IV). Calculations of the fast-neutron dose rates along a single leg of a duct can be handled reasonably well by considering only two components: unscattered neutrons and neutrons that have been reflected from the walls only once. This is a result of the small fraction of dose rate which is incident on a surface

that is reflected. The calculation of the unscattered component is quite straightforward if the angular distribution of the source at the duct entrance is known, and, although the calculation of the singly scattered component is more complex, it can be handled adequately in most cases of interest through the use of the albedo, or reflection coefficient model.

Calculations of the attenuation of gamma radiation incident on a duct configuration can be handled in a similar manner. In most cases, the total albedo (the integral of the differential albedo over all exit solid angles) is even smaller for gamma-ray dose rates than it is for fast-neutron dose rates. Typical values are 0.12 for fast-neutron dose rates and 0.06 for gamma-ray dose rates, thereby rendering the second and higher-order scatterings negligible in most cases.

A significant result of the ORNL experiments was that the dominant radiation component in many complicated duct geometries is the gamma-ray dose rate resulting from the capture of low-energy neutrons in the walls of the duct. An important problem in the calculation of this component is the determination of the spatial distribution of the low-energy neutrons, which involves the processes of the slowing down of the higher-energy neutrons and the transport of the low-energy neutrons themselves. The determination of the distributions of the low-energy neutrons is the problem with which this thesis is concerned.

The complexity of the usual geometries, in practice, precludes the use of many of the common neutron transport calculational techniques.

One technique which can be and is used for this type of calculation is the random-sampling, or Monte Carlo, process. This process can be used to obtain complete descriptions of fast-neutron dose rates and gamma-ray dose rates by following each particle to its death. In practice, it is uneconomical to use the existing codes for a problem as complex as the low-energy neutron problem because excessive machine time is required to follow a neutron completely through the slowing-down and capture processes. Each collision with the wall can result in a large number of nuclear interactions before re-emission, if re-emission occurs at all. It is certainly wasteful to follow a history which does not result in re-emission and possibly terminates so deep in the wall that little contribution is made to the gamma-ray dose rate.

An alternative procedure is the use of the albedo concept to follow the transport of the low-energy neutrons down the duct. However, unlike the albedos for fast neutrons and gamma rays, which are defined on the basis of dose-rate reflection, the albedo for low-energy neutrons, which is defined on the basis of number reflection, is high (on the order of 0.7 or 0.8). Consequently, while the albedos for fast-neutron and gamma-ray dose rates give reasonable results by considering only one reflection, the albedo for low-energy neutrons requires consideration of orders of scatterings higher than the first. If the albedo were low and the geometry simple, direct numerical integrations could be

performed over all possible locations of each scatter point.[5] But when many scatterings must be considered, and when the geometry becomes extremely complicated, these integrals become so complex that the solutions are usually more efficient if the random-sampling technique is used.[6] The technique ordinarily used in particle-transmission problems is the random-walk technique, rather than the technique of random sampling of the multiple integrals directly. It is this technique that was selected for computing the thermal-neutron flux distributions reported in this study.

---

[5]C. W. Terrell et al., Radiation Streaming in Shelter Entranceways, Armour Research Foundation, ARF-1158A01-5 (July, 1961).

[6]H. Kahn, "Random Sampling (Monte Carlo) Techniques in Neutron Attenuation Problems-I," Nucleonics, p. 28 (May, 1950).

CHAPTER II

THE ALBEDO--RANDOM WALK MODEL

The problem of interest is that of predicting the thermal-neutron fluxes at various positions in a multilegged concrete-walled duct, which are due to a neutron radiation field of arbitrary energy distribution incident on the mouth of the duct. It is assumed that this problem can be represented by the transport of particles down the duct according to an albedo model. When used for calculations of fast-neutron or gamma-ray doses, the differential albedo is defined as the fraction of the dose incident on a semi-infinite plane surface that is reflected into a particular solid angle element. In general, the albedo must be a function of the incident direction and energy, the wall material, and the exit direction. Practical considerations of calculational complexity quite often lead to simplifying assumptions, such as the use of an albedo which is an average of the differential albedo over the incident particle energy spectrum or the use of an albedo which has no dependence on the incident direction (and therefore no dependence on the exit azimuthal angle). For the problem considered here, both assumptions given above will be made; specifically, it will be assumed that the albedo is constant and that it is independent of the incident direction. In this case the albedo is defined on the basis of the number of particles reflected rather than on the fraction of dose reflected. The following sections describe the mathematical model chosen to represent the physical case and the

justification of this choice.

Mathematical Model

The basic equation governing particle transmission problems is the transport equation. In such problems random-sampling procedures essentially solve the integral form of the equation,[1] which may be represented as

$$\phi(p) = \int \phi(p')\, K(p',p)\, dp' + S(p) \,, \tag{1}$$

where

p = a vector in phase space, having position and momentum coordinates,

$\phi(p)$ = flux of particles at p,

$K(p',p)$ = a kernel describing the probability of a particle suffering a scattering collision at p' and moving from p' to p without collision,

$S(p)$ = flux at p due to uncollided particles from the source.

---

[1]See, for instance, C. D. Zerby, A Monte Carlo Calculation of Air-Scattered Neutrons, ORNL-2277 (1956), App. A, pp. 61-64; or B. Davison, Neutron Transport Theory (Oxford At the Clarendon Press, 1957) , pp. 22-26, for derivations of integral formulations of the transport equation.

The above equation in the complete form describing a particular problem may be exceedingly complex. The source term, in general, will involve an integration over p, and the kernel may be even more complex, even in simple geometries.

If the source and kernel are known, the above equation may be solved by iteration. It is informative to do this for a few iterations, with the starting approximation $\phi_0(p) = S(p)$. Thus,

$$\phi_1(p) = \int \phi_0(p')\ K(p',p)\ dp' + S(p)\ . \tag{2}$$

It may be noted that $\phi_1(p)$ is the flux at p due to particles reaching p after having one collision (the integral term) plus the flux of uncollided particles. Iterating again,

$$\phi_2(p) = \int \phi_1(p)\ K(p',p)\ dp' + S(p) \tag{3}$$

$$= \iint S(p'')\ K(p'',p)\ K(p',p)\ dp''\ dp' + \int S(p')\ K(p',p)\ dp' + S(p)\ .$$

This gives the flux at p due to particles having had two or less collisions. This iterative solution of the transport equation is therefore equivalent to the Neumann series solution:

$$\phi_n(p) = \sum_{j=0}^{n} I_j(p)\ ,$$

where $I_j(p)$ represents the flux at p from the j<u>th</u> order of scattering.

The random-walk procedure is a statistical analogue of the actual physical process and gives estimates to the I_j's in the following manner. The characteristics of a source particle (i.e., position and momentum) are chosen using randomly distributed variables and applicable distribution functions. The particle starts from the source region with these characteristics and continues to a collision point determined by the known probabilities of interaction. New characteristics are then chosen again, using the appropriate distributions. At this point the particle may make a contribution to $I_1(p)$ by colliding with a detector located at the positional coordinates of p. By following a large number of particles, adding their contributions to various detectors, and then dividing by the number of particles, estimates of each I_j may be obtained. It should be noted that the probability density functions (p.d.f.'s) from which the samplings are taken correspond to the S(p) and K(p',p) of Eqs. 1 through 3.

The form of the transport equation which applies to the albedo model may be described as follows. A duct of arbitrary shape has a position on its surface represented as $\underline{r}$, a position vector. The cosine of the polar angle, defined as the angle at the point $\underline{r}$ between the normal to the surface and an arbitrary direction, will be designated μ. Let $A(\underline{r},\mu)\,d\mu$ be the current of particles entering the duct wall at $\underline{r}$ and in $d\mu$ about μ. $F(\underline{r})$ is the current of particles leaving $\underline{r}$, and $\alpha(\underline{r})$ is the probability of re-emission of a particle entering the surface at $\underline{r}$. Then

$$F(\underline{r}) = \alpha(\underline{r}) \int A(\underline{r},\mu)\ d\mu\ . \tag{4}$$

Associating μ' and ϕ', the cosine of the polar angle and the azimuthal angle, respectively, with a direction measured from a point $\underline{r}'$, there exists a relation G such that $\mu = G(\underline{r},\underline{r}',\mu',\phi')$. The polar angles θ and θ' at the points $\underline{r}$ and $\underline{r}'$ are shown in the sketch below.

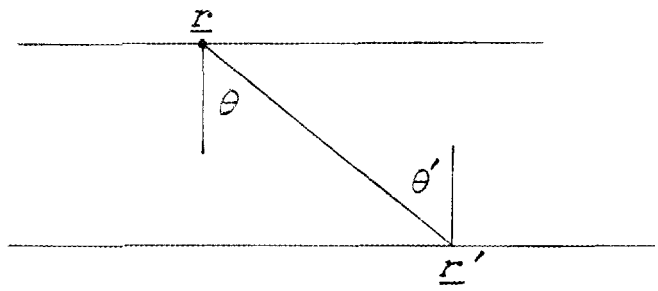

Then

$$A(\underline{r},\mu) = \int d\underline{r}'\ d\mu'\ d\phi'\ F(\underline{r}')\ \frac{dQ}{d\Omega}\ (\mu',\underline{r}')\ \delta[\mu - G(\underline{r},\underline{r}',\mu',\phi')] + A_0(\underline{r},\mu)\ ,$$

where $\frac{dQ}{d\Omega}\ (\mu,\underline{r})$ is the probability per steradian of a particle at $\underline{r}$ being emitted into $d\Omega$ about μ. $A_0(\underline{r},\mu)\ d\mu$ is the current into the surface at $\underline{r}$ and $d\mu$ about μ due to uncollided particles from the source. If Eqs. 4 and 5 are solved by iteration, a sequence of F_j's is generated which approaches F. F_0 is set to zero, since there can be no emergent flux at $\underline{r}$ uncollided from the source. $F_1(\underline{r})$, the current of singly scattered particles leaving $\underline{r}$, is then

$$F_1(\underline{r}) = \alpha(\underline{r}) \int A_0(\underline{r},\mu)\ d\mu\ .$$

As before, repeated iterations give higher-ordered approximations to $F(\underline{r})$. Knowing $F(\underline{r})$, the flux of particles can be obtained by integrating over the duct walls and adding the unscattered contribution from the source.

The details of how the procedure outlined above is actually handled in the computer code are as follows:

A source plane is defined from which all particles originate, located at the mouth of a duct which may have either a rectangular cross section or a cross section defined by the zeros of a general quadratic function, i.e., $ax^2 + by^2 + cxy + dx + ey + f$, with $a/b > 0$ and $a \neq 0$. The duct may have multiple right-angle bends when the rectangular cross section is used. The source may be either located at a point or uniformly distributed on the source plane. The angular distribution of the particles leaving the source plane may be specified (in terms of a probability density function) as a power series in the cosine of the polar angle of emission (the angle between the particle direction and the normal to the surface). The particle undergoing the random walk has no characteristics associated with it at any time other than its position, direction, and weight, which is unity upon emission from the source plane. Upon a collision with a wall surface, the weight of the particle is changed by a constant factor (corresponding to the albedo, or probability of re-emission, associated with the actual wall and the physical particle whose behavior is being simulated). A direction of emission

is then selected which is assumed to be independent of the incident direction. It is therefore not a function of the azimuthal angle and, as before, is selected from a probability density function expressed as a power series in the cosine of the polar angle of emission. Fluxes at various positions along the duct are computed from this random walk by one of two procedures. One technique which can be used is that of statistical estimation. In this technique, at every scatter point, including the source point, an estimate is made of the flux contribution to a series of point detectors. This is calculated using the known probability of the particle reaching each of these detector locations from the wall scatter point. An alternate procedure is to add track lengths from the particle track which occur in each of a series of finite volume detectors. The flux in a particular detector is the sum of all the track lengths which occurred in it divided by the volume of the detector. The detector which has proved to be the most satisfactory for the problem under consideration is a detector which is thin in the dimension parallel to the duct center line and which occupies the entire cross section of the duct. The flux which is obtained from this detector is, of course, an average flux over the volume of the detector, but since the flux does not vary rapidly along a plane normal to the center line this average flux is a fairly good measure of the flux along the duct center line. The particles are followed until they completely traverse the duct, re-enter the source plane, or exceed a predetermined number of wall scatterings.

Applicability to the Physical Case

The applicability of the mathematical model described above to a physical case may be established in several ways. One possible procedure would be to vary the value of the albedo and its angular distribution until the calculation agreed with experimental results. This by itself might provide some actual knowledge or understanding of the behavior which could extend the number of problems that could be solved. Combined with a certain amount of information from other sources, it can be a useful technique.

A preferable procedure would be to study the physical behavior of a single wall-scattering process, possibly by experimental techniques or by detailed Monte Carlo calculations of the conventional type, in order to establish the validity of various assumptions and to establish the nature of the changes which must be made for different physical configurations. The combination of this detailed examination of a single wall-scattering process, which results in an albedo model, with a calculation which uses the albedo model in the correct geometry would certainly seem to be a more economical and versatile calculational technique than the full-scale Monte Carlo calculation.

Detailed investigations of the type described above are under way at ORNL, but the knowledge available at this point is derived substantially from experimental experience. Consider now the information available which is applicable to the physical cases of interest. The

cases to be considered will be restricted to concrete-walled ducts having an arbitrary cross section (man-sized rectangular cross sections are of the most interest) and an arbitrary number of bends which are subjected to the radiations present in air at distances on the order of a mile from a fission-type nuclear weapon. Actually, only the wall material and the neutron spectrum have substantial effect on the nature of the albedo.

The distances of interest are far enough from the source that the lower energy regions of the neutron differential energy spectrum are in equilibrium; i.e., the shape of the neutron spectrum below, say 100 keV, is not changing significantly with distance. This shape may be considered loosely as consisting of a 1/E spectrum between thermal energy and 100 keV plus a thermal group. As this spectrum traverses the duct, drastic changes would not be expected to occur. The most noticeable change will be that the number of thermal neutrons relative to the 1/E region will increase, since the ratio of scattering to absorption cross section for neutrons of thermal and intermediate energies is larger for concrete than for air. The spectrum of fast neutrons might undergo rather drastic changes, but this should not affect the lower energy regions to a great extent until extremely long ducts are traversed, in which case intensities would be so low that all dose rates would be insignificant in most practical cases.

If the physical case could be adequately simulated by consideration

of the transport from a pure thermal-neutron source, the specification of the albedo would be rather straightforward. The integral albedo, or total probability of reflection, would be on the order of 0.7; the assumption of independence with respect to incident direction is probably adequate, although the value of the albedo does change somewhat (see Appendix F). The assumption of independence with respect to the exit azimuthal angle is probably quite good, and the angular distribution should be fairly flat, probably a function which could be adequately represented as a sum of an isotropic component and a component proportional to the cosine of the polar angle. This statement on the nature of the angular distribution can be, at least partially, justified as follows: The angular distribution would be nearly isotropic for the case where the first collisions occur exactly on the wall surface. (The contribution to the distribution from singly scattered particles is precisely isotropic if isotropic scattering in the laboratory system is assumed.) If the scattering sources are distributed uniformly with distance into the wall, the resulting outward current should resemble a cosine distribution (Lambert's law). The distribution of scattering sources from the thermal source outside the wall will lie somewhere between these two extremes; therefore the conclusions as stated above are drawn.

Returning to consideration of the actual neutron spectrum, experiments at the Tower Shielding Facility (TSF) have shown that a spectrum of this general nature incident onto a concrete surface will result in an almost constant density of neutrons with energies below 0.4 eV as

a function of the distance into the wall. Actually, this distribution has a slight peak at a penetration distance of about 5 cm, but the net result is an almost constant density for distances on the order of 20 or 30 cm. This spatial distribution results, of course, from the slowing down of intermediate-energy neutrons combined with the transport of the thermal neutrons. In any case, this spatial distribution may be assumed to result in an angular distribution of the outgoing current quite closely resembling the cosine distribution. As to the value of the albedo, there seems to be no reason to expect the albedo of intermediate-energy neutrons to be drastically different from that of the pure thermal neutrons.

In summary, it is concluded that the spatial distribution of the thermal-neutron flux in a concrete-walled duct may be calculated by a random-walk process which utilizes at every wall collision an idealized albedo model. The albedo may be assumed to have the value on the order of that found for thermal neutrons and to have an angular distribution proportional to the cosine of the polar angle.

CHAPTER III

STRAIGHT DUCTS

The albedo model described in the previous chapter was incorporated into a digital computer code which was used both on the Control Data Corporation (CDC) 1604A computer at ORNL and on the International Business Machines (IBM) 7090 computer at the Union Carbide Central Data Processing Facility in Oak Ridge. A detailed description of the code and its use is given in Appendices A, B, and C.

A large number of calculations performed with the computer code were for straight ducts, both circular and rectangular in cross section. The results are presented below, along with comparisons of the calculations with an analytic approximation given by Simon and Clifford.[1]

All the straight-duct results are presented as particle flux (particles/cm^2) along the center line of the duct normalized to an incoming current of 1 particle/cm^2 at the source plane. The flux was obtained by totalling the particle track lengths in each of a series of detector volumes occupying the entire cross section of the duct and having a thickness of 0.5 ft, and then dividing by the volume of the detector. In each case the source was assumed to be uniform over the mouth of the duct and to have a distribution of angular current proportional to the

---

[1]A. Simon and C. E. Clifford, "The Attenuation of Neutrons in Air Ducts in Shields," Nuclear Science and Engineering 1, 156 (1956).

cosine of the angle measured from the line normal to the source plane. (This corresponds to an isotropic flux outside the duct; i.e., the number of neutrons per unit solid angle arriving at the duct mouth is constant for all directions.)

Calculations for Cylindrical Ducts

The cylindrical duct calculations were for a duct length of 30 ft and diameters varying from 0.5 to 6.0 ft. Albedos of 0.12 and 0.8 and albedo distributions of isotropic, cosine, and cosine[2] were used.

The calculated fluxes for a straight 0.5-ft-diam cylindrical duct and an albedo of 0.8 are presented in Figs. 1 and 2 for isotropic and cosine distributions, respectively. The error points shown in these figures and for all subsequent data from the computer code calculations represent $\pm 2\sigma$, where σ is the standard deviation, or square root of the variance.[2] It can be shown that there is a 95% probability that a new, independent calculation would be within the error bars.

The results of the calculations for 1-ft-diam ducts using albedos of 0.12 and 0.8 and isotropic and cosine distributions are shown in Figs. 3 through 6. Here the data represent scattered fluxes only, as opposed

---

[2]See Appendix A for the definition of variance and methods for obtaining the estimate of the variance.

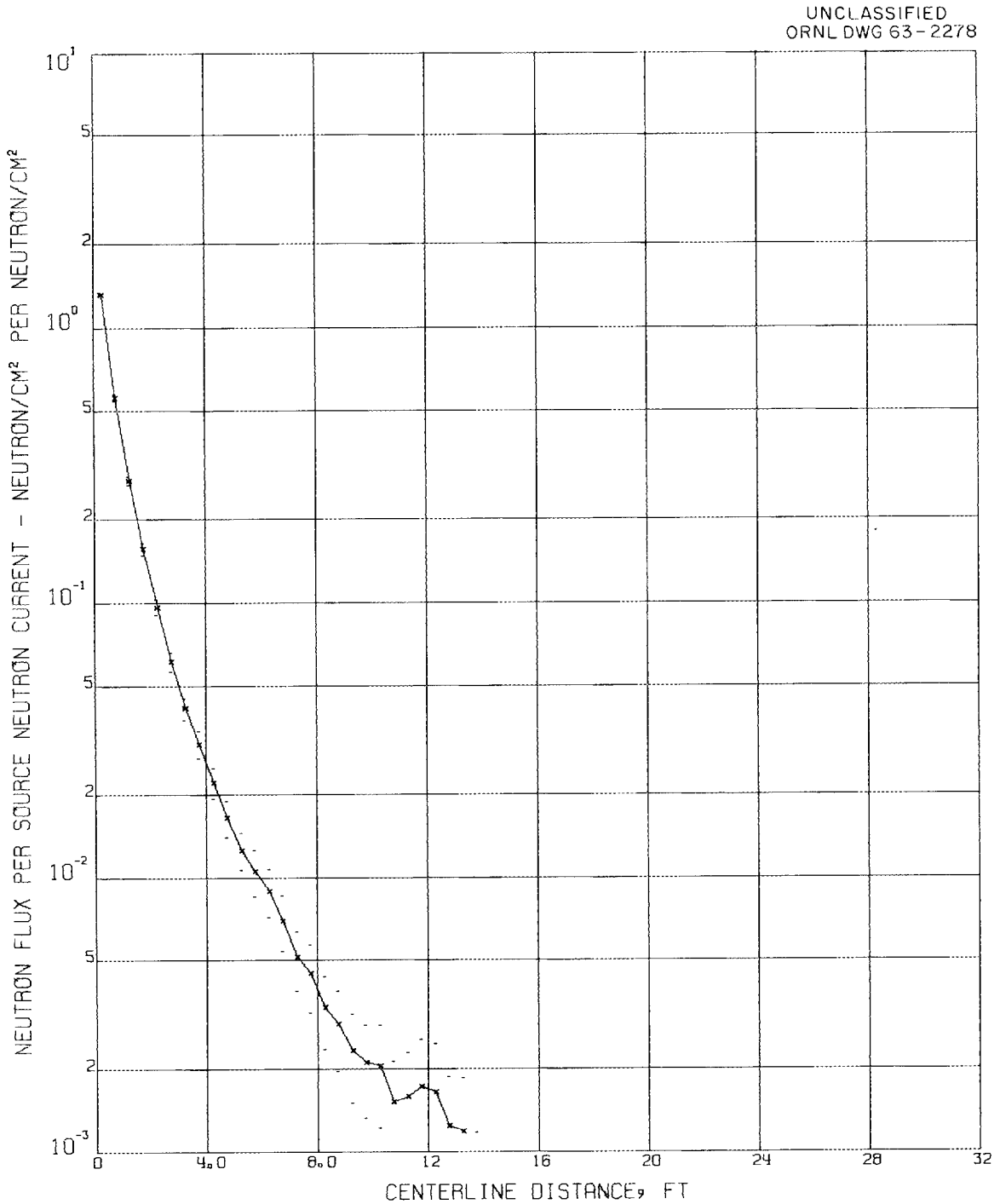

Fig. 1. Total Neutron Flux Calculated for 0.5-ft-diam Cylindrical Duct Using an Isotropic Albedo of 0.80 (10,000 Histories).

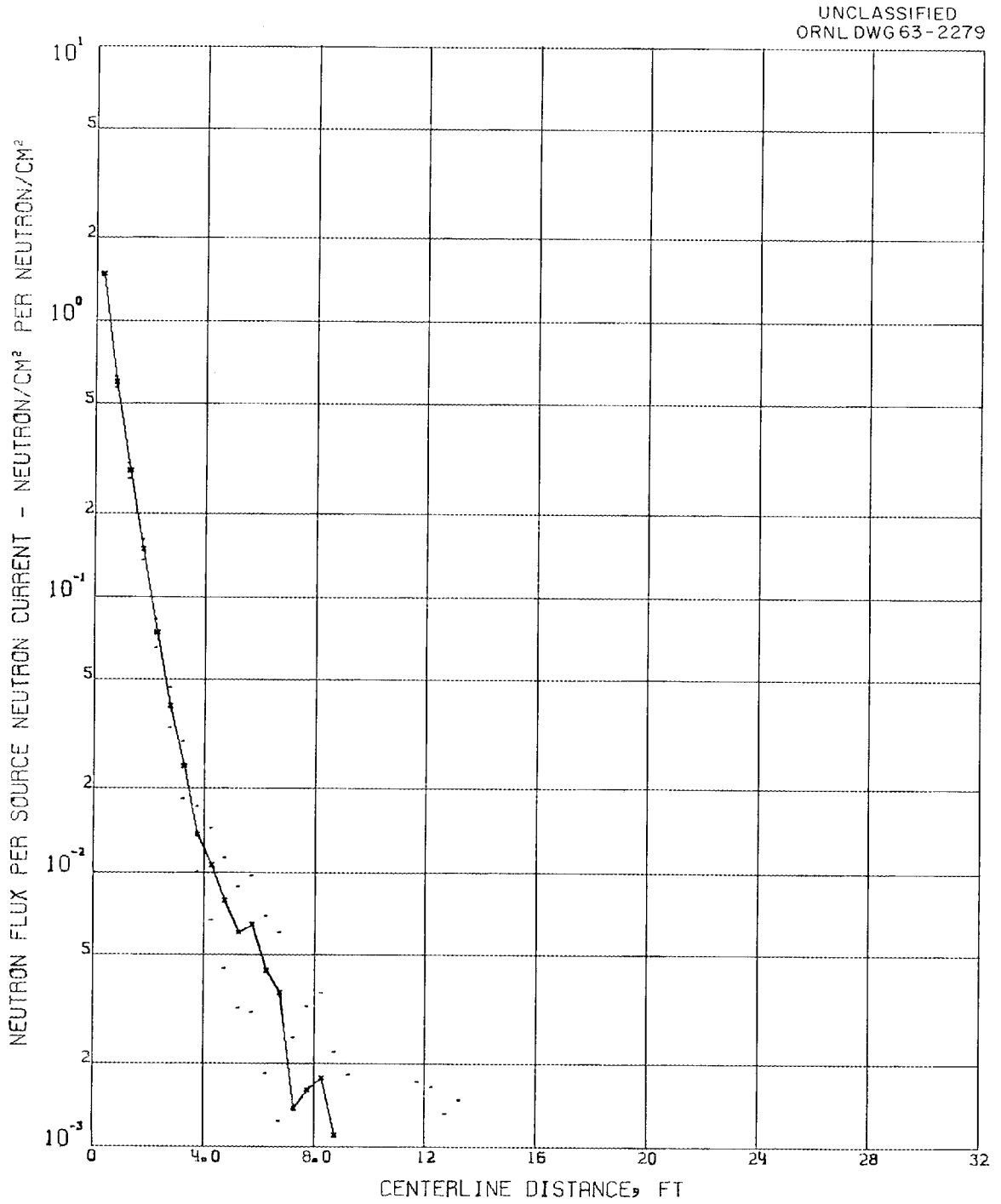

Fig. 2. Total Neutron Flux Calculated for 0.5-ft-diam Cylindrical Duct Using a Cosine Albedo of 0.8 (4,000 Histories).

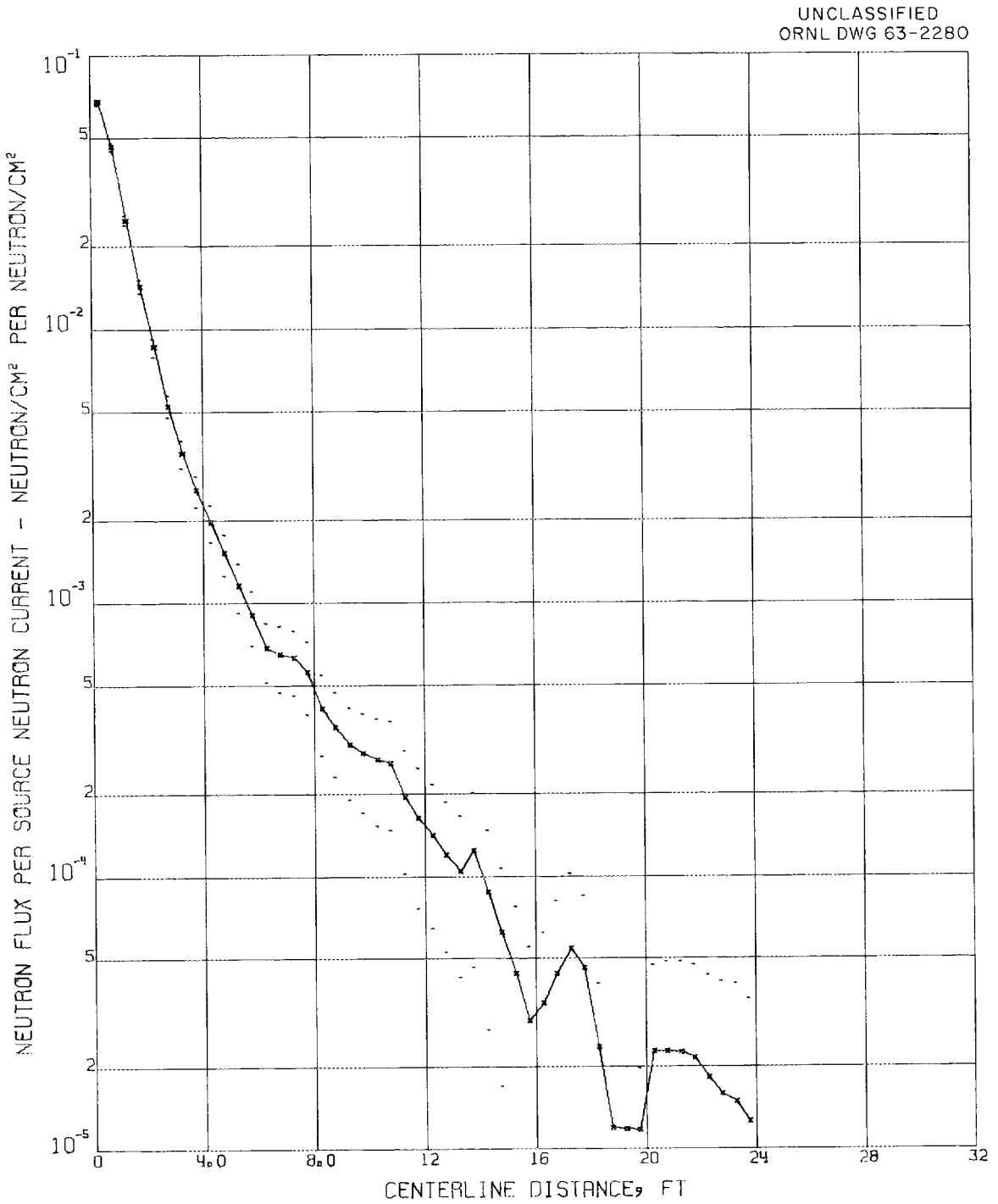

Fig. 3. Scattered Neutron Flux Calculated for 1-ft-diam Cylindrical Duct Using an Isotropic Albedo of 0.12 (10,000 Histories).

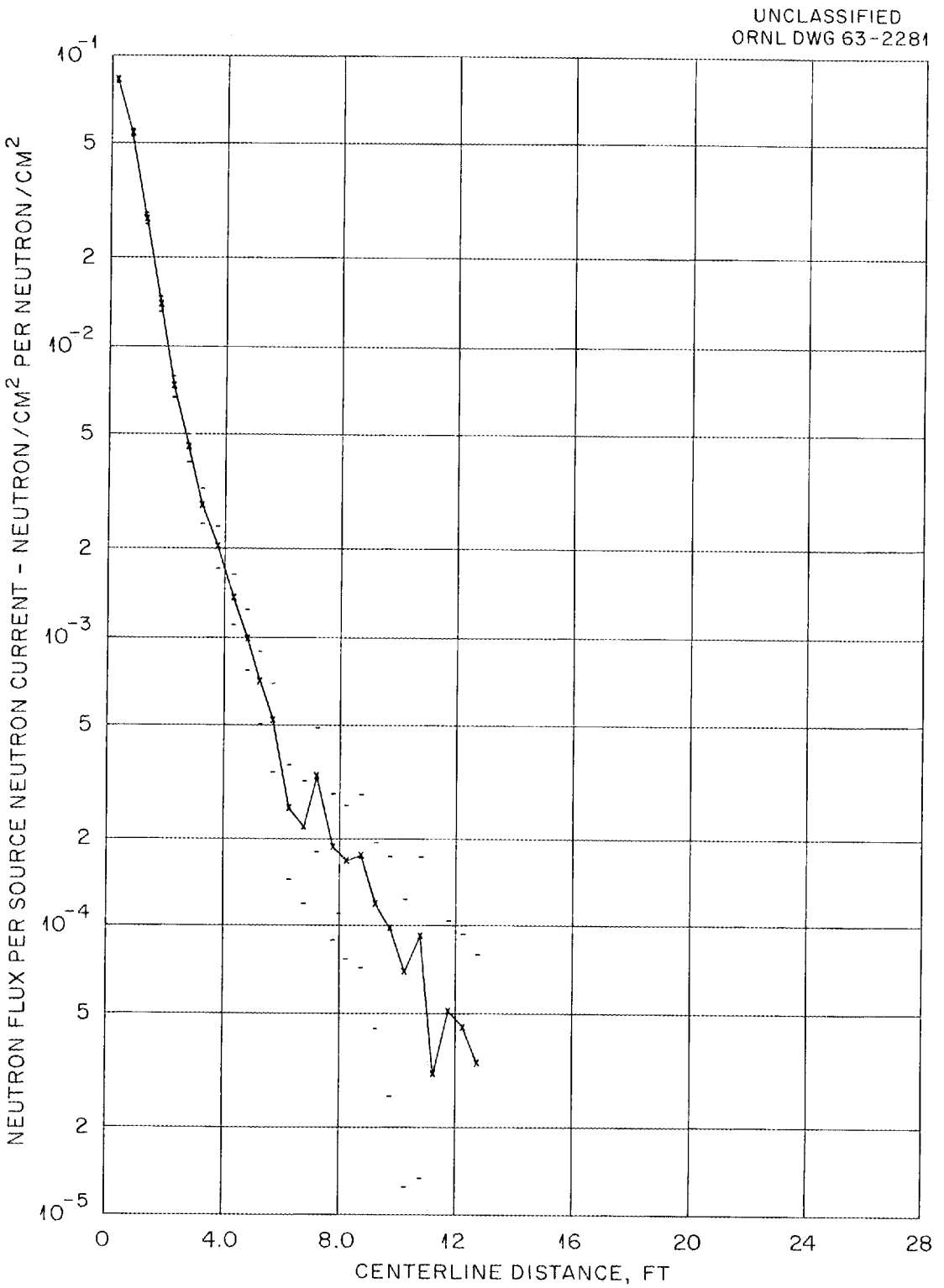

Fig. 4. Scattered Neutron Flux Calculated for 1-ft-diam Cylindrical Duct Using a Cosine Albedo of 0.12 (10,000 Histories).

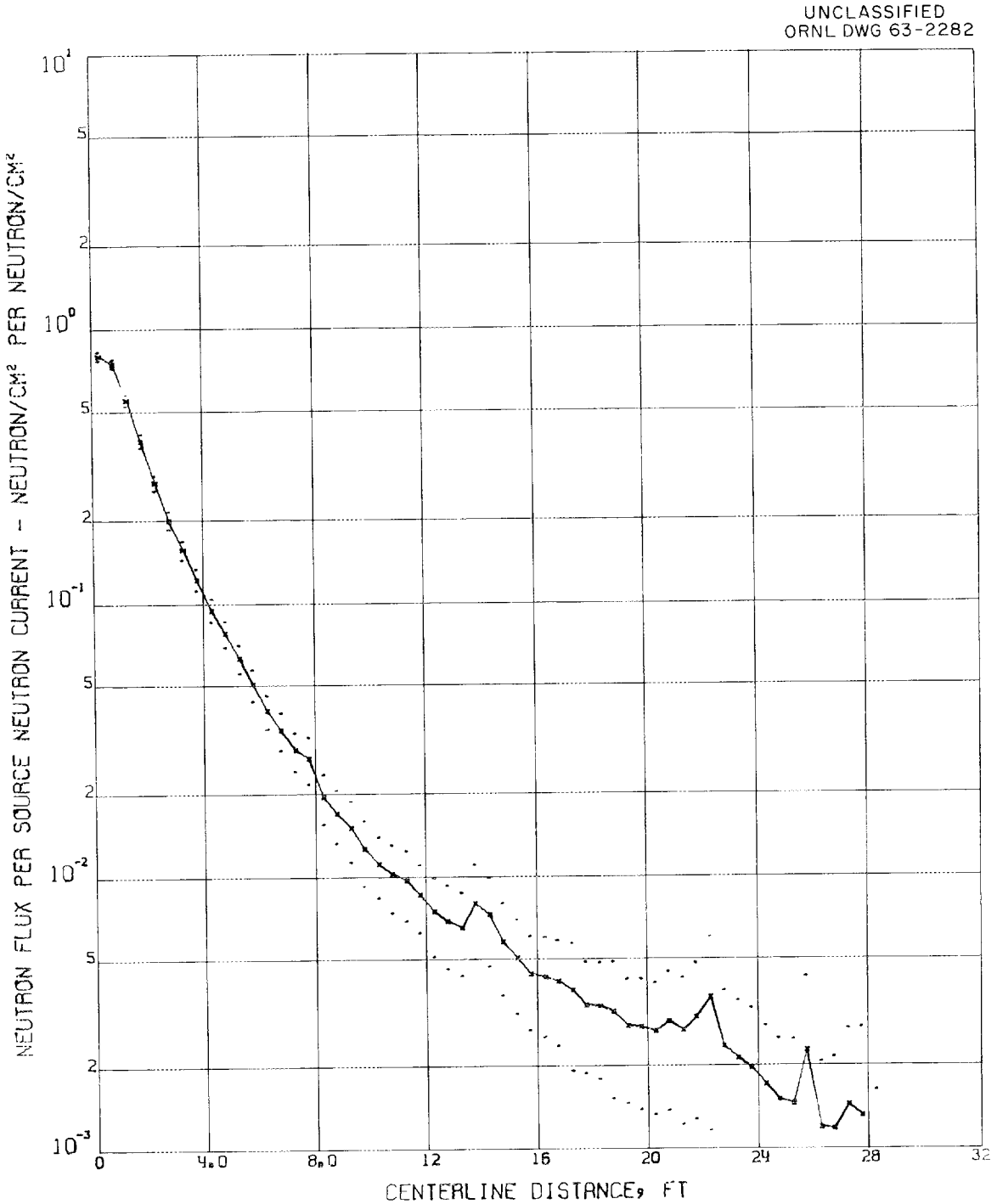

Fig. 5. Scattered Neutron Flux Calculated for 1-ft-diam Cylindrical Duct Using an Isotropic Albedo of 0.8 (4,000 Histories).

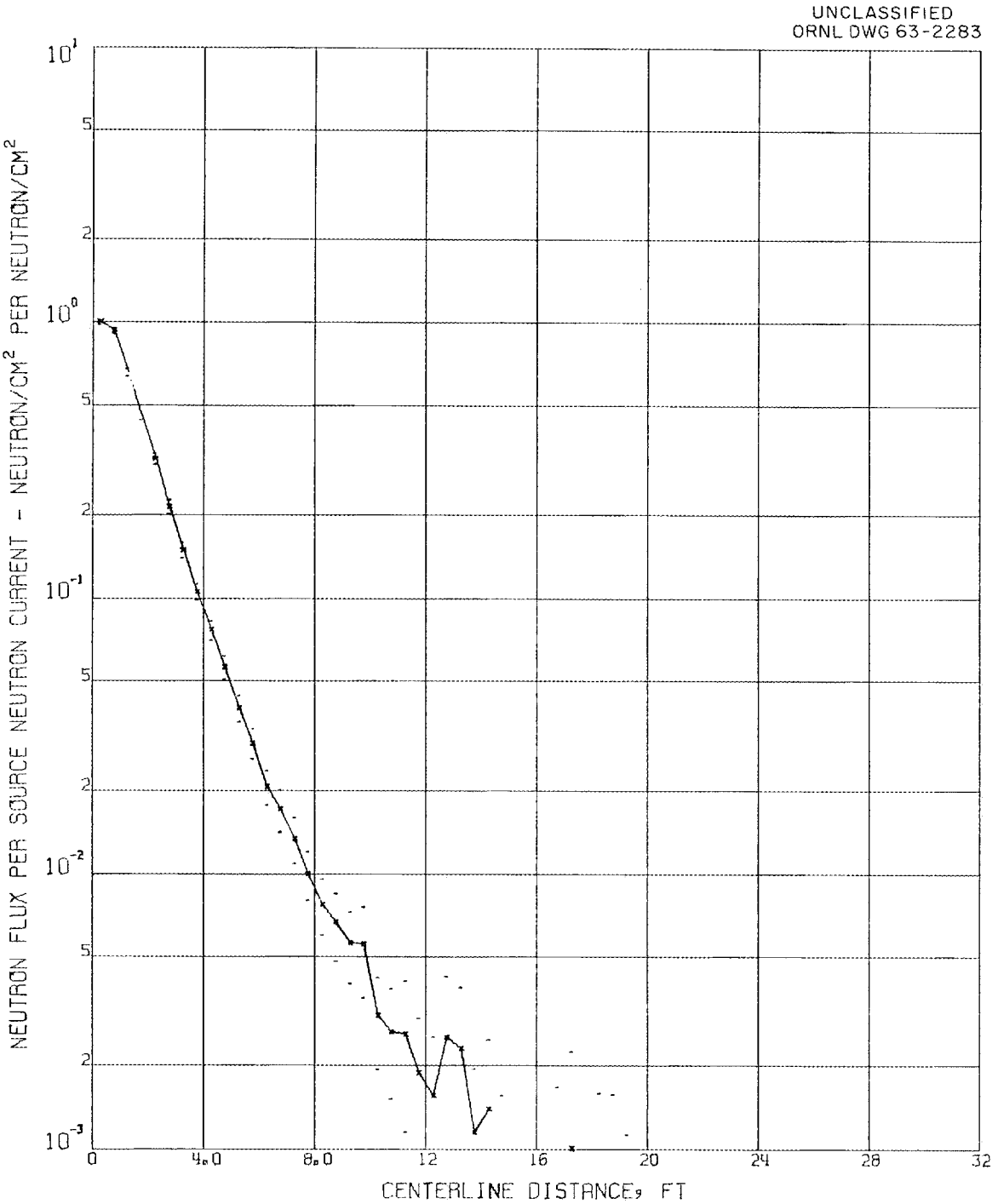

Fig. 6. Scattered Neutron Flux Calculated for 1-ft-diam Cylindrical Duct Using a Cosine Albedo of 0.8 (10,000 Histories).

to total fluxes given in Figs. 1 and 2 and in most of the plots that follow. Figures 5 and 6 demonstrate quite well the difference between an isotropic distribution and a cosine distribution of the albedo. The two curves are virtually identical for distances within 4 ft of the source, but for greater distances the isotropic albedo gives a much larger flux.

Total fluxes for a 1.38198-ft-diam duct (cross-sectional area of 1.5 ft^2) and an albedo of 0.8 are shown for isotropic and cosine distributions in Figs. 7 and 8, respectively. Figures 9 and 10 are similar except that the diameter is 1.95441 ft, resulting in a cross-sectional area of 3.0 ft^2. The calculations for these four cases were performed for later comparisons (pages 41, 48—57) with calculations for rectangular ducts having cross sections of 3 by 0.5 ft and 3 by 1 ft.

Total fluxes for a 6-ft-diam duct and an albedo of 0.8 are given for isotropic, cosine, and $cosine^2$ distributions in Figs. 11, 12, and 13, respectively. In these cases, where the calculation extends to only five diameters from the source, the angular distribution of the albedo has little effect on the results. The difference between the isotropic and $cosine^2$ distributions is less than a factor of 2 at any point.

Calculations for Rectangular Ducts

The calculations for straight rectangular ducts were performed for duct cross sections of 3 by 0.5 ft, 3 by 1 ft, and 3 by 6 ft and a duct length of 30 ft. Figures 14 through 20 show the results for the

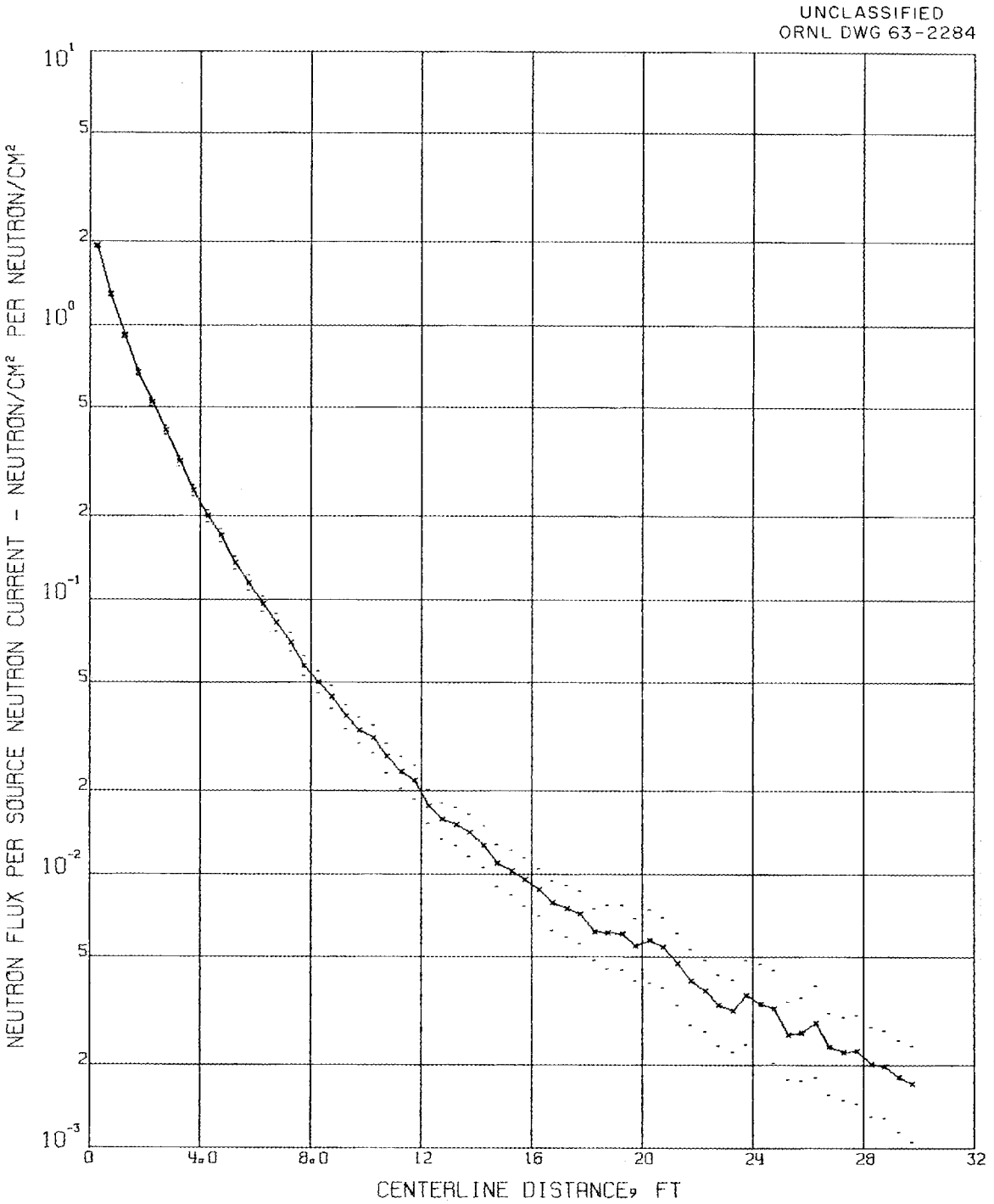

Fig. 7. Total Neutron Flux Calculated for 1.382-ft-diam Cylindrical Duct Using an Isotropic Albedo of 0.8 (10,000 Histories).

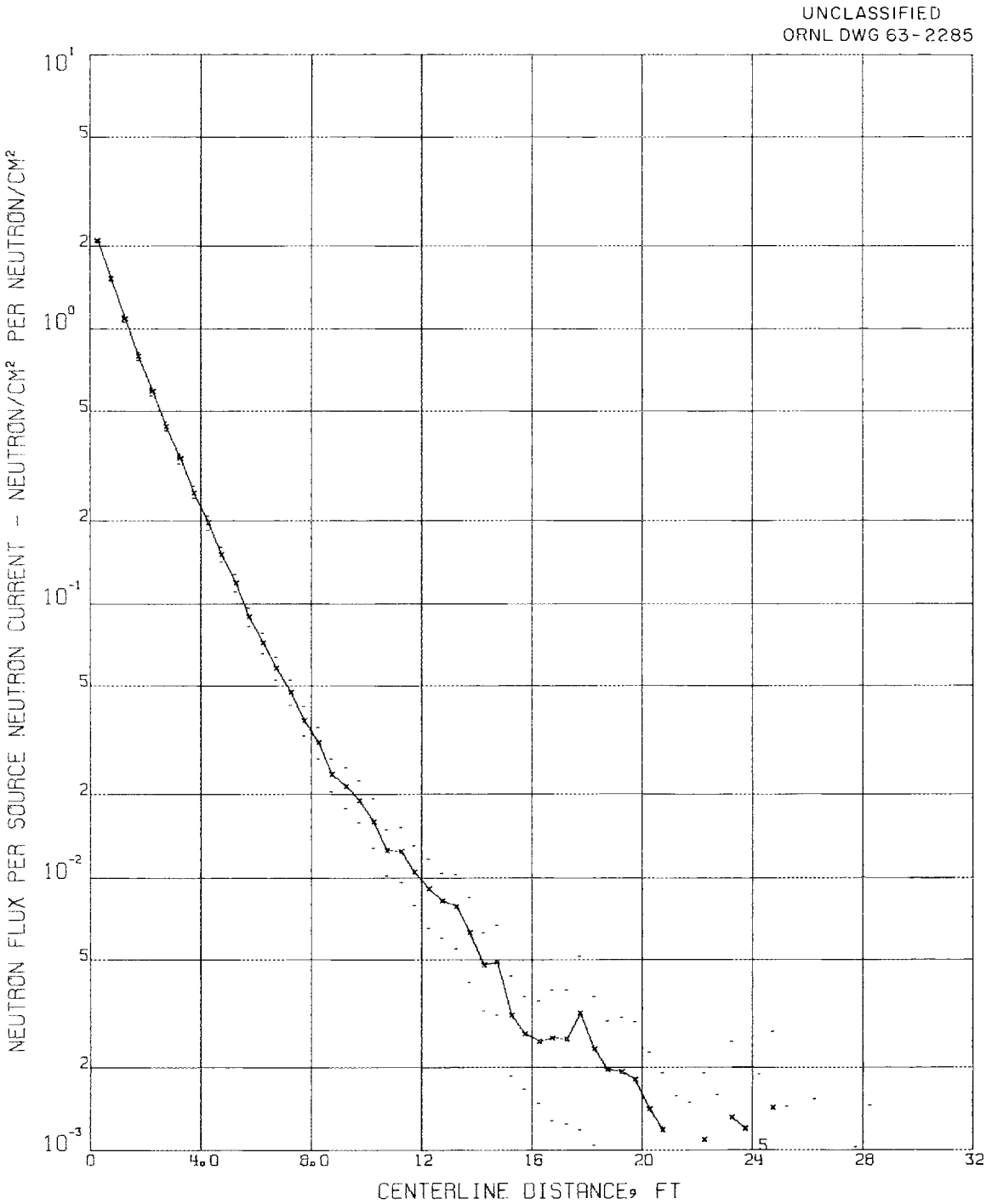

Fig. 8. Total Neutron Flux Calculated for 1.382-ft-diam Cylindrical Duct Using a Cosine Albedo of 0.8 (10,000 Histories).

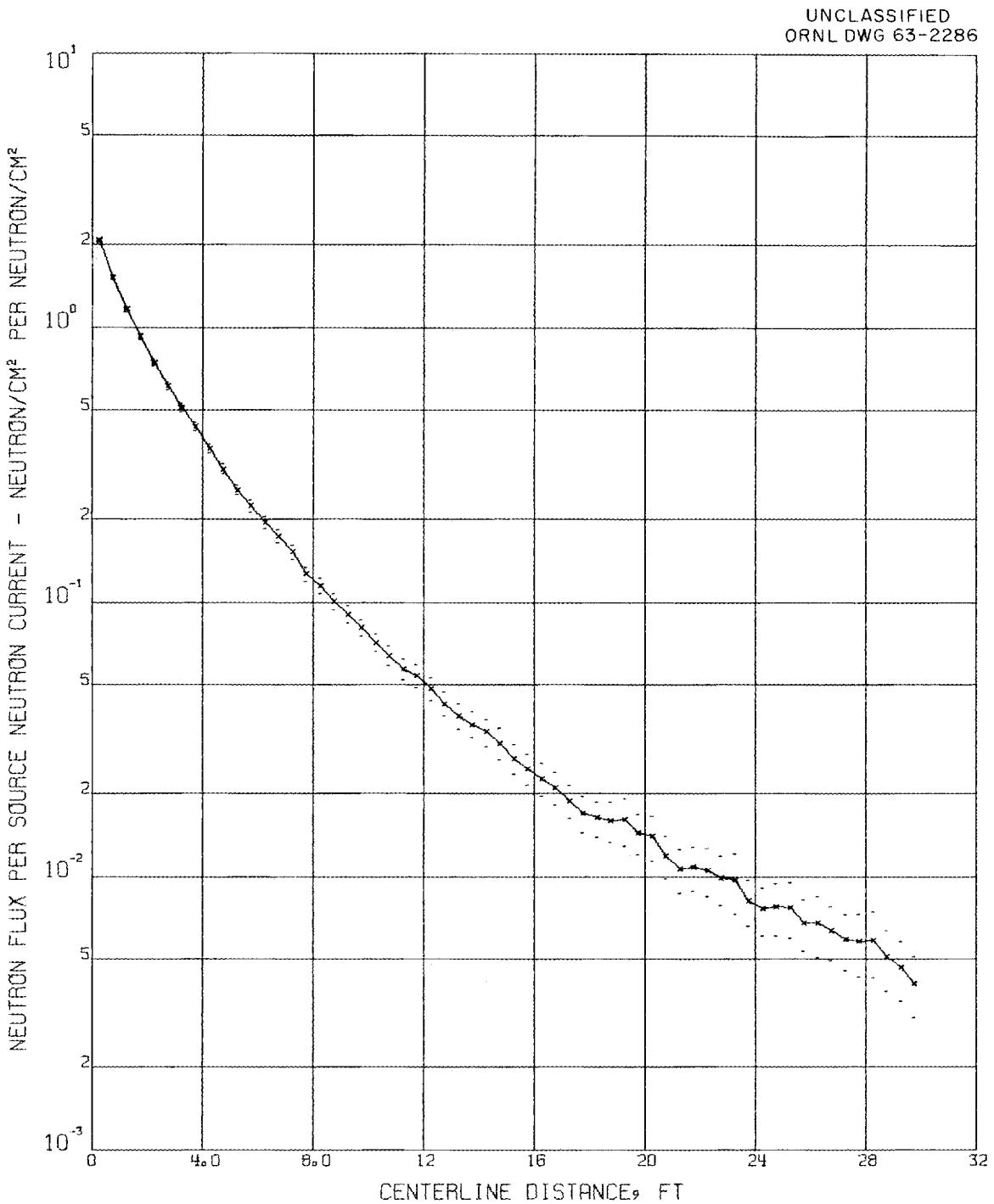

Fig. 9. Total Neutron Flux Calculated for 1.9544-ft-diam Cylindrical Duct Using an Isotropic Albedo of 0.8 (10,000 Histories).

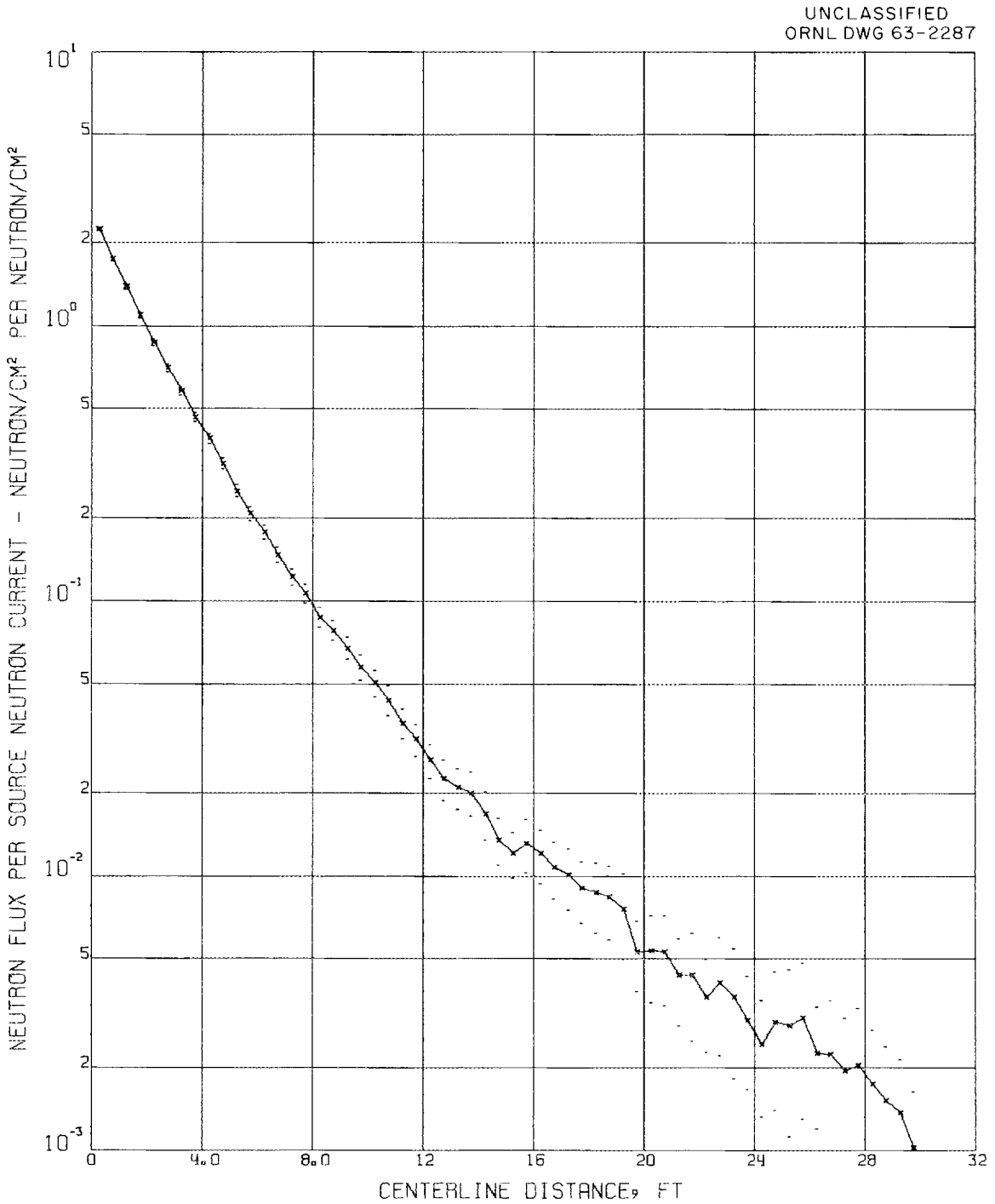

Fig. 10. Total Neutron Flux Calculated for 1.9544-ft-diam Cylindrical Duct Using a Cosine Albedo of 0.8 (10,000 Histories).

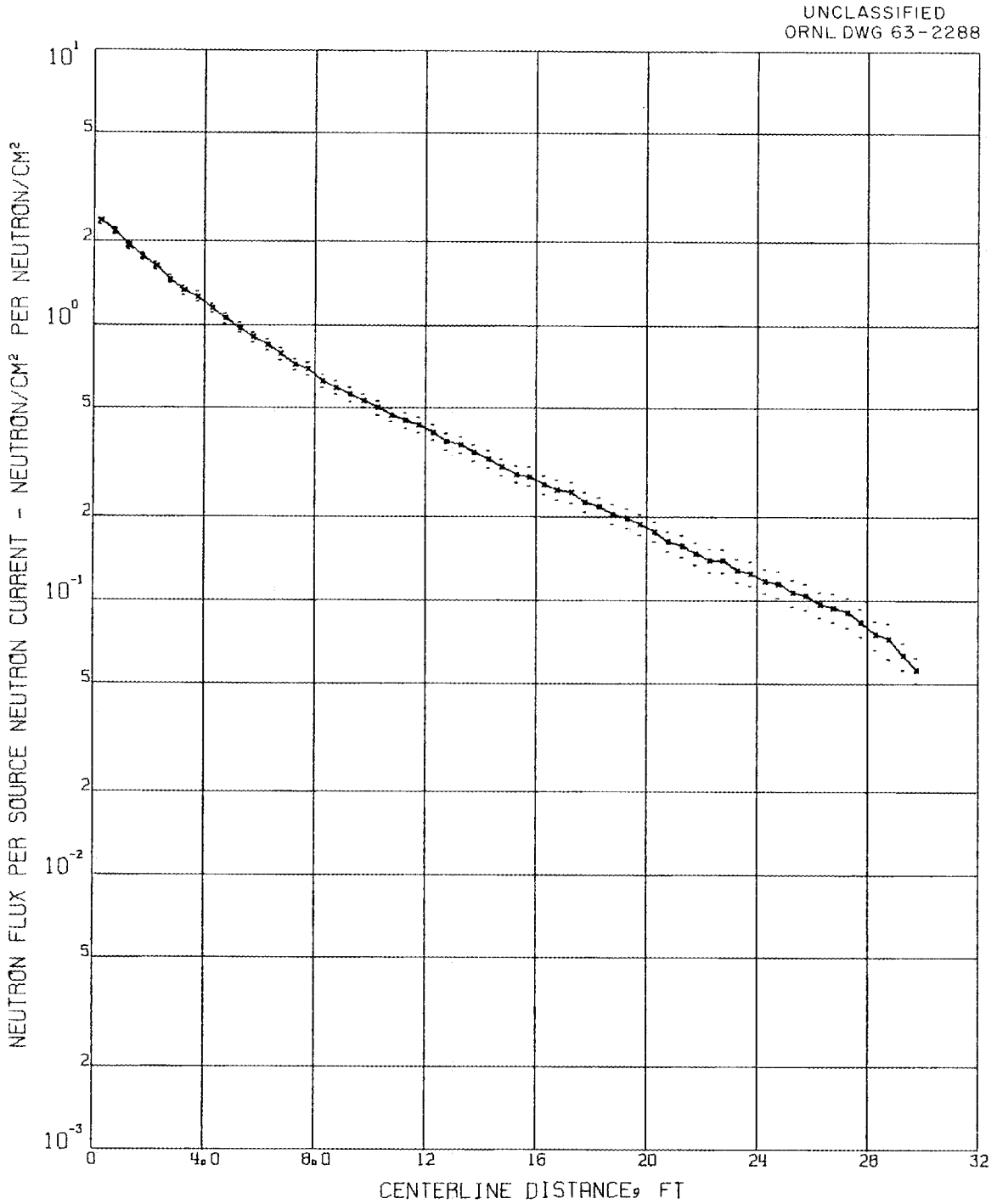

Fig. 11. Total Neutron Flux Calculated for 6-ft-diam Cylindrical Duct Using an Isotropic Albedo of 0.8 (4,000 Histories).

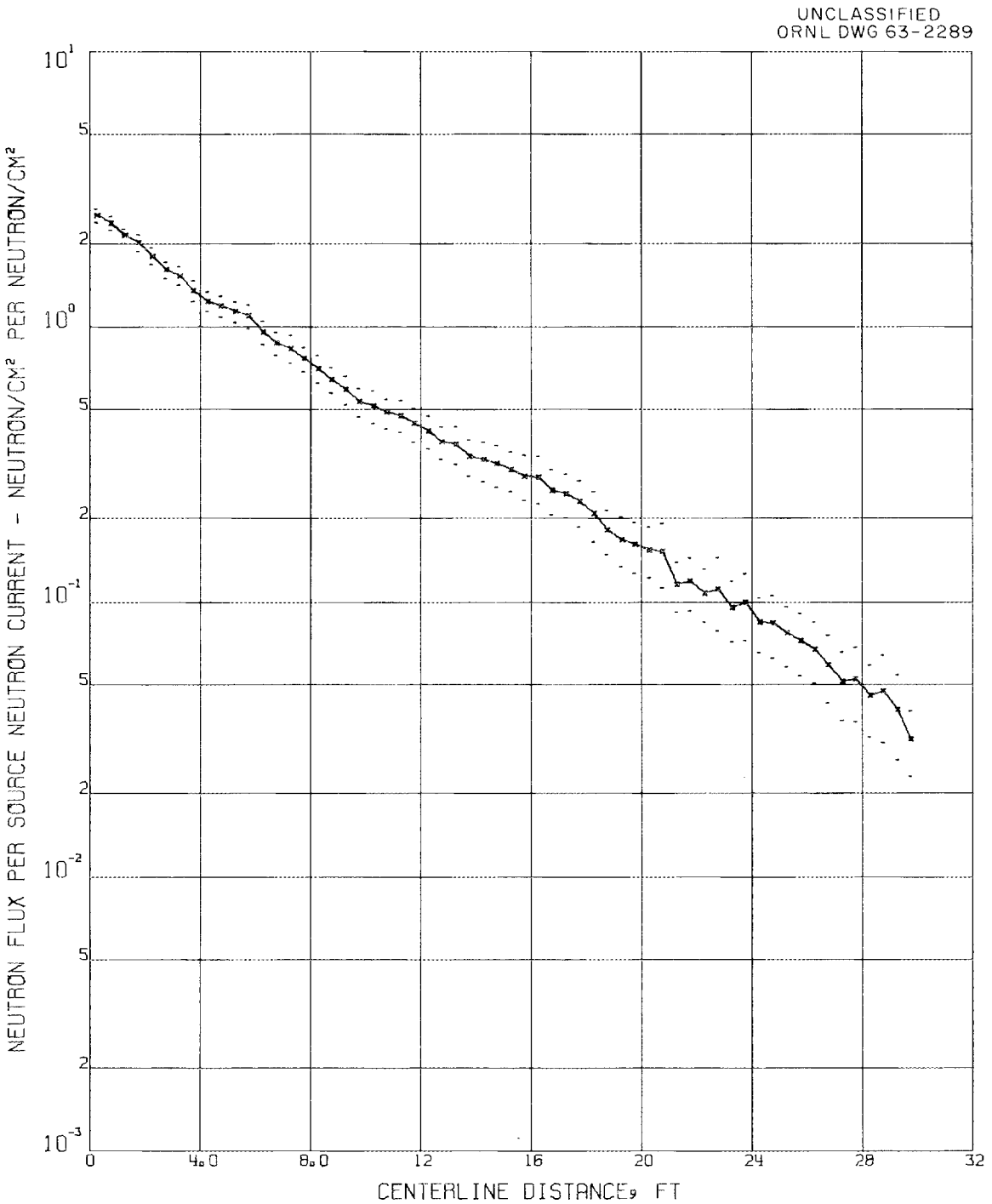

Fig. 12. Total Neutron Flux Calculated for 6-ft-diam Cylindrical Duct Using a Cosine Albedo of 0.8 (1,000 Histories).

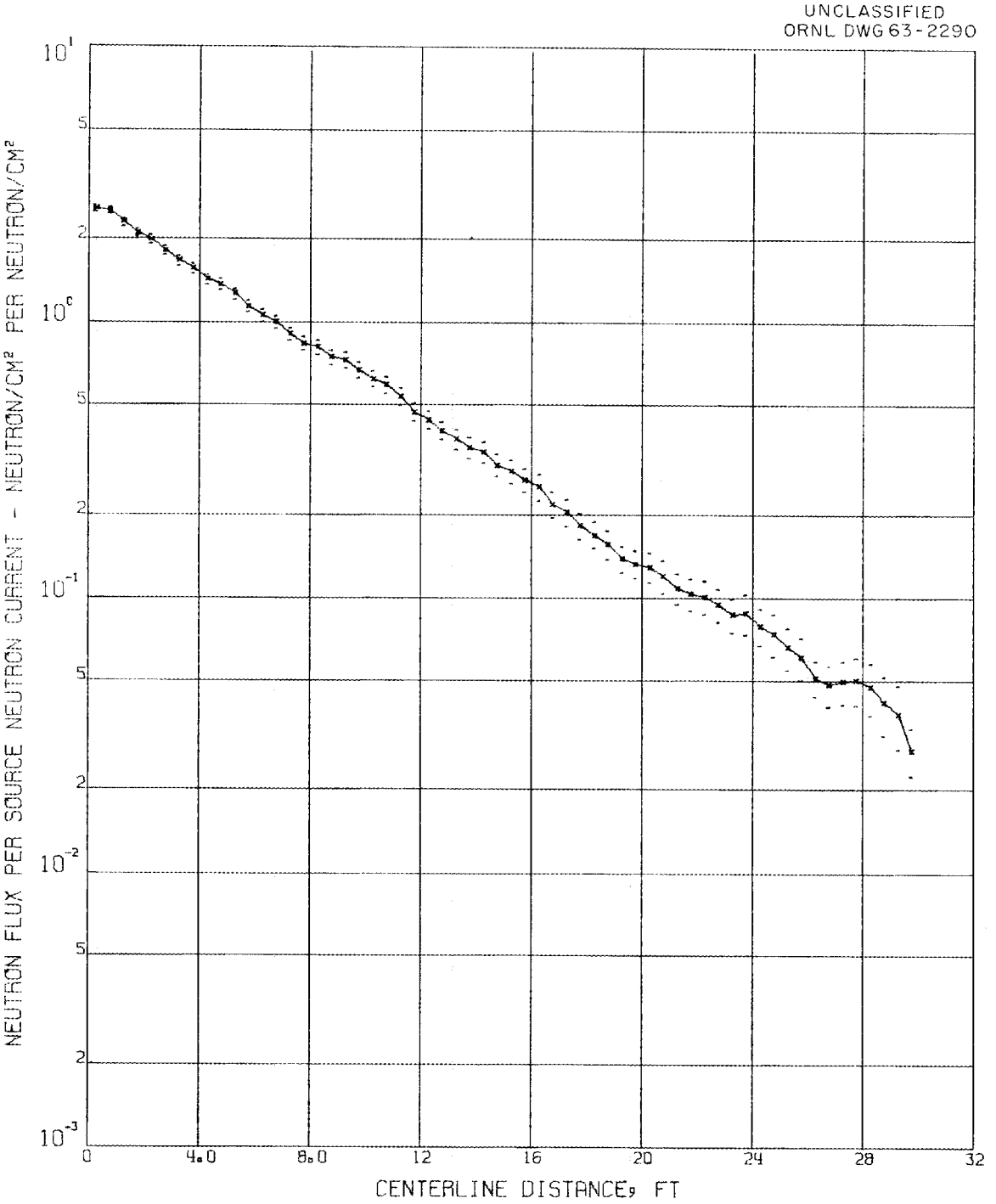

Fig. 13. Total Neutron Flux Calculated for 6-ft-diam Cylindrical Duct Using a Cosine^2 Albedo of 0.8 (4,000 Histories).

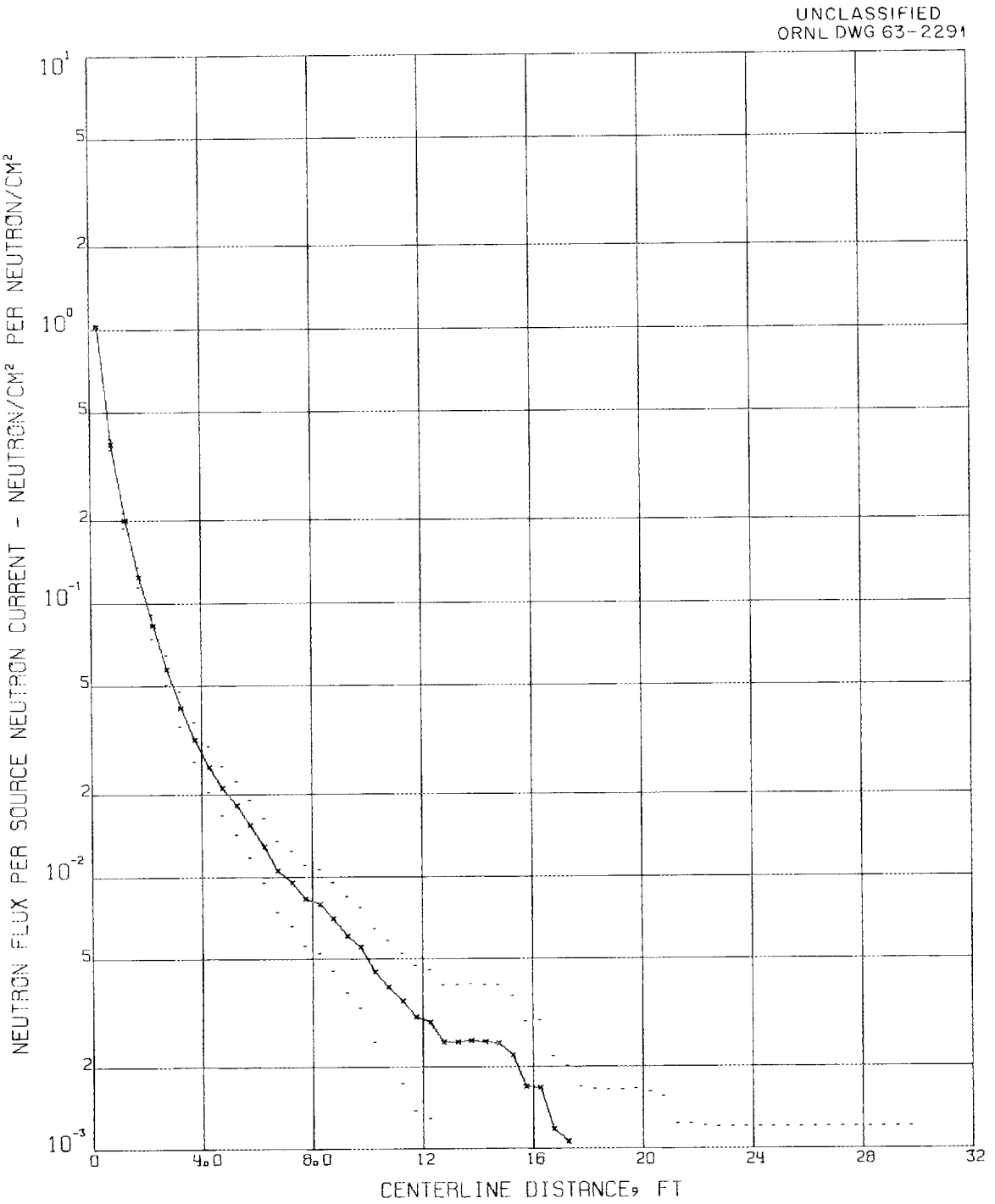

Fig. 14. Total Neutron Flux Calculated for 3 by 0.5 ft Rectangular Duct Using an Isotropic Albedo of 0.12 (4,000 Histories).

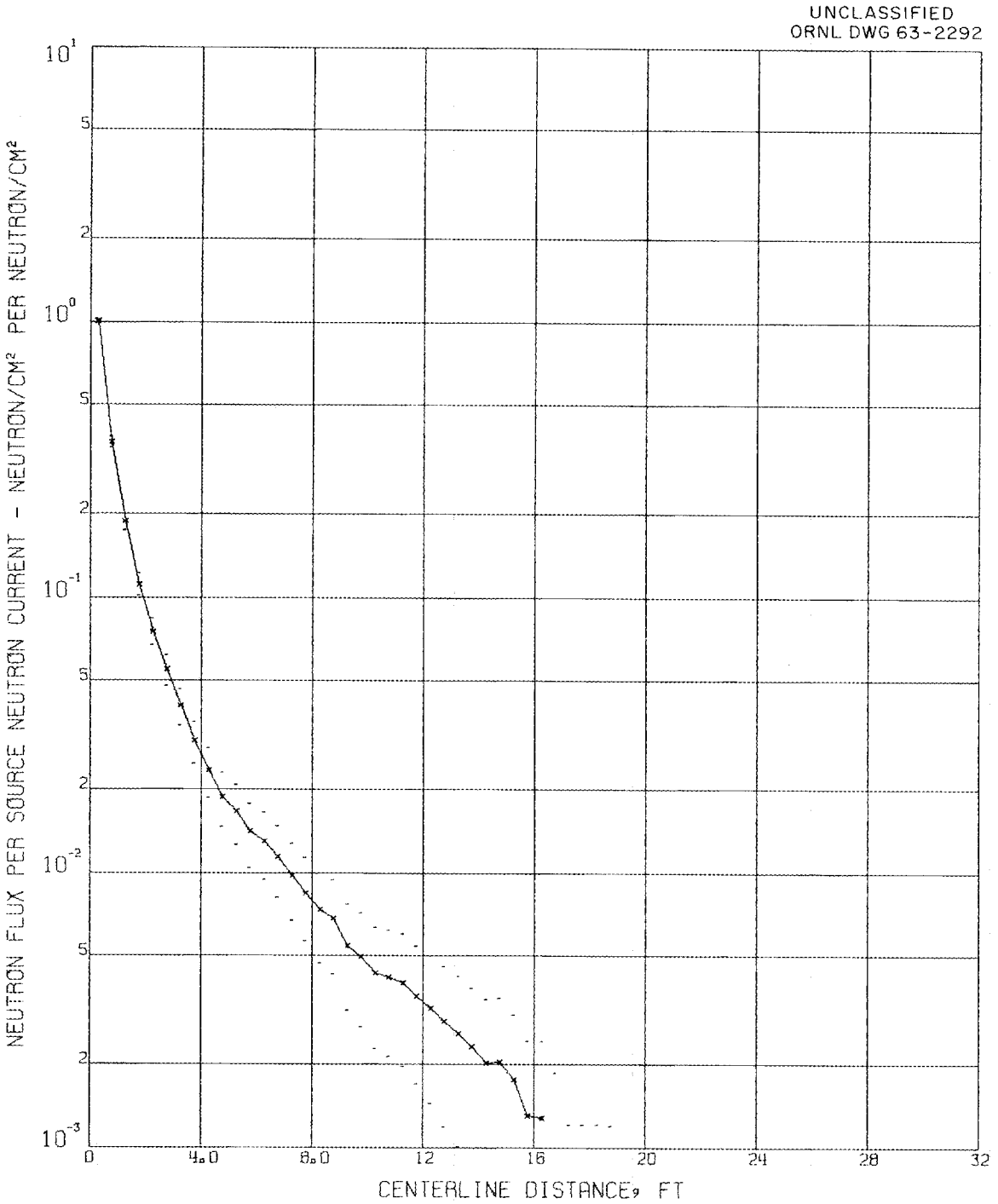

Fig. 15. Total Neutron Flux Calculated for 3 by 0.5 ft Rectangular Duct Using a Cosine Albedo of 0.12 (4,000 Histories).

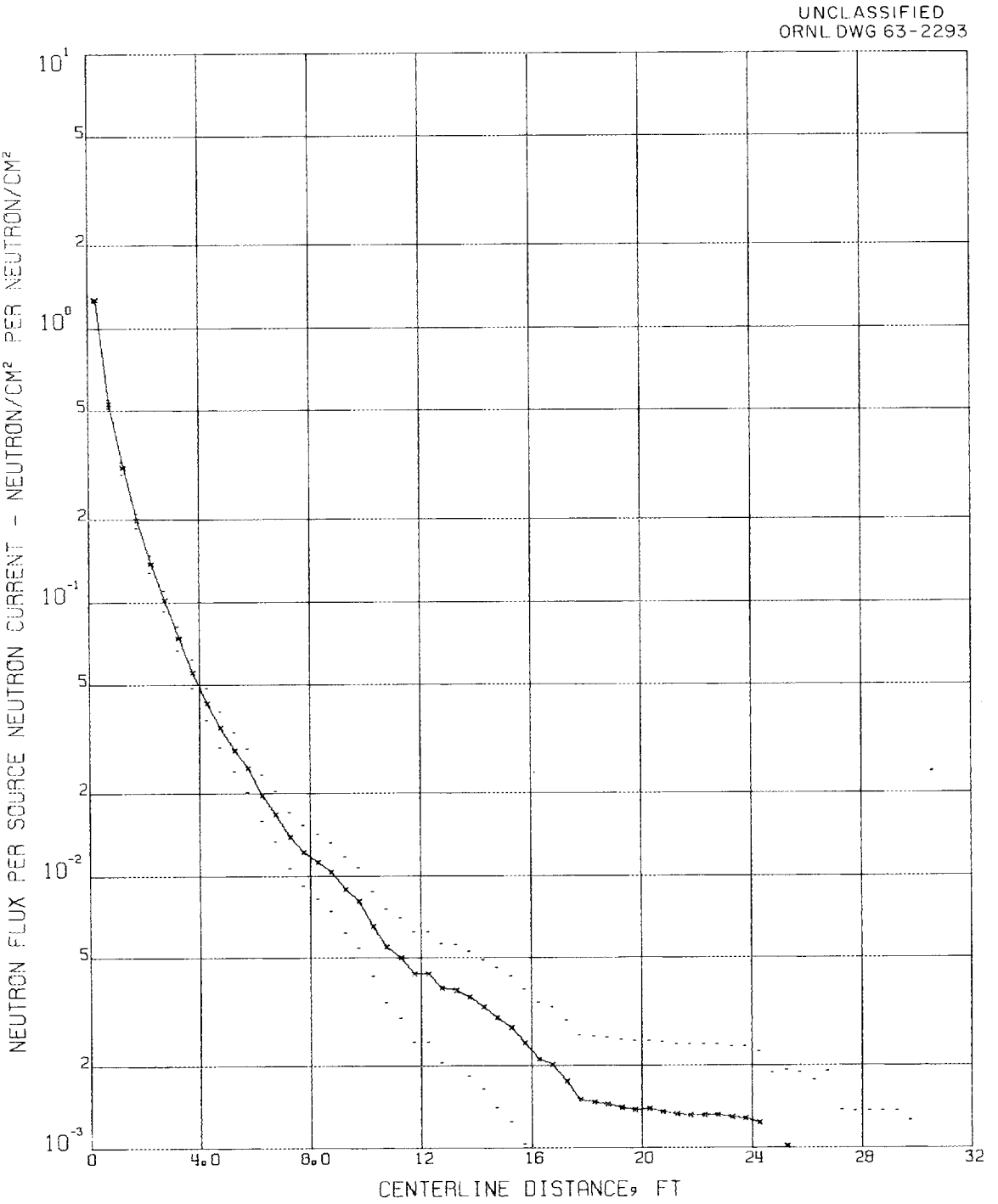

Fig. 16. Total Neutron Flux Calculated for 3 by 0.5 ft Rectangular Duct Using an Isotropic Albedo of 0.4 (4,000 Histories).

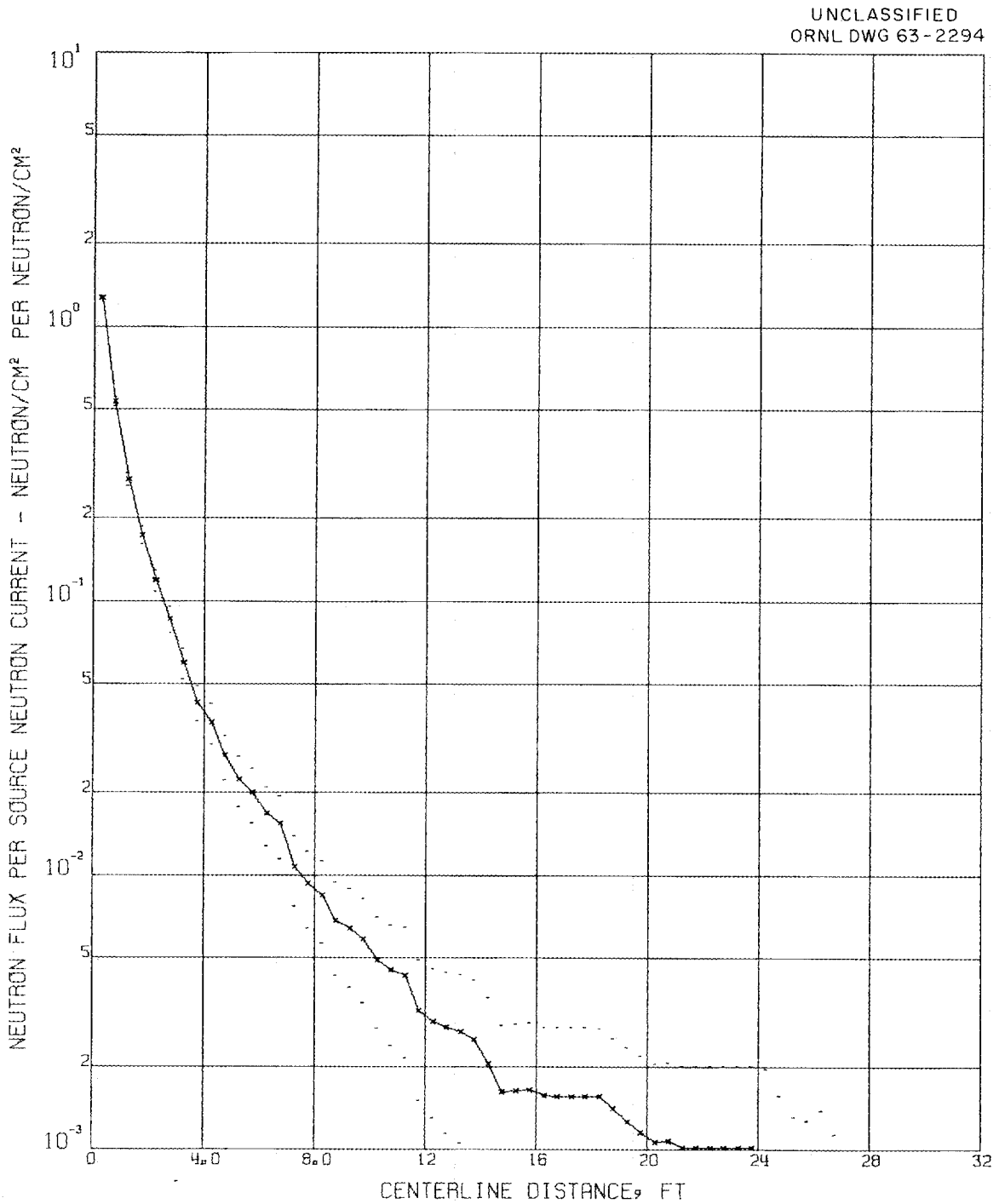

Fig. 17. Total Neutron Flux Calculated for 3 by 0.5 ft Rectangular Duct Using a Cosine Albedo of 0.4 (4,000 Histories).

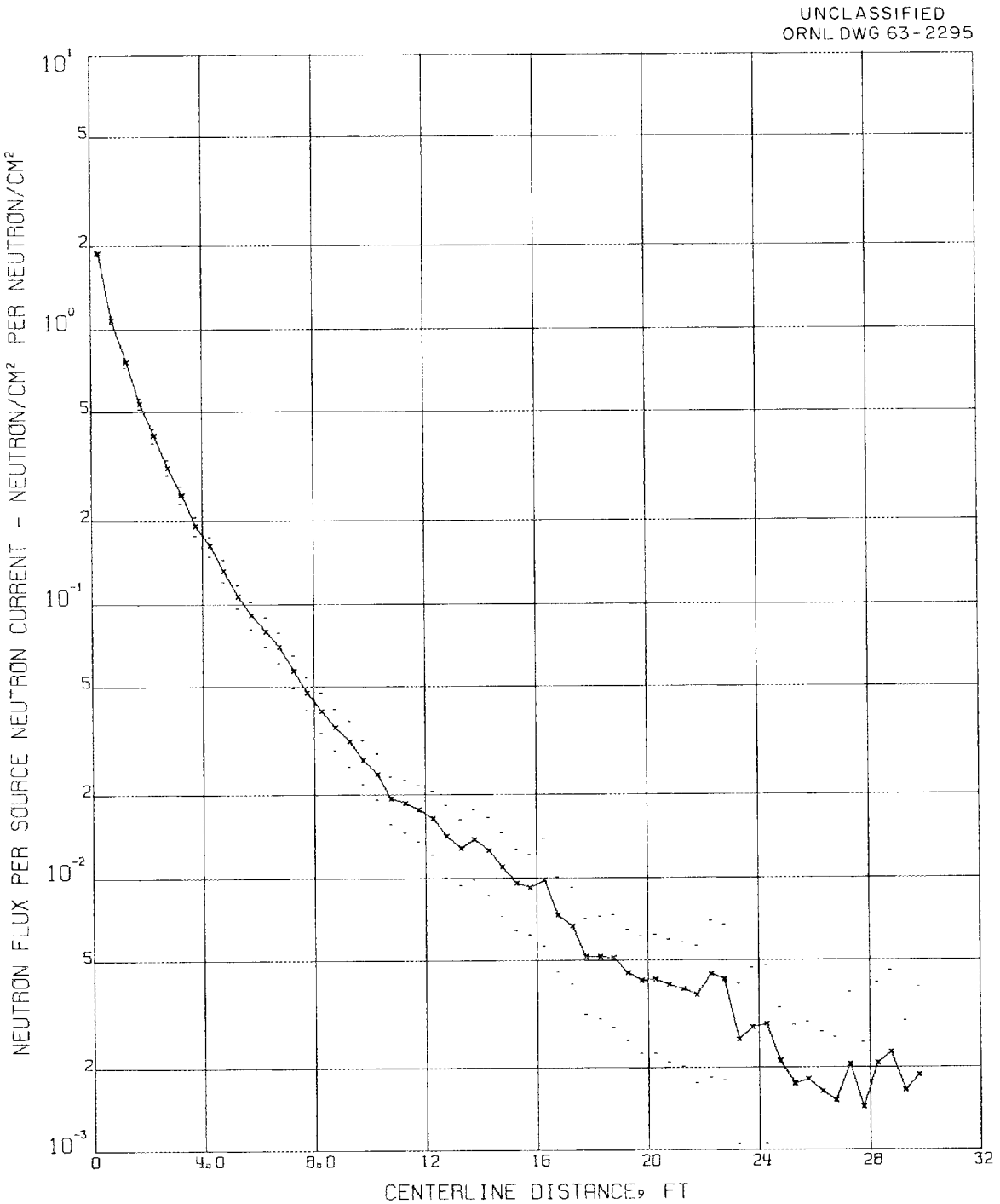

Fig. 18. Total Neutron Flux Calculated for 3 by 0.5 ft Rectangular Duct Using an Isotropic Albedo of 0.8 (4,000 Histories).

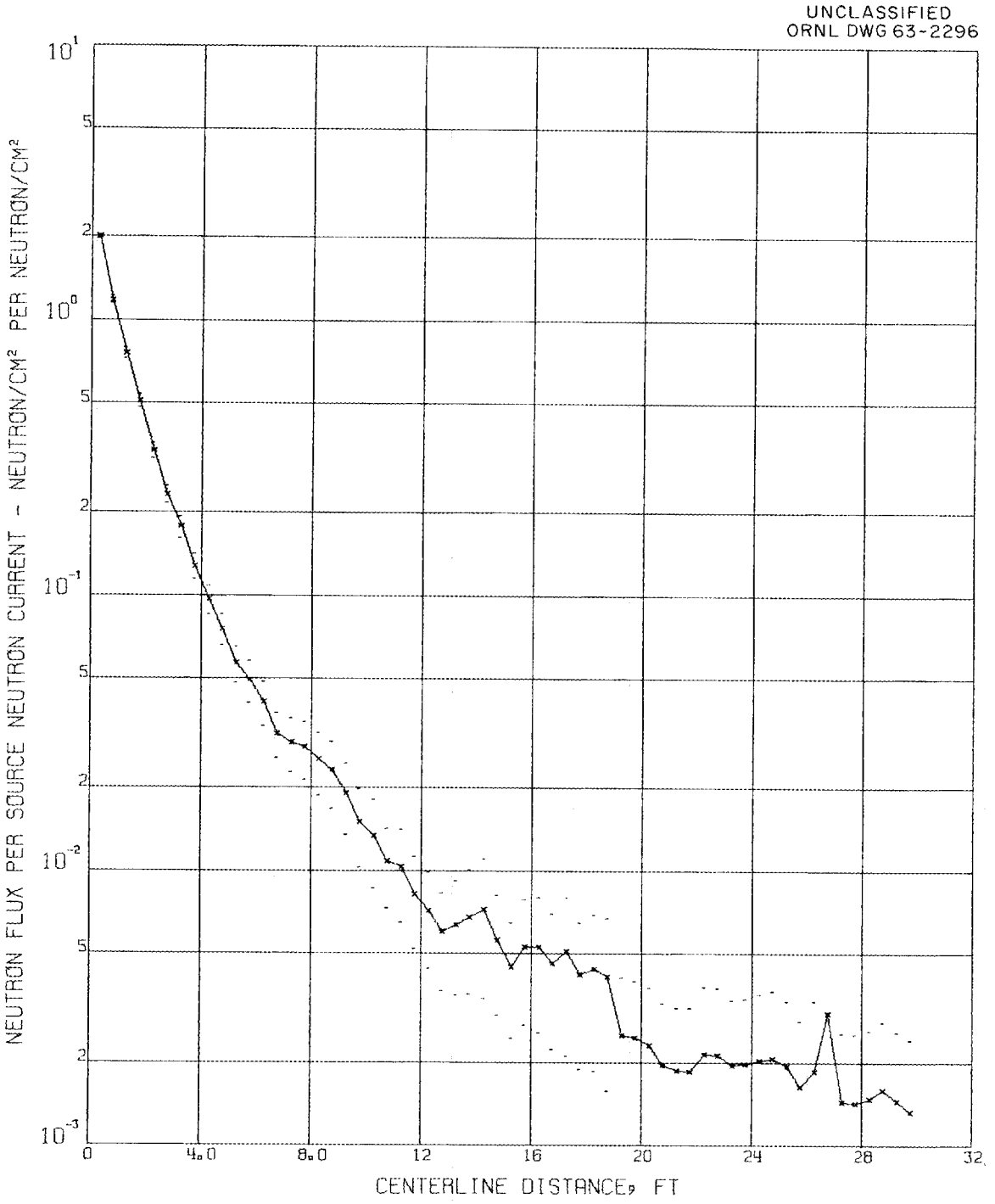

Fig. 19. Total Neutron Flux Calculated for 3 by 0.5 ft Rectangular Duct Using a Cosine Albedo of 0.8 (4,000 Histories).

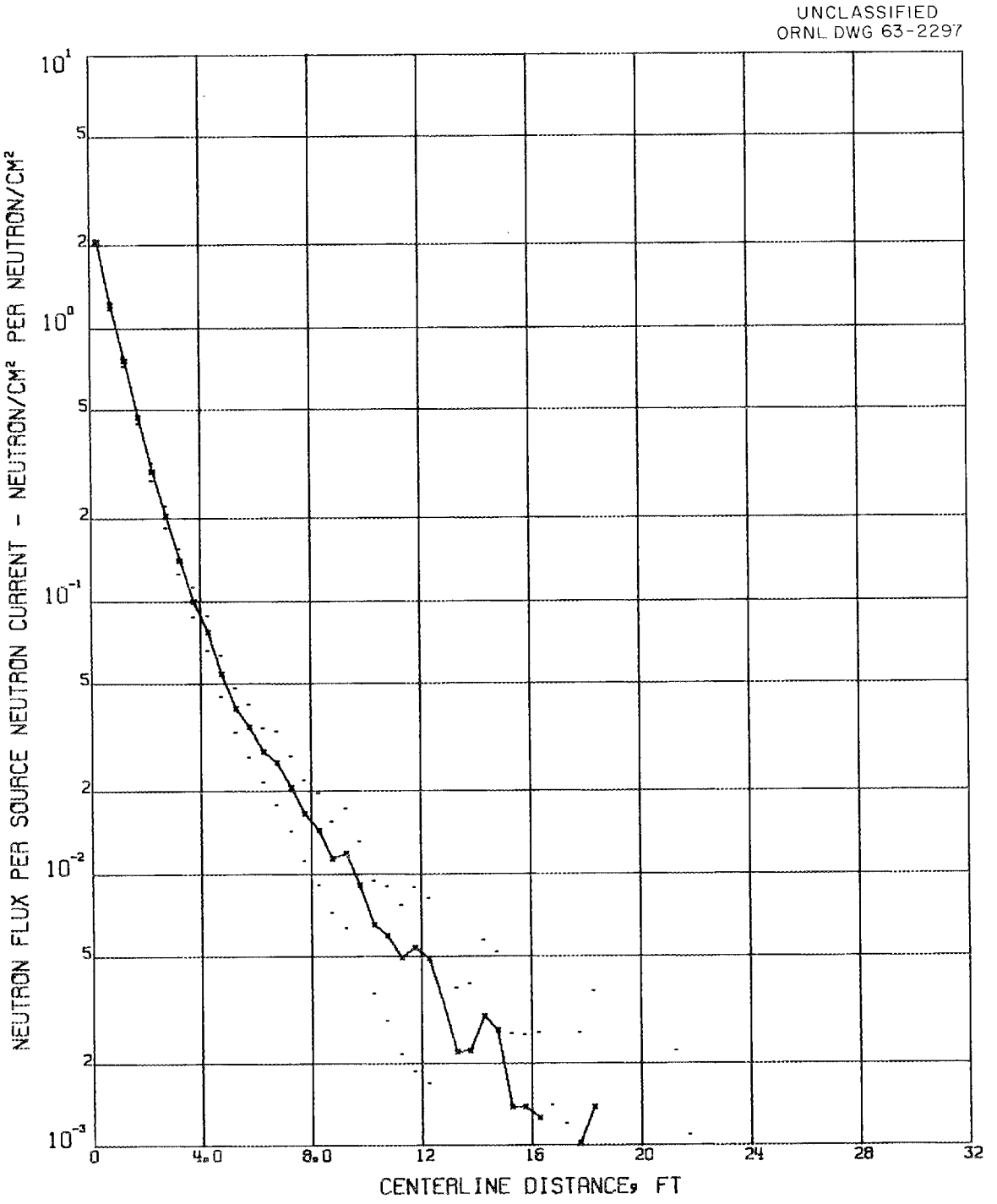

Fig. 20. Total Neutron Flux Calculated for 3 by 0.5 ft Rectangular Duct Using a Cosine^2 Albedo of 0.8 (4,000 Histories).

3 by 0.5 ft cross section, with Figs. 14 and 15 presenting the total fluxes for an albedo of 0.12 and isotropic and cosine distributions, Figs. 16 and 17 the fluxes for an albedo of 0.4 and isotropic and cosine distributions, and Figs. 18, 19, and 20 the fluxes for an albedo of 0.8 and isotropic, cosine, and cosine^2 distributions.

Figures 21, 22, and 23 give the results for a 3 by 1 ft cross section, an albedo of 0.8, and distributions of isotropic, cosine, and cosine^2, respectively. Figures 24 through 26 correspond to Figs. 21 through 23 except that a 3 by 6 ft cross section was used.

As presented here, the rectangular duct data have only limited significance, but they are used in comparisons given in later sections.

Comparisons with an Analytic Approximation

One of the primary purposes in performing the straight-duct calculations was to enable comparisons with calculations based on an equation reported by Simon and Clifford.[3] The Simon-Clifford equation which was used for the comparison was derived for very long straight circular ducts with an azimuthally independent albedo expressed as a sum of isotropic and cosine distribution components as follows:

$$\alpha = \alpha'(A + 2B \cos\theta) \ , \tag{1}$$

---

[3]Simon and Clifford, loc. cit.

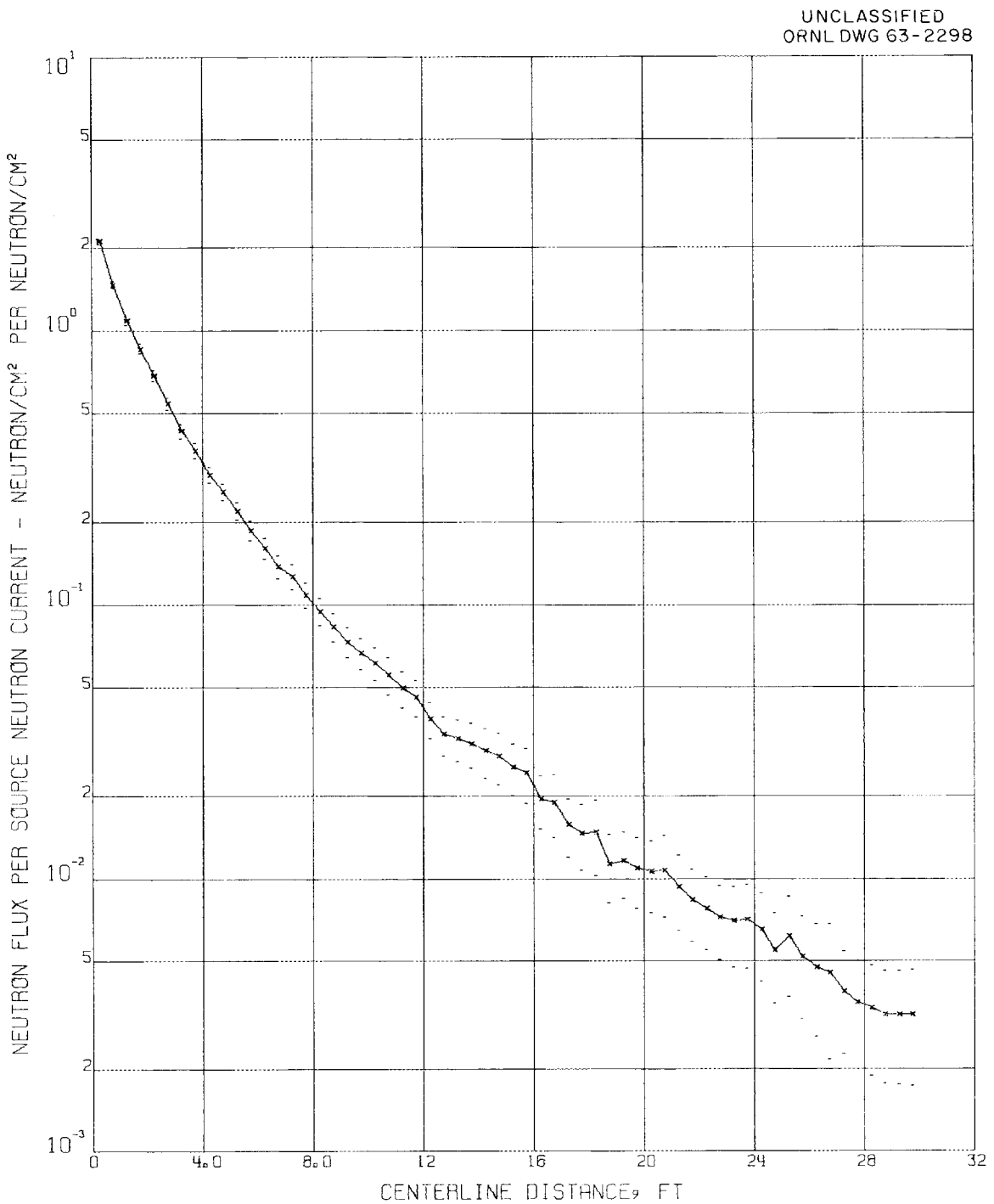

Fig. 21. Total Neutron Flux Calculated for 3 by 1 ft Rectangular Duct Using an Isotropic Albedo of 0.8 (4,000 Histories).

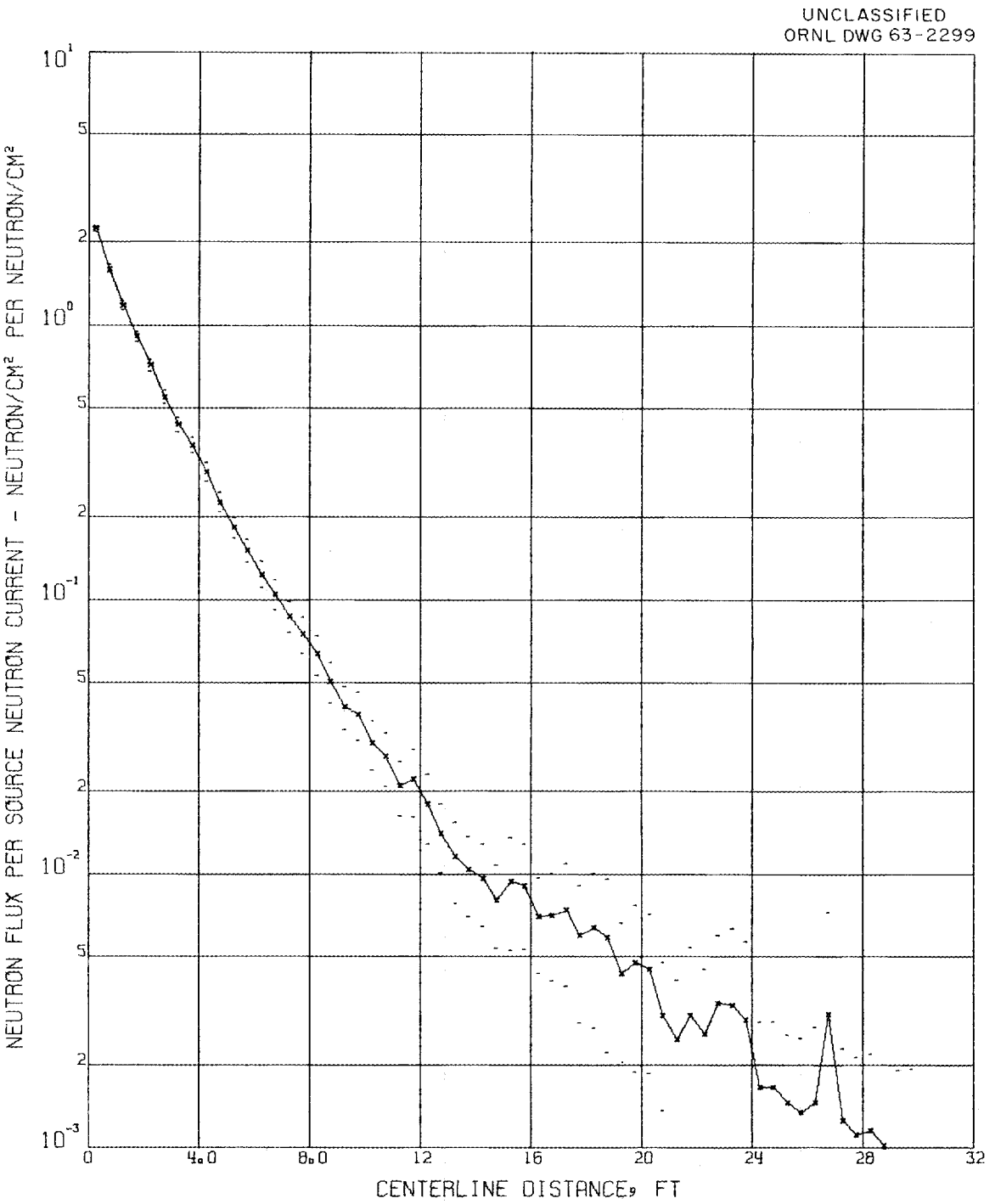

Fig. 22. Total Neutron Flux Calculated for 3 by 1 ft Rectangular Duct Using a Cosine Albedo of 0.8 (4,000 Histories).

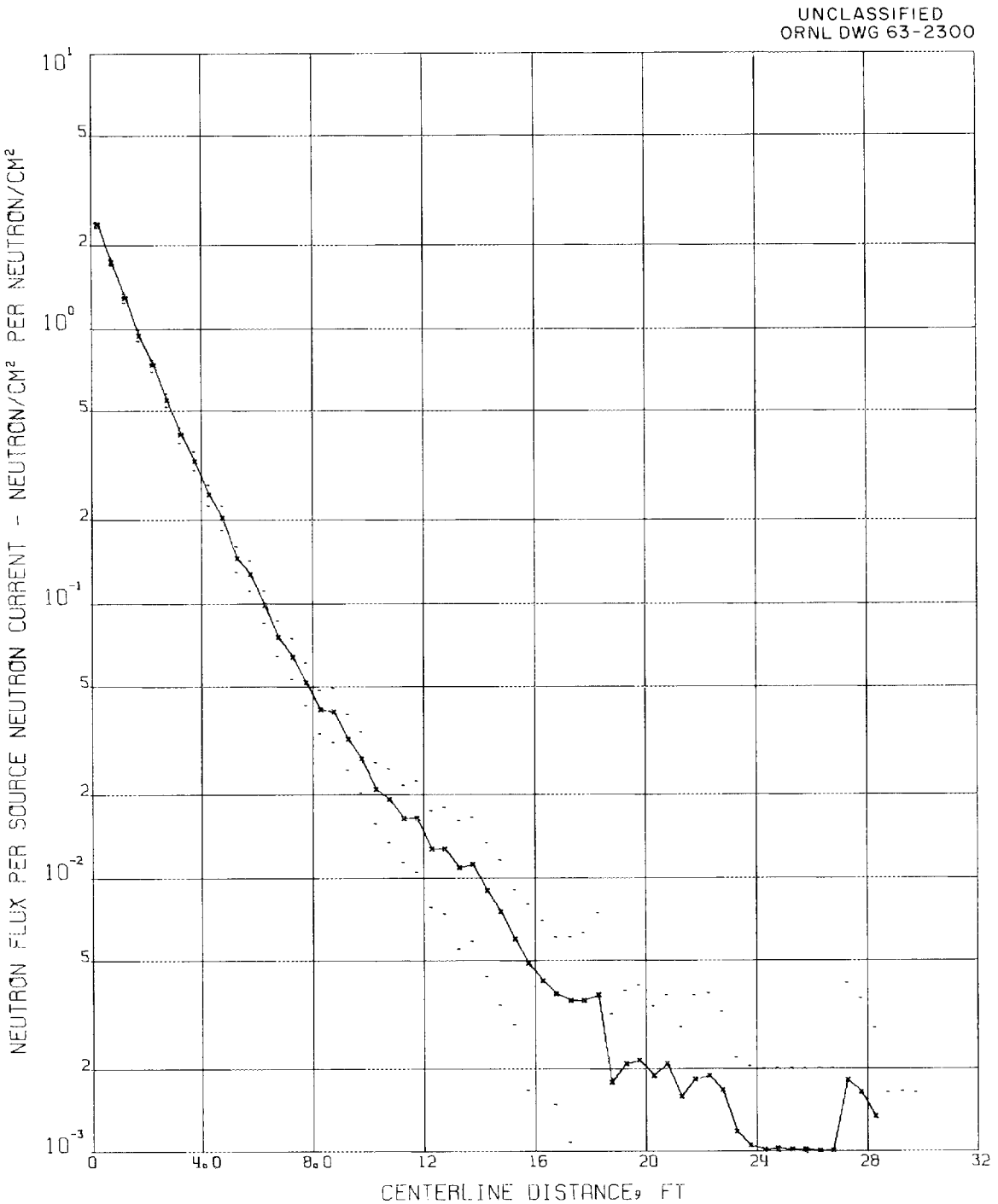

Fig. 23. Total Neutron Flux Calculated for 3 by 1 ft Rectangular Duct Using a Cosine^2 Albedo of 0.8 (4,000 Histories).

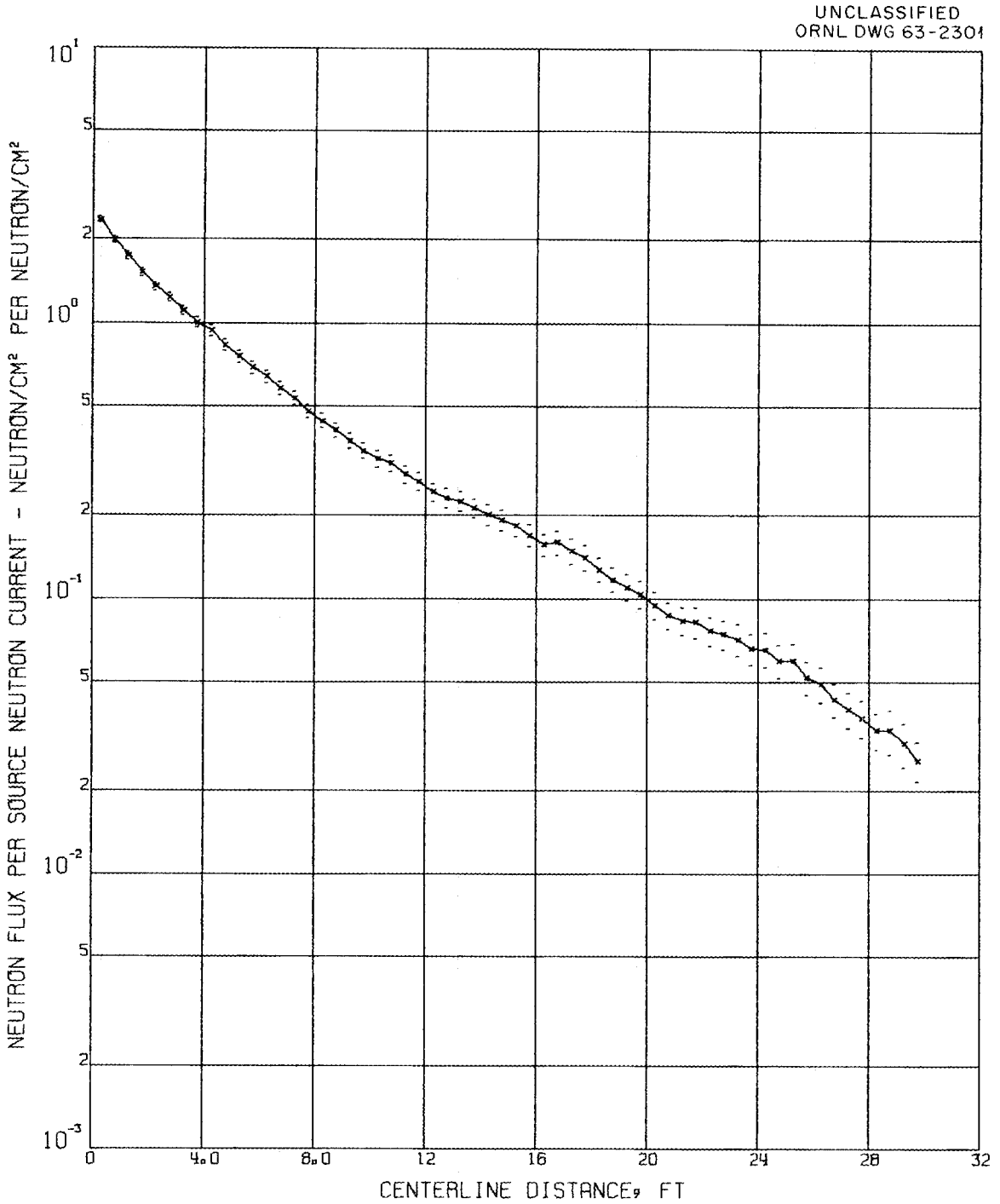

Fig. 24. Total Neutron Flux Calculated for 3 by 6 ft Rectangular Duct Using an Isotropic Albedo of 0.8 (4,000 Histories).

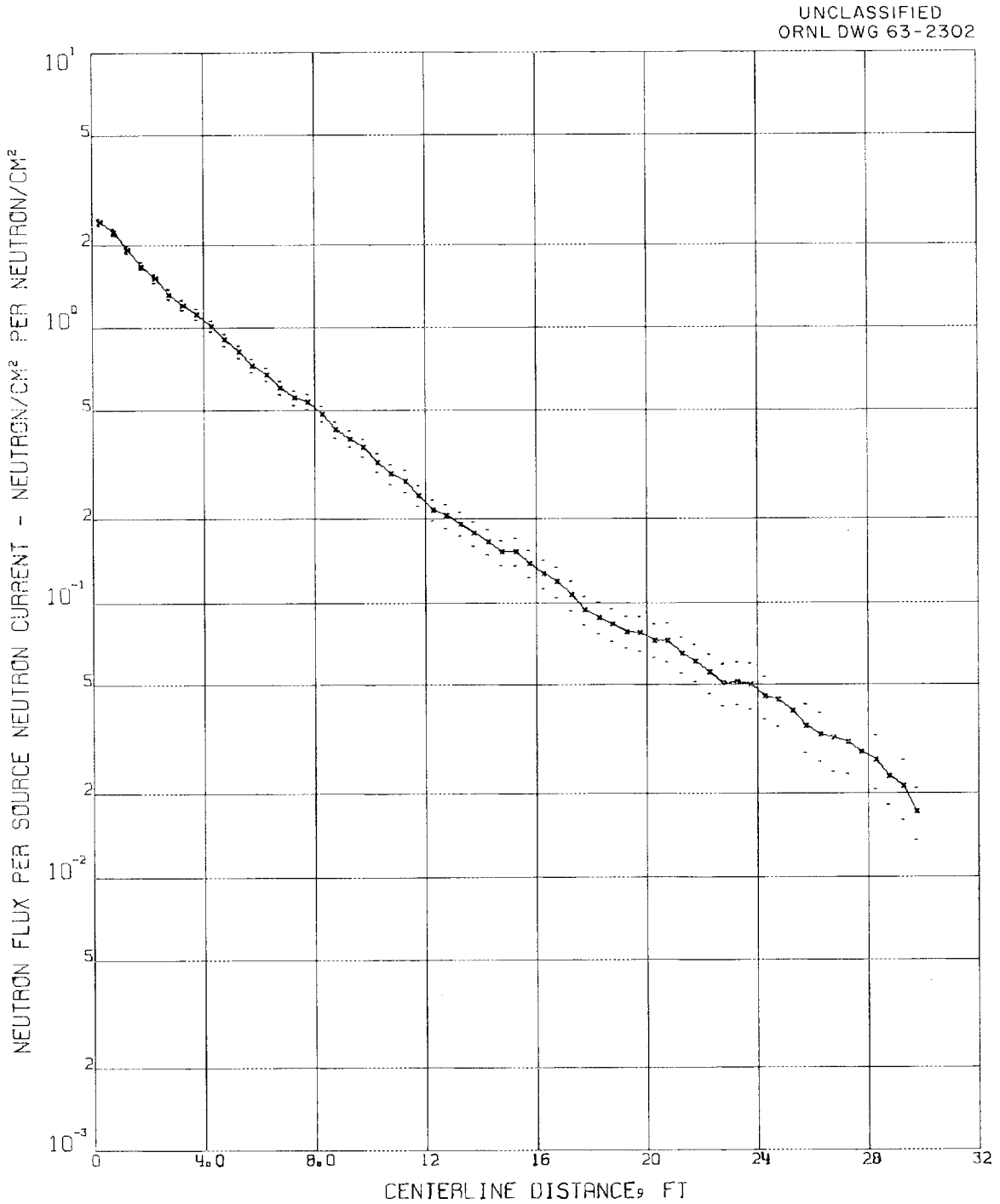

Fig. 25. Total Neutron Flux Calculated for 3 by 6 ft Rectangular Duct Using a Cosine Albedo of 0.8 (4,000 Histories).

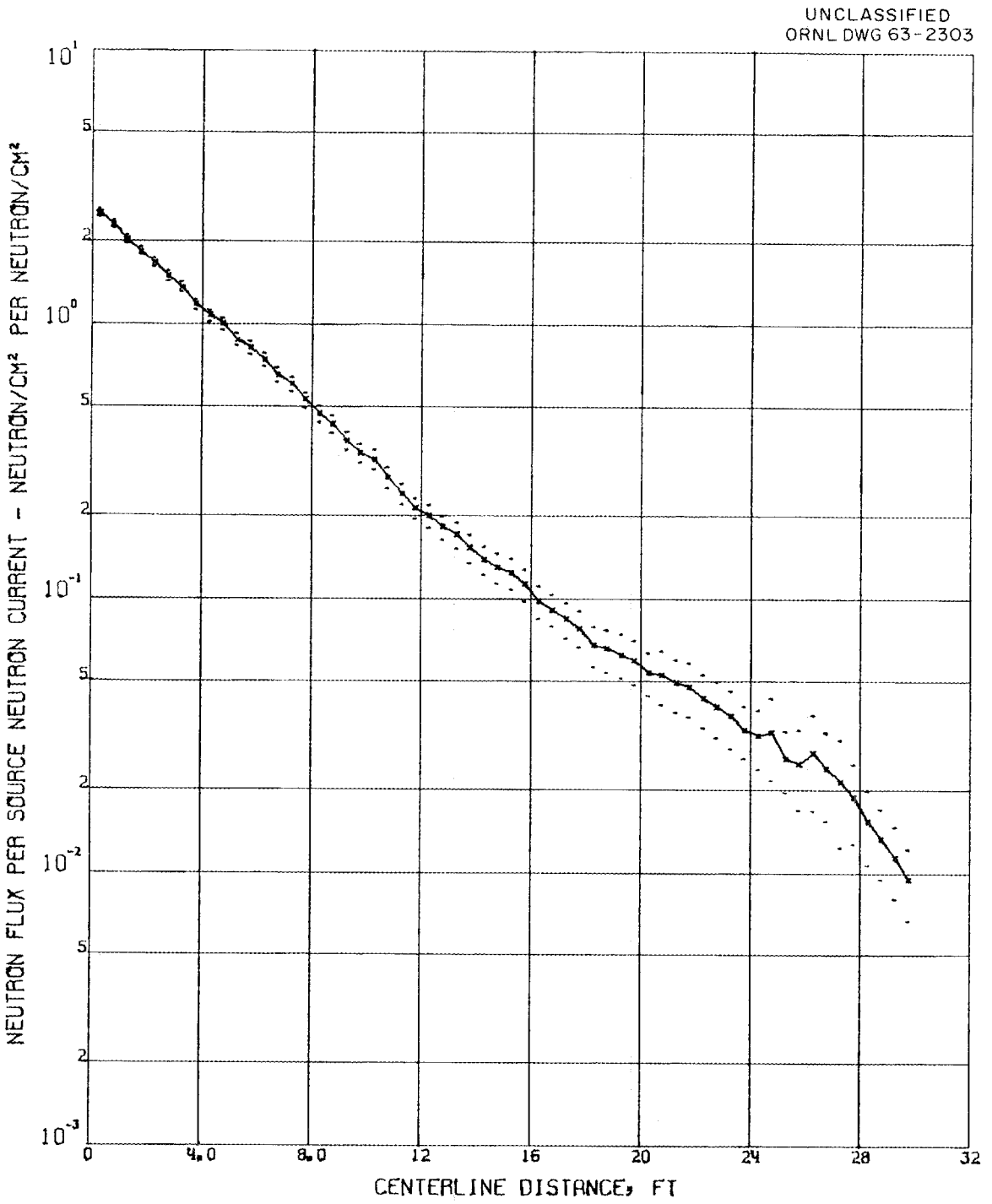

Fig. 26. Total Neutron Flux Calculated for 3 by 6 ft Rectangular Duct Using a Cosine^2 Albedo of 0.8 (4,000 Histories).

where

α = differential albedo (per unit cosine),

α' = total albedo,

A = fraction of albedo represented by an isotropic distribution,

B = fraction of albedo represented by a cosine distribution ($A + B = 1$),

θ = polar angle of emission, measured from the normal to the reflecting surface.

The albedo is an average over the incident neutron spectrum and therefore does not include an energy dependence. The Simon-Clifford equation using this albedo is:

$$\Phi = \Phi_0 \left(1 + A \frac{\alpha'}{1 - \alpha'} + \frac{4B\delta}{\ell} \frac{\alpha'}{1 - \alpha'} \right) , \qquad (2)$$

where

ℓ = distance along the center line of the duct,

Φ = neutron flux at ℓ,

Φ_0 = uncollided neutron flux at ℓ,

δ = radius at the duct,

and α', A, and B are as described above. The equation was actually derived for a plane isotropic source at the duct mouth, but when given in the form of Eq. 2, it applies as well to the cosine source used for the calculations of this paper.

Scattered fluxes obtained with Eq. 2 for a 1-ft-diam cylindrical duct and isotropic and cosine albedos of magnitude 0.12 are compared with scattered fluxes from the Monte Carlo calculations in Fig. 27, in which all the data are normalized to unit particle flux from the source plane. For an isotropic albedo the two calculations (upper curve and triangular points) agree, within the 2σ limits of the Monte Carlo calculation, from about 3 to 12 ft. Beyond 12 ft, the statistics of the Monte Carlo calculation are very poor and probably not meaningful. For a cosine albedo (lower curve and circular points), the agreement is within the 2σ limits beyond about 5 ft. Since the albedo is small, the unscattered flux accounts for most of the total flux (over 85% with the isotropic albedo and more than 85% with the cosine albedo), so that Eq. 2 may be expected to yield results that are correct to within about 5% beyond 2 ft (or two diameters from the source).

Figure 28 corresponds to Fig. 27 except that the albedo is 0.8. With this large albedo, the scattered flux is as much as 80 or 85% of the total, so that errors in calculating the scattered component are significant. It can be seen that Eq. 2 does describe the actual behavior well at large distances, but it does not lie within the 2σ limits of the Monte Carlo calculation except for distances beyond 10 ft. Even at 10 ft, the Monte Carlo calculations indicate that errors on the order of 15% (isotropic albedo) to 50% (cosine albedo) might be expected in the total flux calculation by Eq. 2.

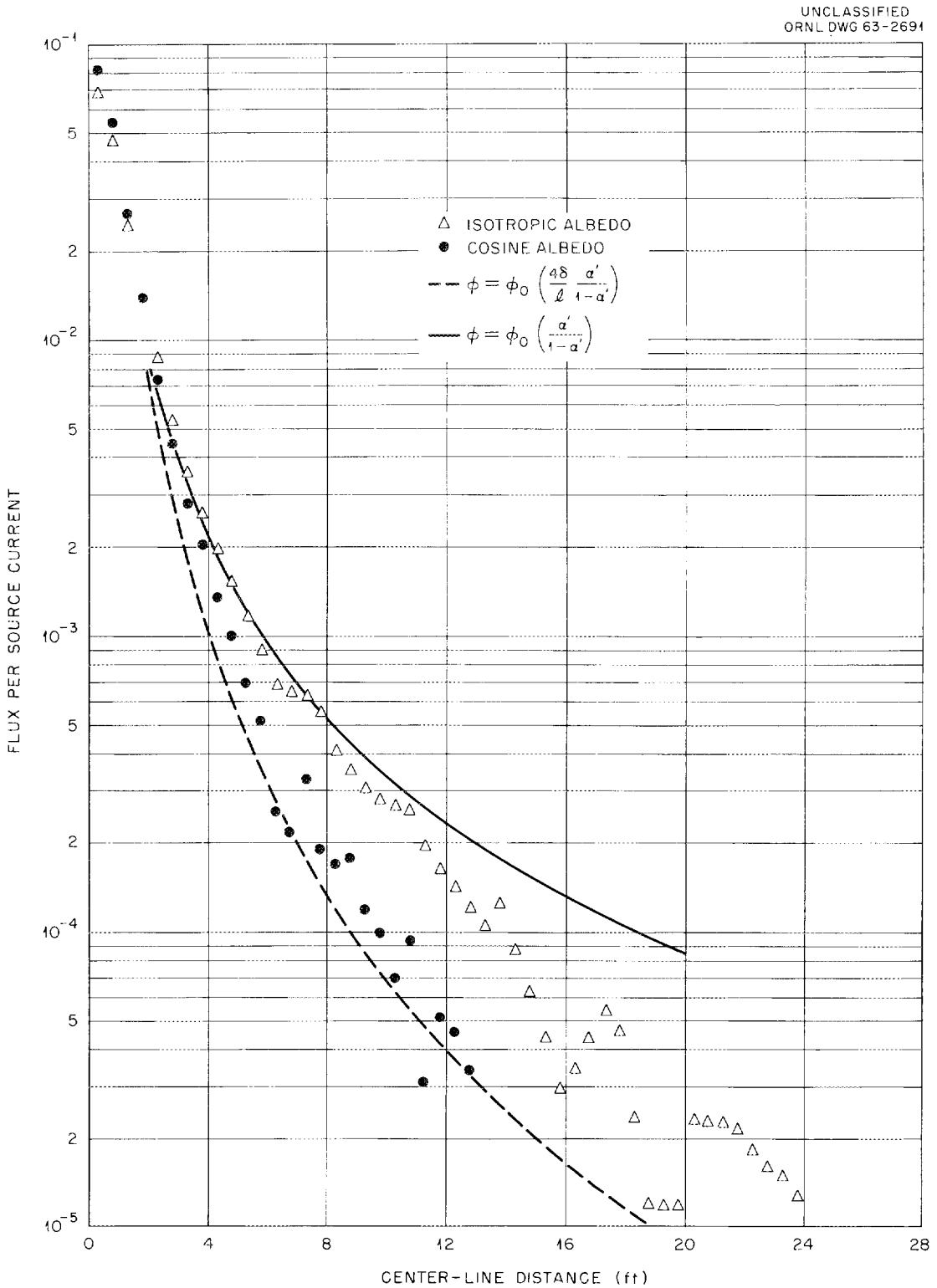

Fig. 27. Scattered Neutron Flux in a 1-ft-diam Cylindrical Duct: Comparison of Calculations Using Isotropic and Cosine Albedos of 0.12 with an Analytic Approximation.

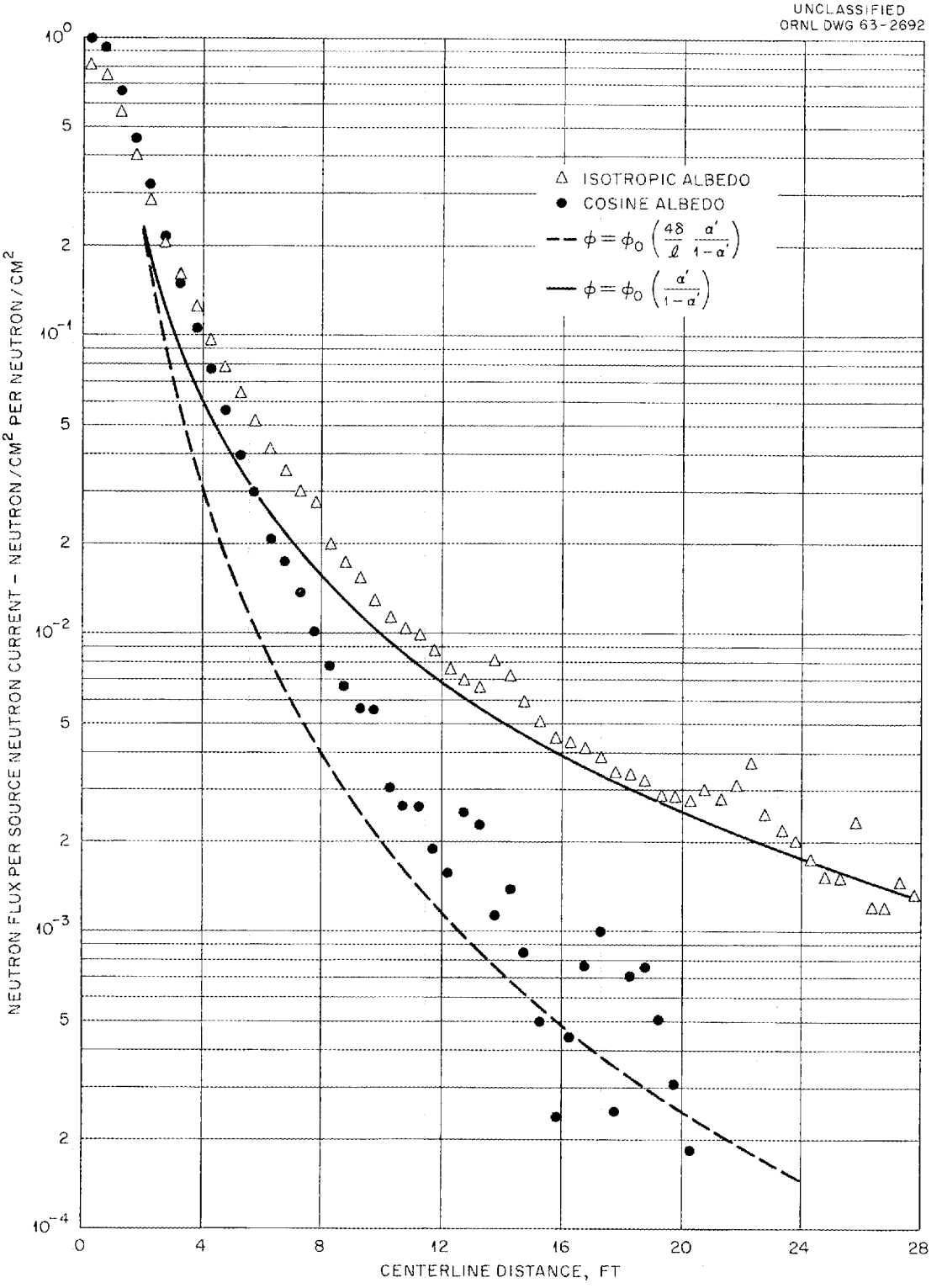

Fig. 28. Scattered Neutron Flux in a 1-ft-diam Cylindrical Duct: Comparison of Calculations Using Isotropic and Cosine Albedos of 0.8 With an Analytic Approximation.

Figures 29 and 30 show results of total flux calculations with an isotropic albedo of value 0.8 in four different geometries. Shown in Fig. 29 are the Monte Carlo calculations for a 3 by 0.5-ft rectangular duct and for a 1.38198-ft-diam cylindrical duct. Also shown are the uncollided flux and the results of Eq. 2 for the cylindrical duct. The uncollided flux is not shown for the rectangular duct, but it is not too different from that for the cylindrical duct, especially at large distances, since the two ducts are of equal cross-sectional area. (See Appendix E for proof of this.) The ratio of the unscattered fluxes for the cylindrical duct to those for the rectangular duct is approximately 16, 4.5, 2, and 1.2% for distances of 2, 4, 6, and 8 ft, respectively. The prediction of Eq. 2 agrees within 2σ with the rectangular duct results for distances greater than 8 ft and with the cylindrical duct results for distances greater than 12 ft. Equation 2 gives an underestimate of the cylindrical duct results between about 2 and 10 diameters from the source in almost every case. As will be seen, the rectangular duct results are consistently lower than the cylindrical duct results and thereby are in better agreement with Eq. 2.

Figure 30 presents similar results for two larger ducts, a 3 by 1 ft rectangular duct and a 1.95441-ft-diam cylindrical duct. Qualitatively the comments about Fig. 29 apply to these data as well. It may be noted from both Fig. 29 and Fig. 30 that there is an indication that the rectangular duct results are approaching a lower asymptotic value for the isotropic albedo than Eq. 2 predicts.

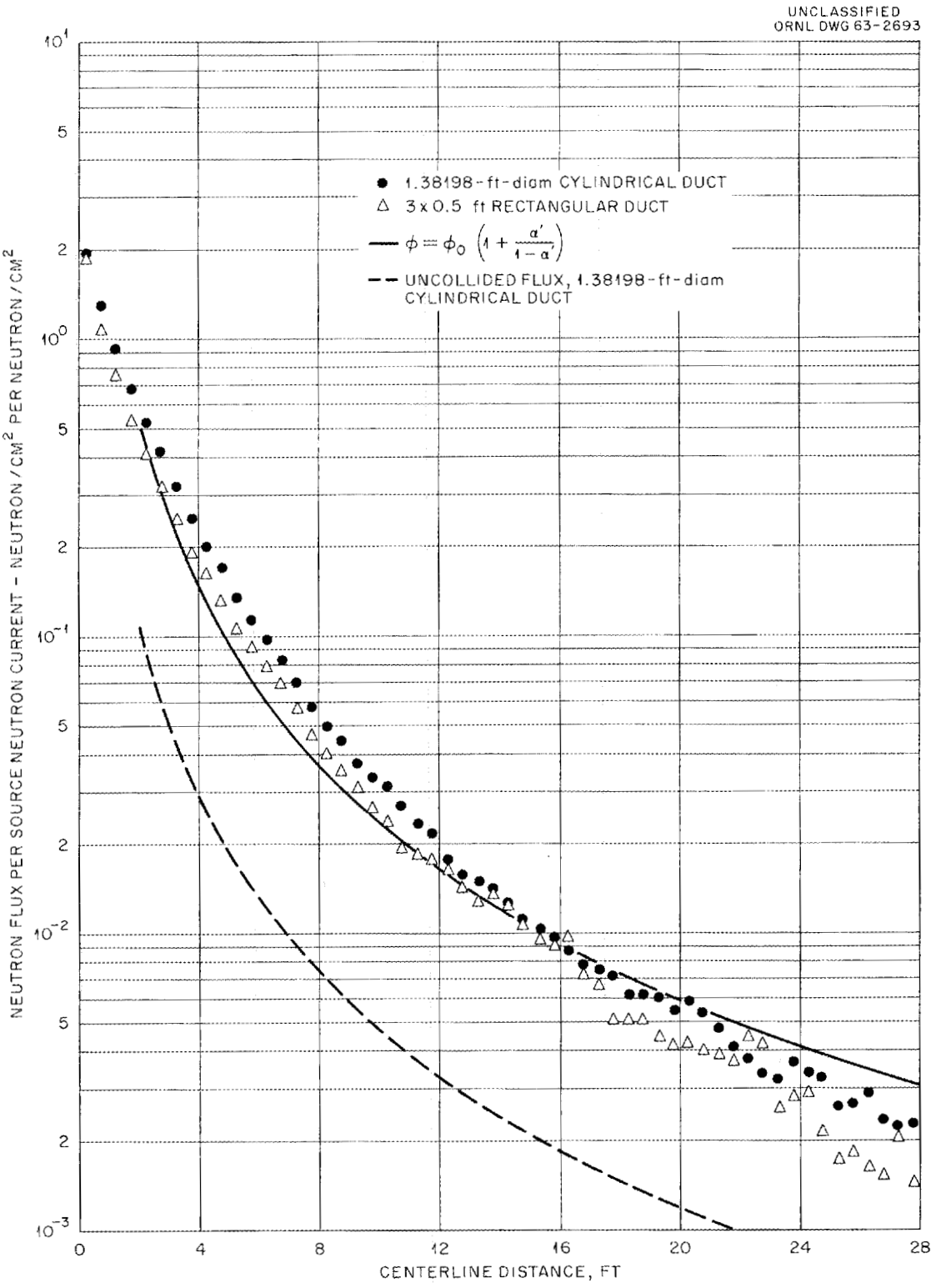

Fig. 29. Total Neutron Flux Using an Isotropic Albedo of 0.8: Comparison of Calculations for a 1.38198-ft-diam Cylindrical Duct, a 3 by 0.5 ft Rectangular Duct, and an Analytic Approximation.

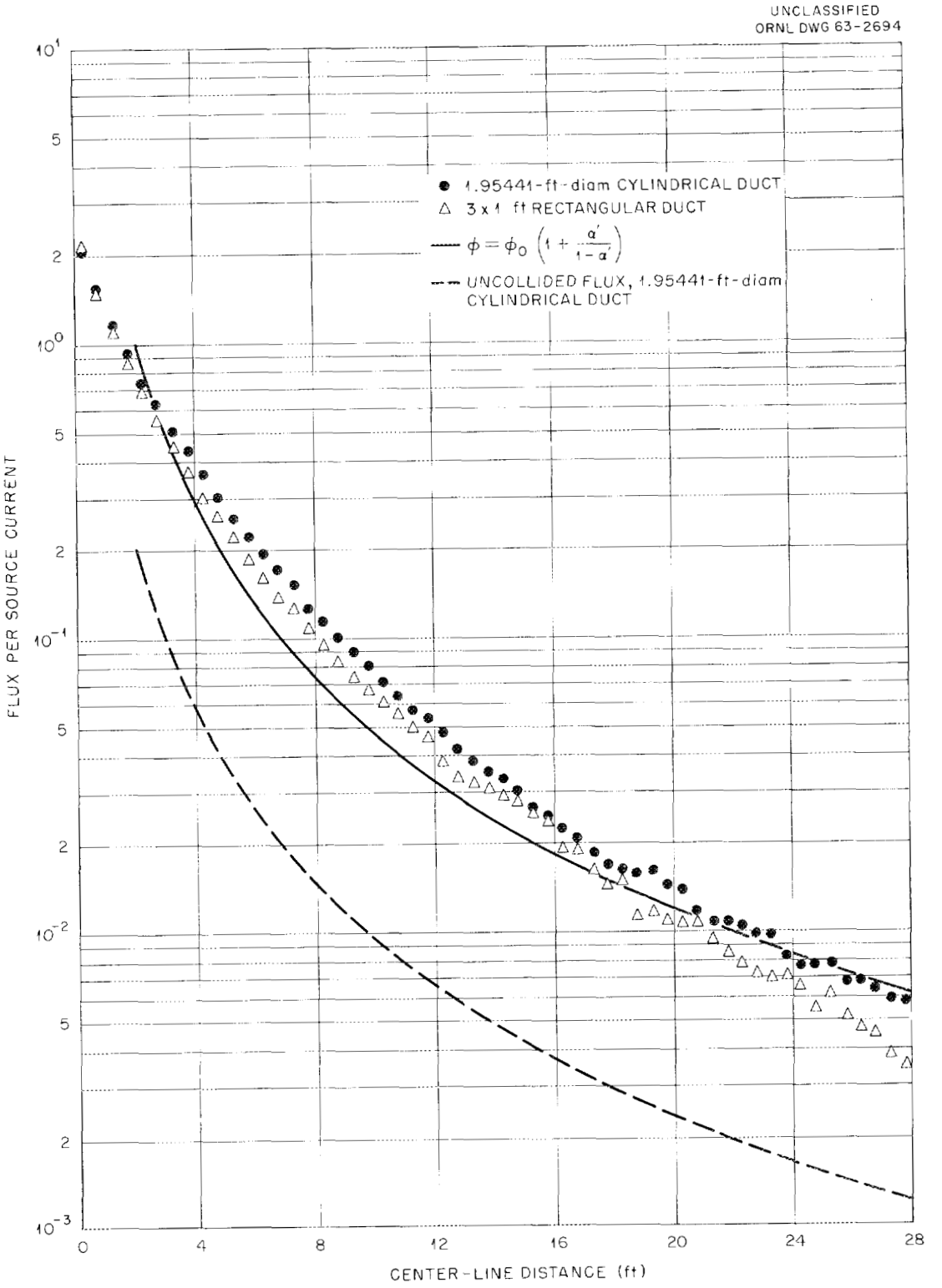

Fig. 30. Total Neutron Flux Using an Isotropic Albedo of 0.8: Comparison of Calculations for a 1.95441-ft-diam Cylindrical Duct, a 3 by 1-ft Rectangular Duct, and an Analytic Approximation.

Figures 31 and 32 are comparable to Figs. 29 and 30 except that a cosine albedo distribution is used. Agreement with Eq. 2 is somewhat better, but this is partially because the scattered flux is not as large a fraction of the total flux as it is with the isotropic albedo.

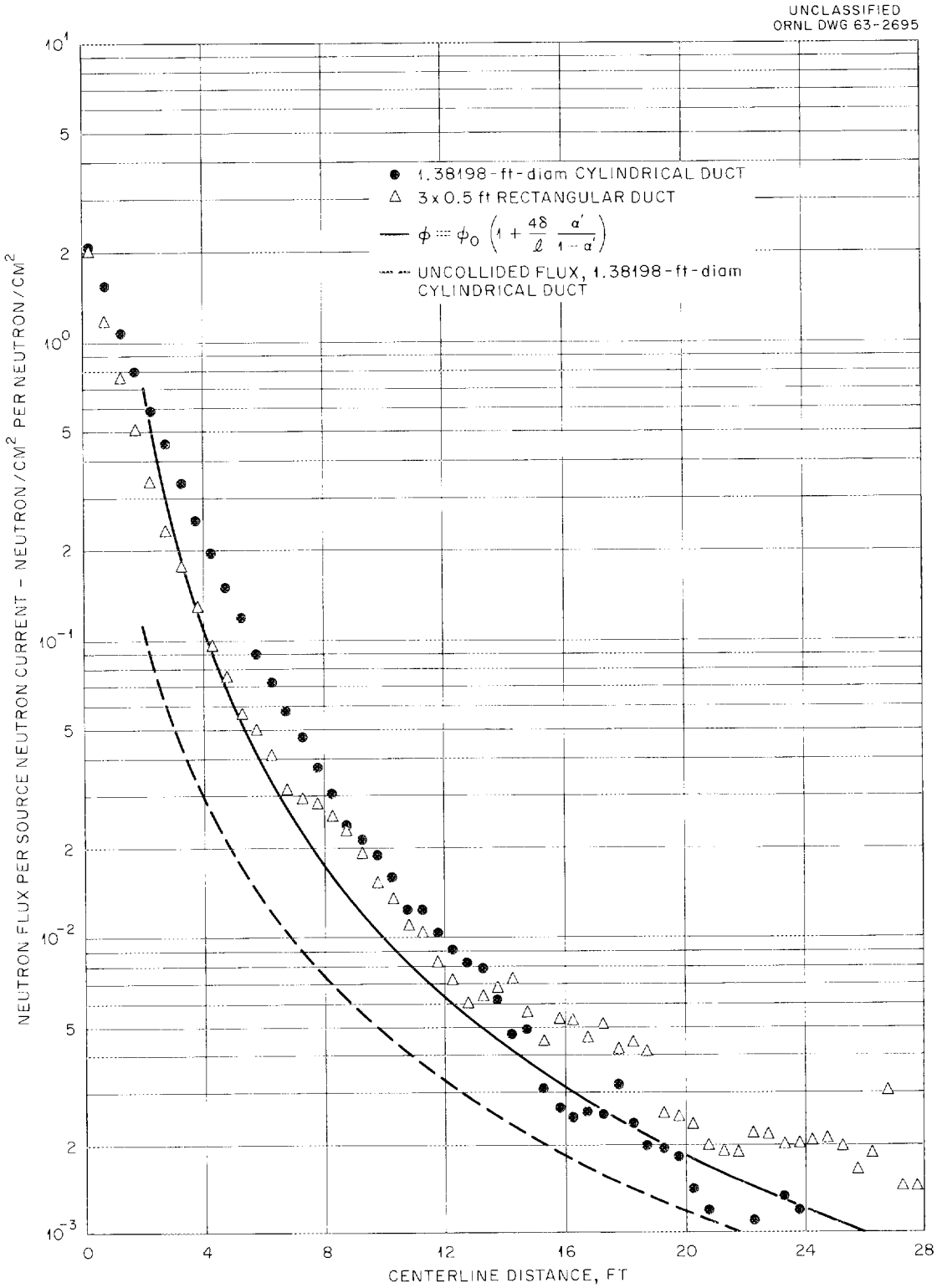

Fig. 31. Total Neutron Flux Using a Cosine Albedo of 0.8: Comparison of Calculations for a 1.38198-ft-diam Cylindrical Duct, a 3 by 0.5 ft Rectangular Duct, and an Analytic Approximation.

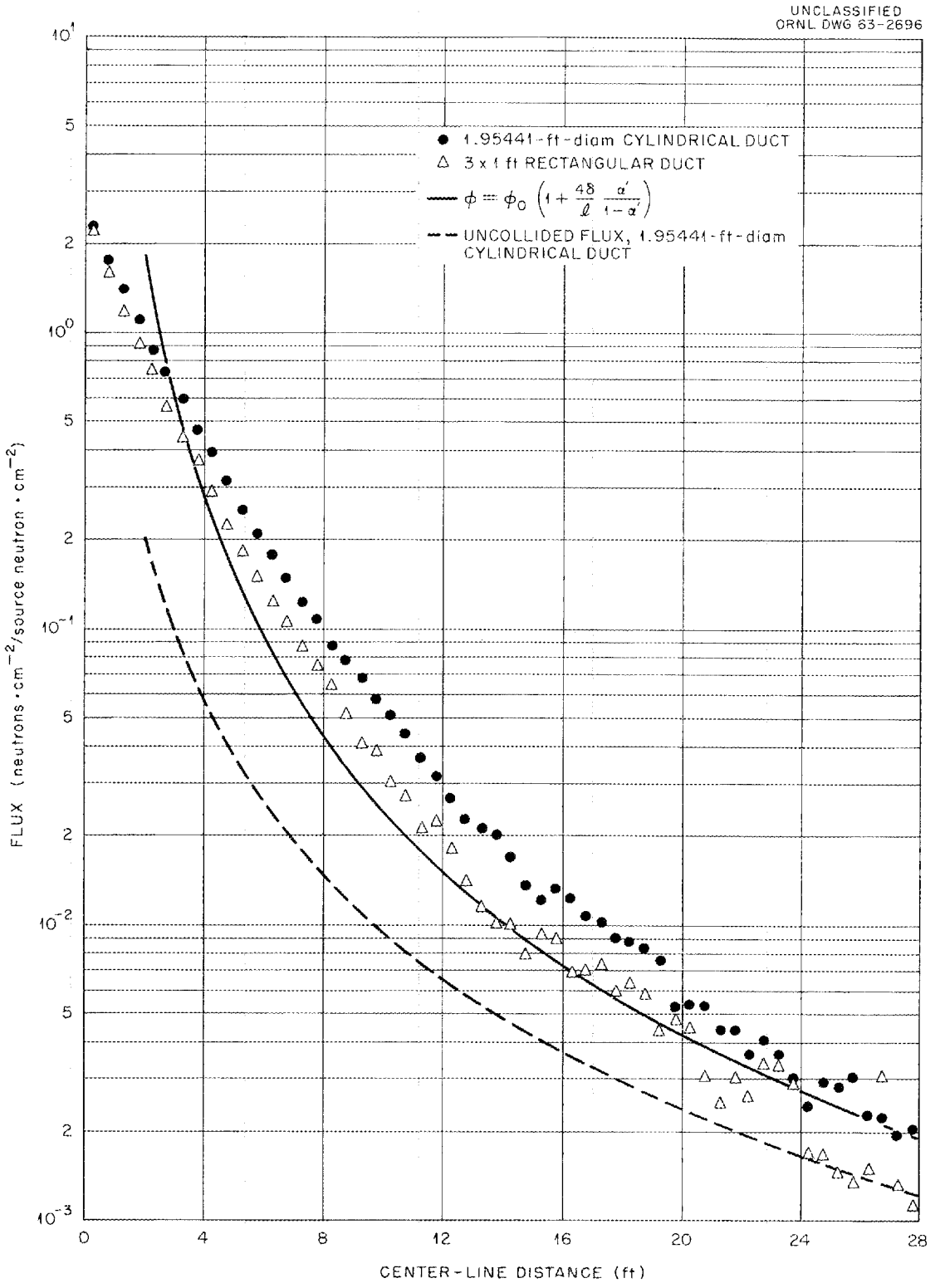

Fig. 32. Total Neutron Flux Using a Cosine Albedo of 0.8: Comparison of Calculations for a 1.95441-ft-diam Cylindrical Duct, a 3 by 1-ft Rectangular Duct, and an Analytic Approximation.

CHAPTER IV

DUCTS WITH BENDS

Calculations

Most of the calculated results presented in this section were obtained for the three-legged 54-slab detector configuration described in Appendix C. Duct heights of 1, 6, and 8 ft were used with the cross section shown in Fig. 33 (detectors 1 through 54 only). Two other configurations, resembling a room containing a source on one wall and having a two-legged duct extending from an adjacent wall, were also used by adding detectors 55 through 63 as shown in Fig. 33. The source is distributed uniformly on the plane at $x = 0$ from $z = 0$ to H (the duct height) and either from $y = 0$ to 3 ft in the case of the three-legged duct or from $y = 0$ to 7.5 ft in the case of the configuration consisting of a room and two legs.

All data are plotted as particle flux due to a unit particle current source versus the distance along the center line of the duct. Referring to Fig. 33, it may be noted that detectors 13, 14, and 15 and detectors 34, 35, and 36 are not located on the center line. The data from the detectors are plotted in numerical order; so the points at 6.25, 6.75, 7.25, 16.75, 17.25, and 17.75 ft are not actually flux along the duct center line. As before, the error bars above and

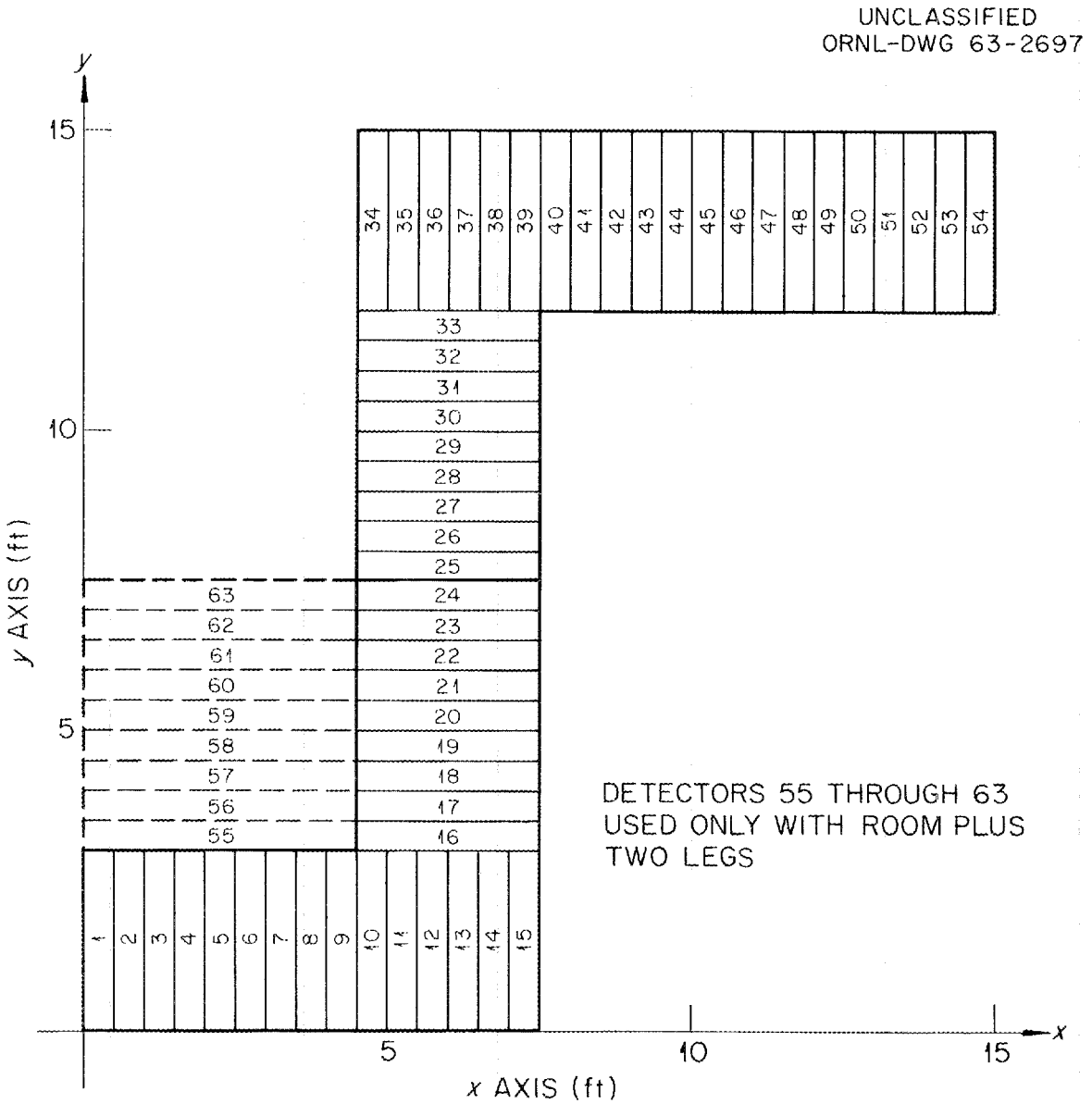

Fig. 33. Cross Section of x-y Plane Showing Detector Locations and Numbers for Three-Legged Duct Geometry and Room Plus Two-Legged Duct Geometry.

below the plotted points represent 2σ or 2 standard deviations.

Figures 34 through 36 present the results for the three-legged duct geometry with a 3 by 1 ft cross section (duct height = 1 ft). Figure 34 is for cosine albedo of magnitude 0.24, while Figs. 35 and 36 are for isotropic and cosine albedos, respectively, both of magnitude 0.8.

Figures 37 through 43 give the calculated fluxes for the same three-legged duct geometry but for a duct height of 6 ft (3 by 6 ft cross section). A cosine distribution of the albedo was used in each case, Figs. 37, 38, 39, 40, and 41 using albedo values of 0.12, 0.24, 0.7, 0.8, and 0.9, respectively.

Figures 42 and 43, both for a cosine albedo of 0.8, compare the results of two different calculational techniques. The data shown in Fig. 42 are from a calculation using the slab detectors defined in Fig. 33, while the data given in Fig. 43 are from a calculation using the second geometry described in Appendix C and statistical estimation of the flux. Exactly the same histories are used in both calculations. This pair of calculations demonstrates quite well that statistical estimation is not always desirable.[1] In this case, the machine time required for the statistical estimation calculation was longer by a factor of 12 (approximately 1 hr compared with 5 min). The calculation does reduce the variance for a given number of histories and would be preferable in most cases where the flux at only one or two points is required.

---

[1]M. H. Kalos, "On the Estimation of Flux at a Point by Monte Carlo." Nuclear Science and Engineering 16, 111 (1963).

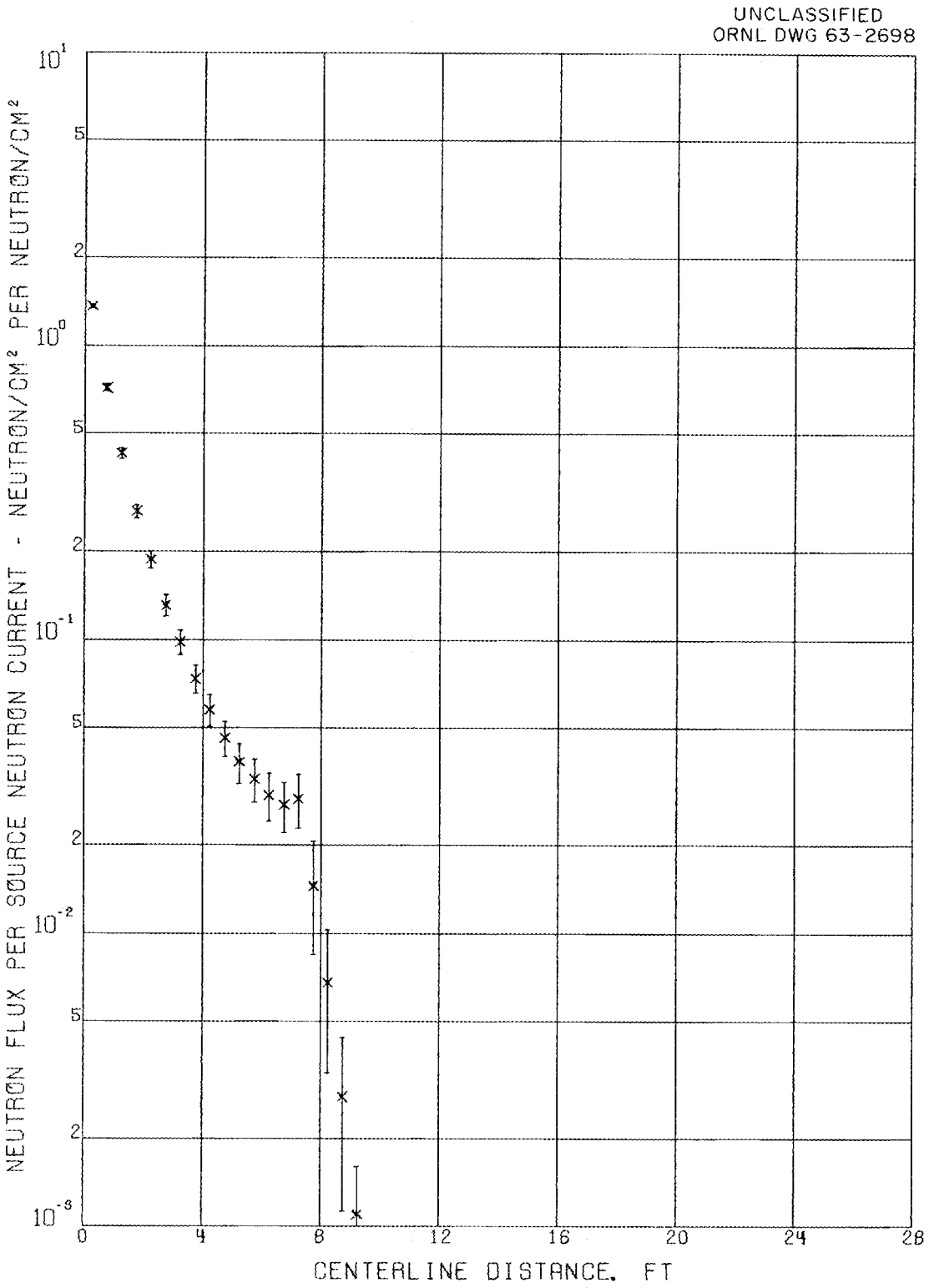

Fig. 34. Total Neutron Flux Calculated for Three-Legged 3 by 1 ft Rectangular Duct Using a Cosine Albedo of 0.24 (4,000 Histories).

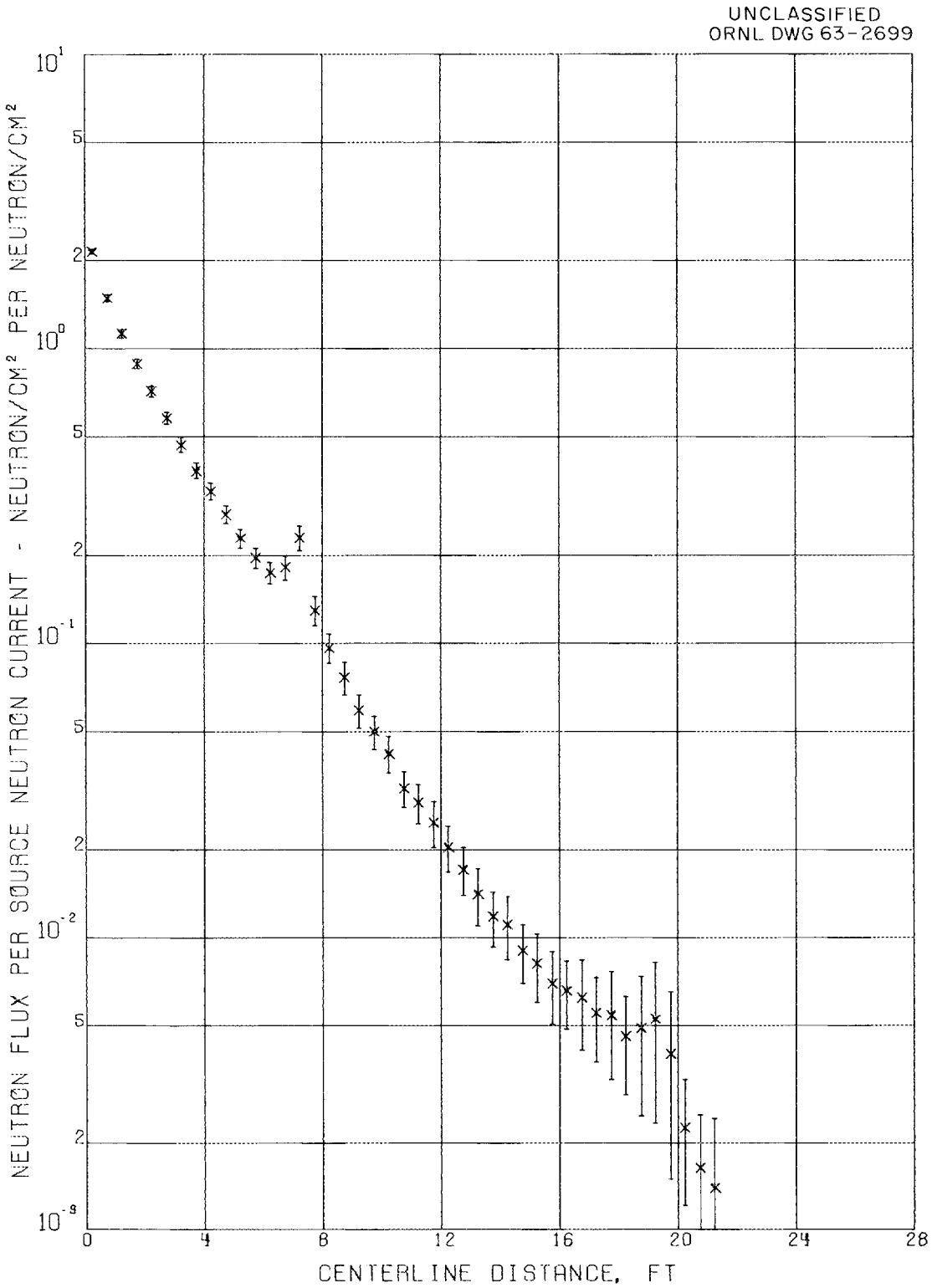

Fig. 35. Total Neutron Flux Calculated for Three-Legged 3 by 1 ft Rectangular Duct Using an Isotropic Albedo of 0.8 (4,000 Histories).

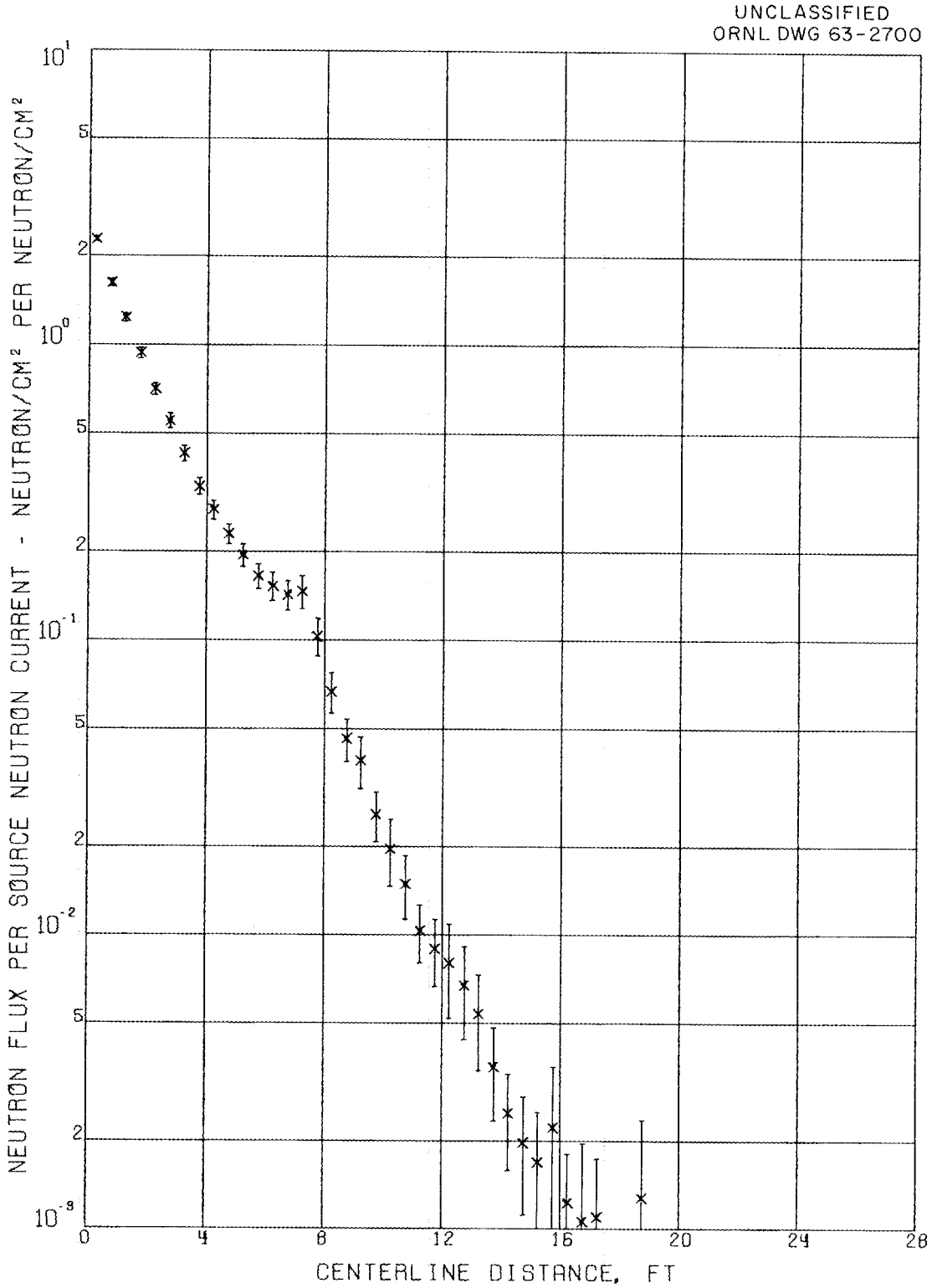

Fig. 36. Total Neutron Flux Calculated for Three-Legged 3 by 1 ft Rectangular Duct Using a Cosine Albedo of 0.80 (4,000 Histories).

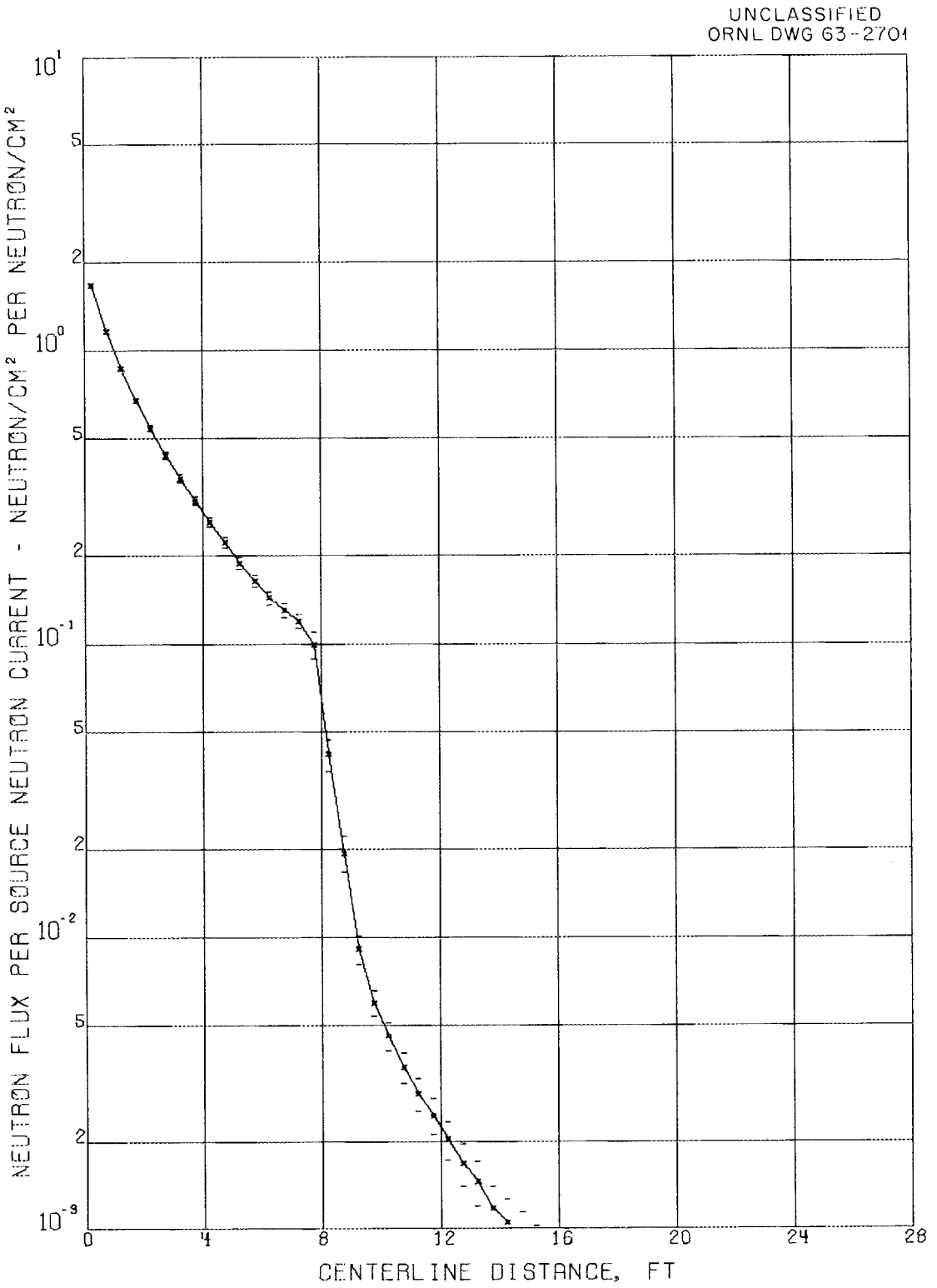

Fig. 37. Total Neutron Flux Calculated for Three-Legged 3 by 6 ft Rectangular Duct Using a Cosine Albedo of 0.12 (10,000 Histories).

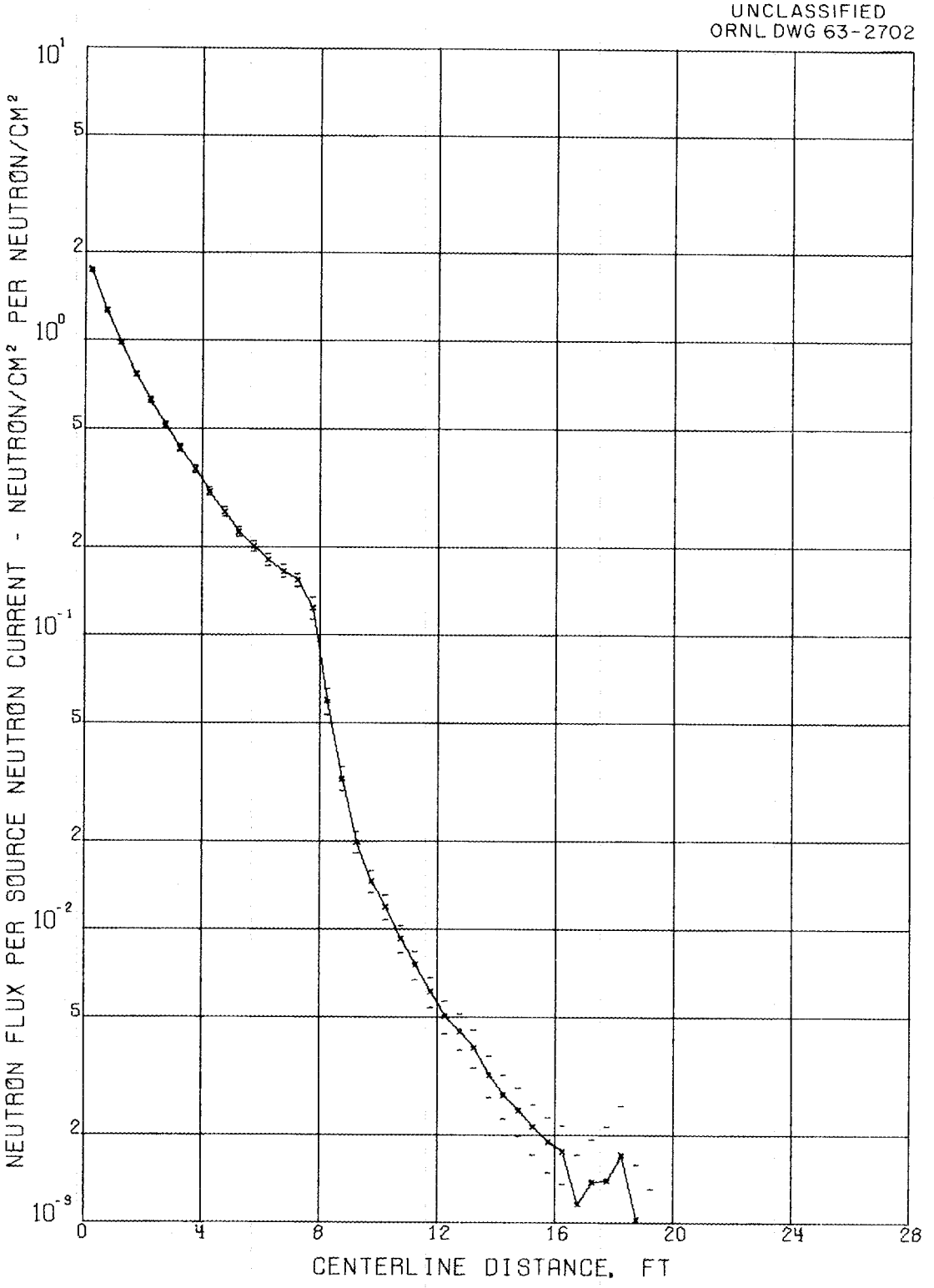

Fig. 38. Total Neutron Flux Calculated for Three-Legged 3 by 6 ft Rectangular Duct Using a Cosine Albedo of 0.24 (10,000 Histories).

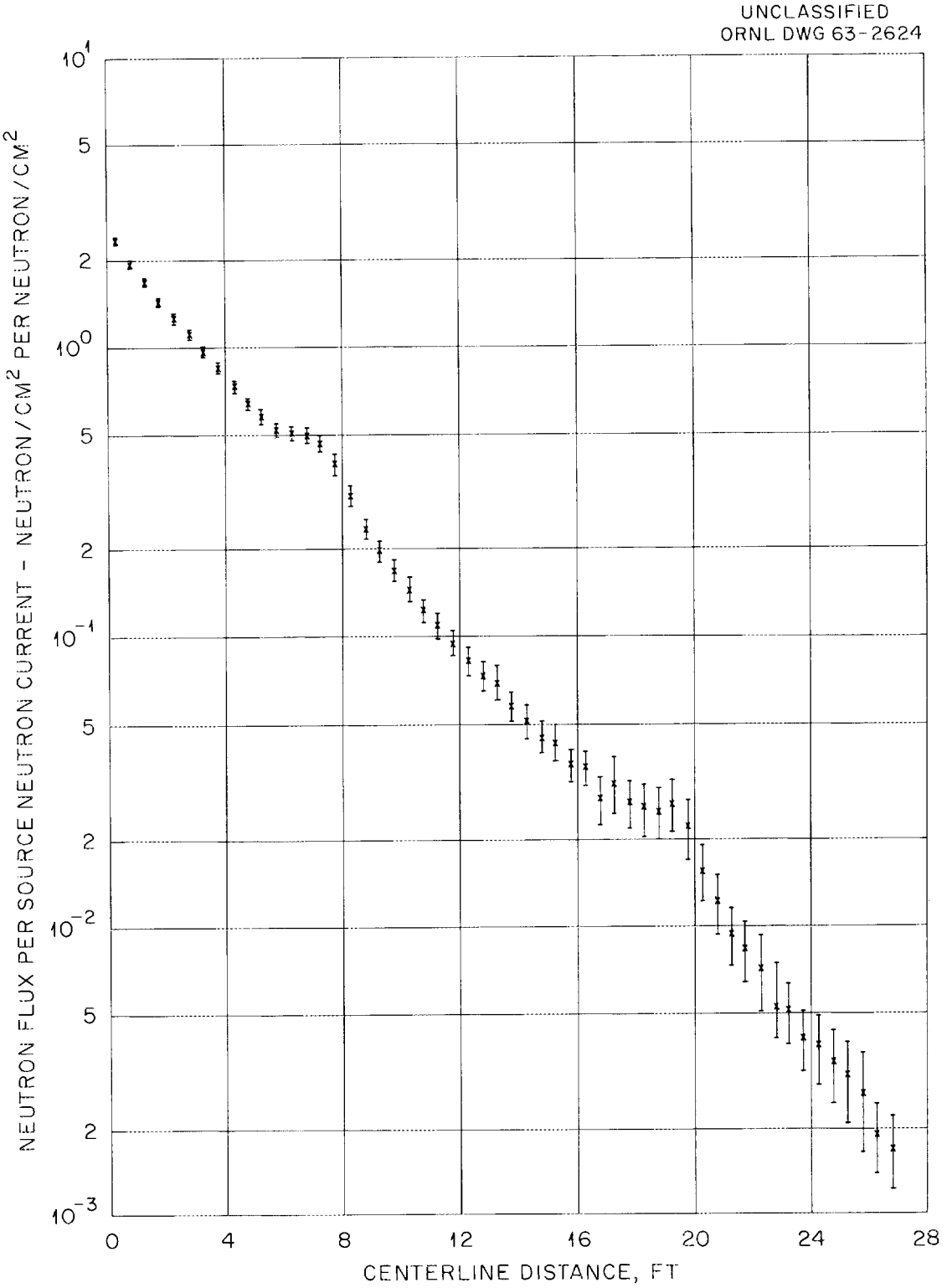

Fig. 39. Total Neutron Flux Calculated for Three-Legged 3 by 6 ft Rectangular Duct Using a Cosine Albedo of 0.7 (4,000 Histories).

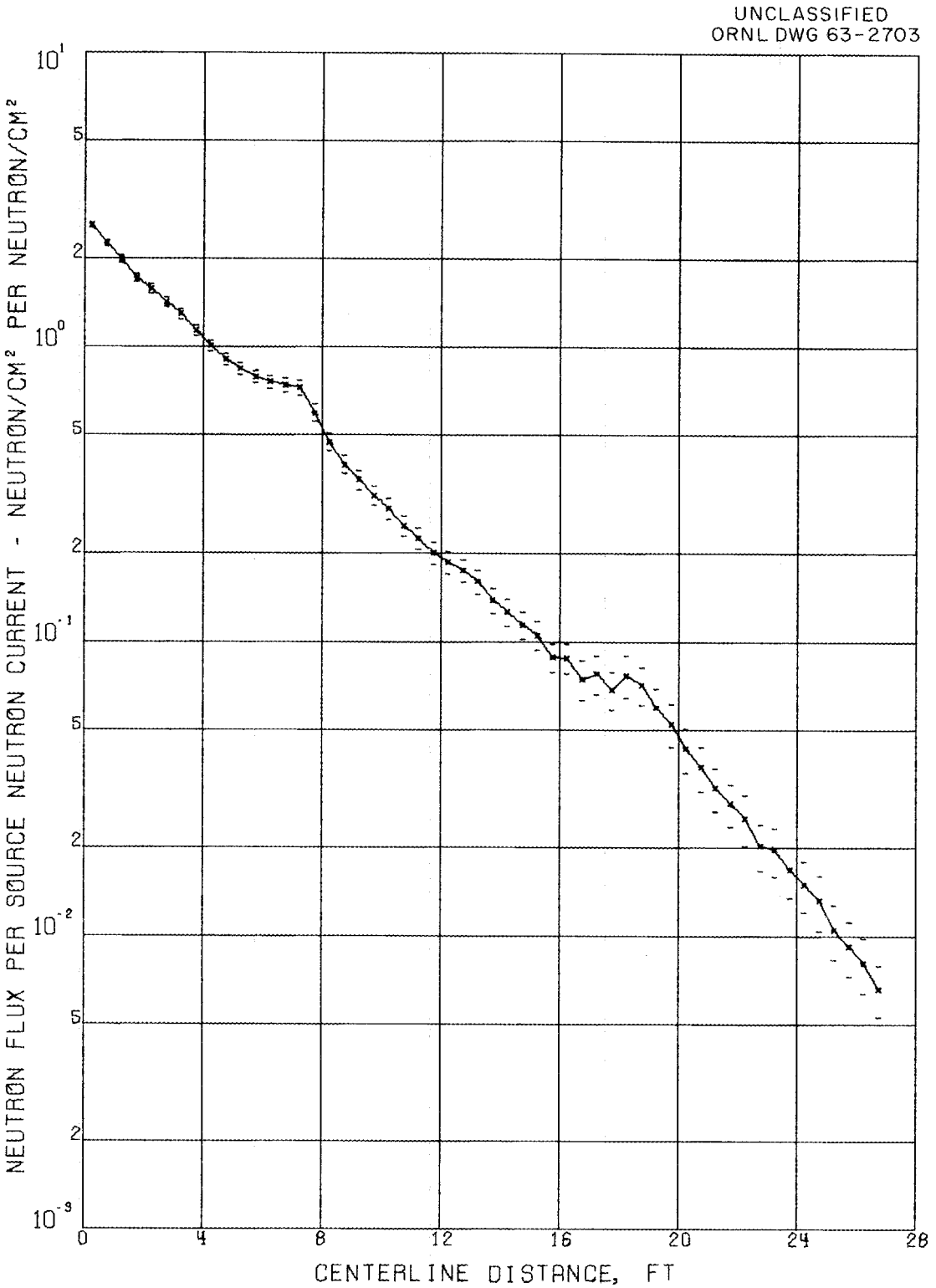

Fig. 40. Total Neutron Flux Calculated for Three-Legged 3 by 6 ft Rectangular Duct Using a Cosine Albedo of 0.8 (4,000 Histories).

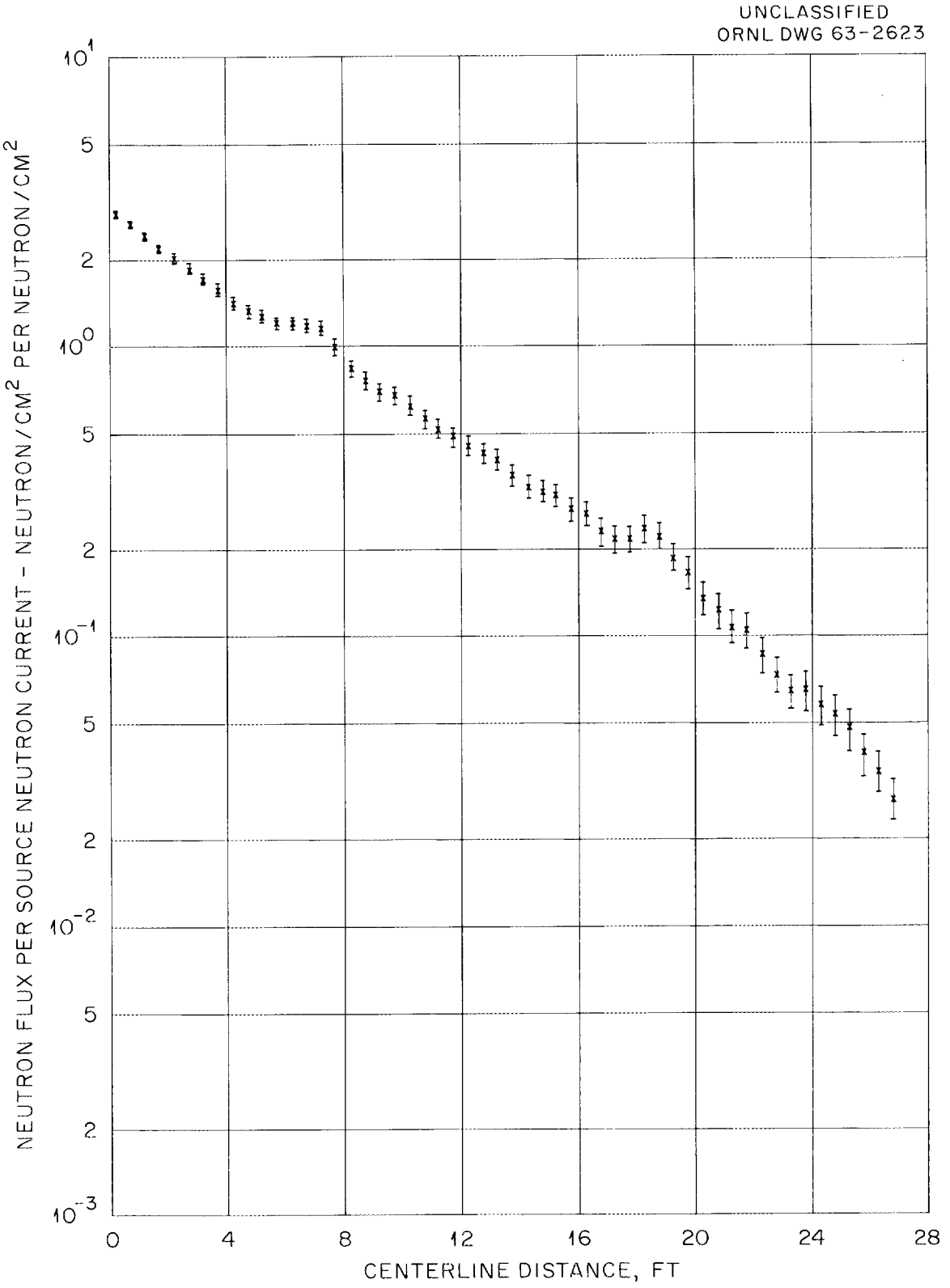

Fig. 41. Total Neutron Flux Calculated for Three-Legged 3 by 6 ft Rectangular Duct Using a Cosine Albedo of 0.9 (4,000 Histories).

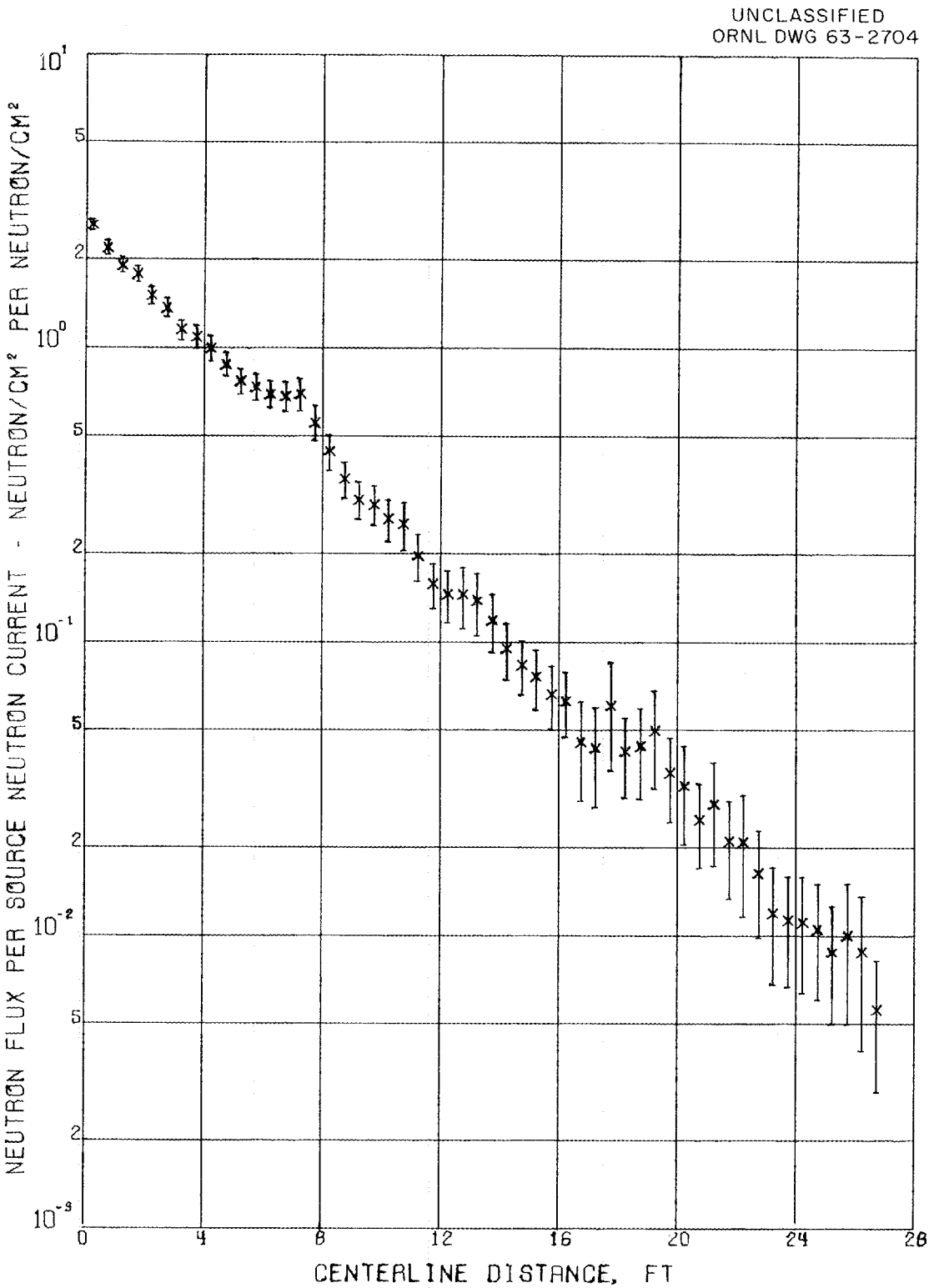

Fig. 42. Total Neutron Flux Calculated for Three-Legged 3 by 6 ft Rectangular Duct Using a Cosine Albedo of 0.8 (1,000 Histories).

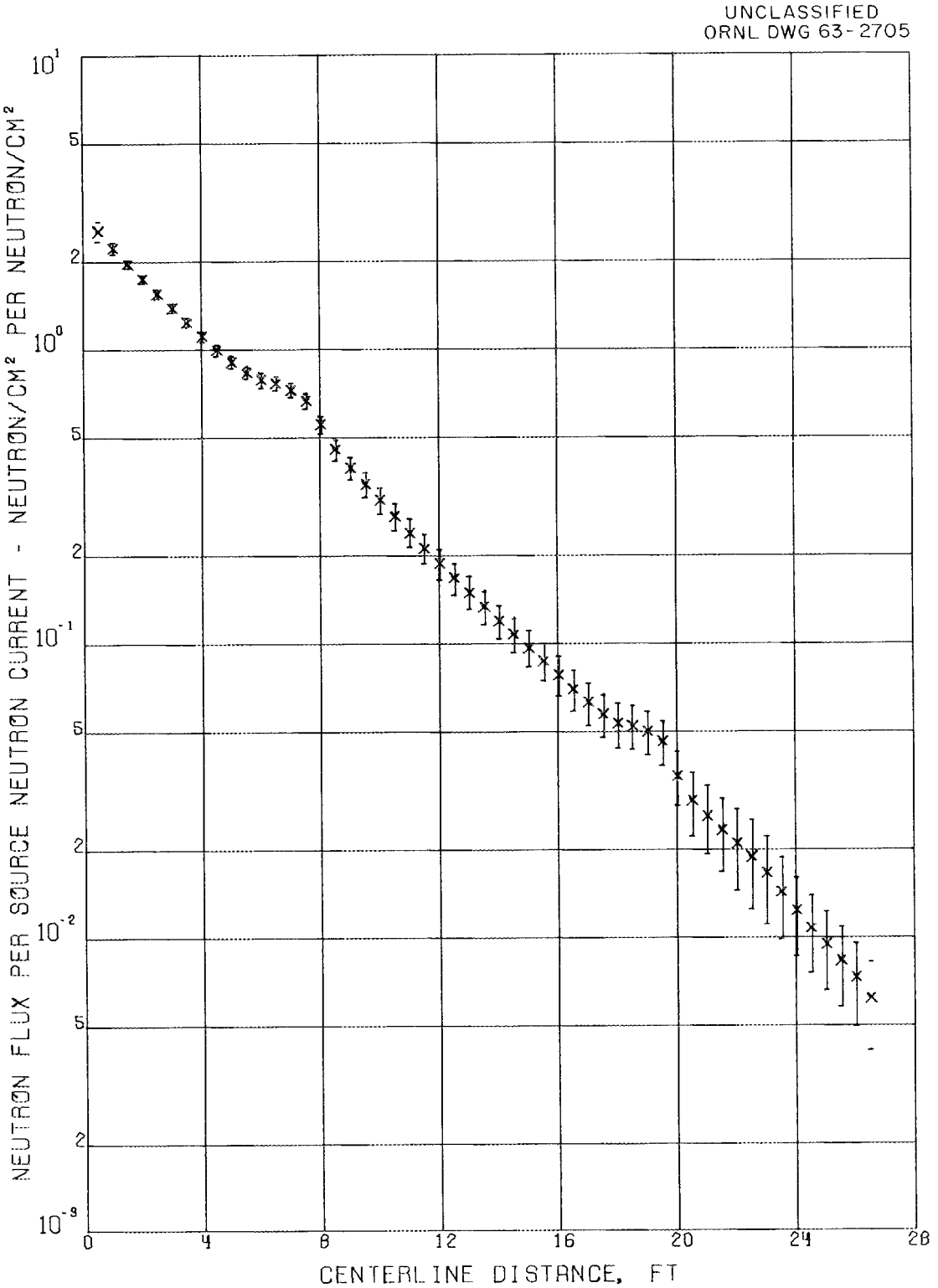

Fig. 43. Total Neutron Flux Calculated for Three-Legged 3 by 6 ft Rectangular Duct Using a Cosine Albedo of 0.8 (1,000 Histories). Calculation based on statistical estimation.

It should also be noted that the statistical estimation technique results in a much smoother curve. This is because the detector estimates are not statistically independent; estimates are made to each detector from every scatter point. An advantage of the statistical estimation calculation is that the answers are direct estimates of the flux as a function of distance down the duct center line. As mentioned previously, the particle flux obtained with the slab detectors is one which is an average over the volume of the detector, and, because of the way the geometry is set up, six of the detectors are not located on the duct center line. Comparison of the two figures indicates that the center-line flux is not much larger than the average flux; the 2σ limits of the two calculations overlap.

Figures 44 and 45 give the results of calculations using the same three-legged geometry, but for an 8-ft-high duct. An albedo of 0.8 was used in both cases, Fig. 44 being for an isotropic distribution and Fig. 45 for a cosine distribution.

Figures 46 and 47 present data from calculations using the nine additional detectors (55-63) shown in Fig. 33. By adding these detectors a 7.5 by 7.5 ft room is formed with two legs of a duct leading from the room. The calculations used a cosine albedo of 0.8 and duct heights of 6 and 8 ft for Figs. 46 and 47, respectively. The data for detectors 55 through 63 are plotted at the same center-line positions as detectors 16 through 24, respectively.

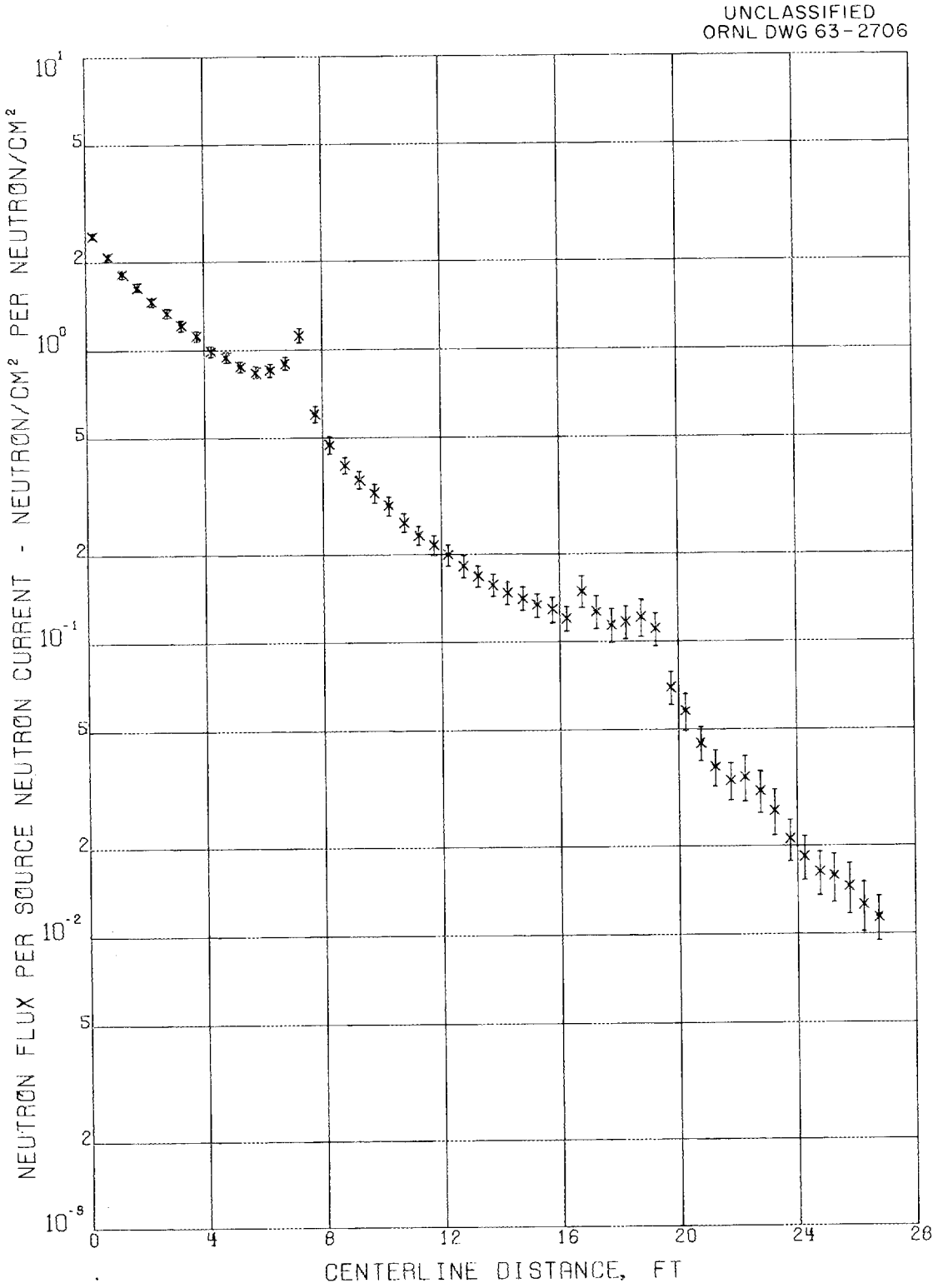

Fig. 44. Total Neutron Flux Calculated for Three-Legged 3 by 8 ft Rectangular Duct Using an Isotropic Albedo of 0.8 (4,000 Histories).

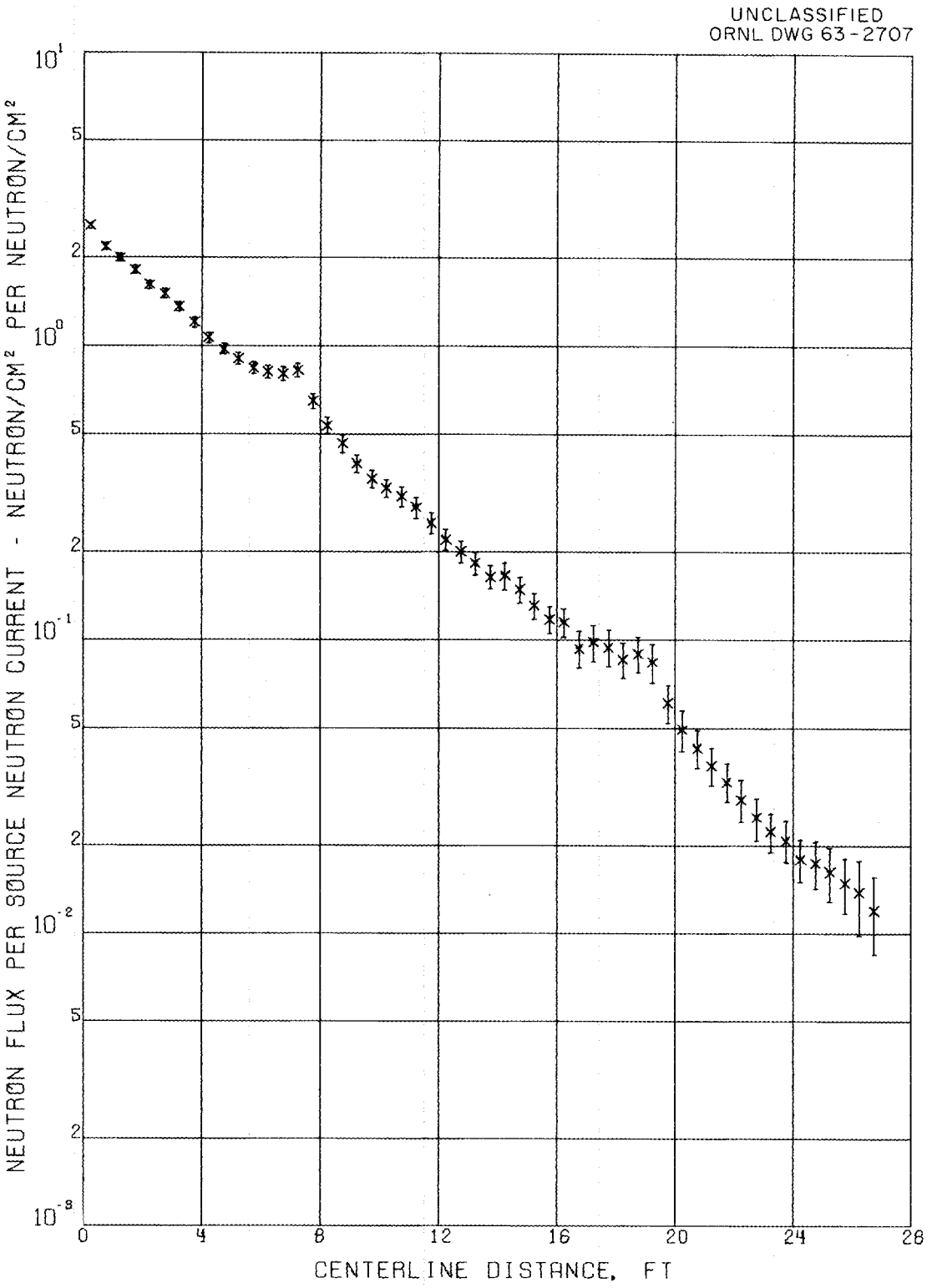

Fig. 45. Total Neutron Flux Calculated for Three-Legged 3 by 8 ft Rectangular Duct Using a Cosine Albedo of 0.8 (4,000 Histories).

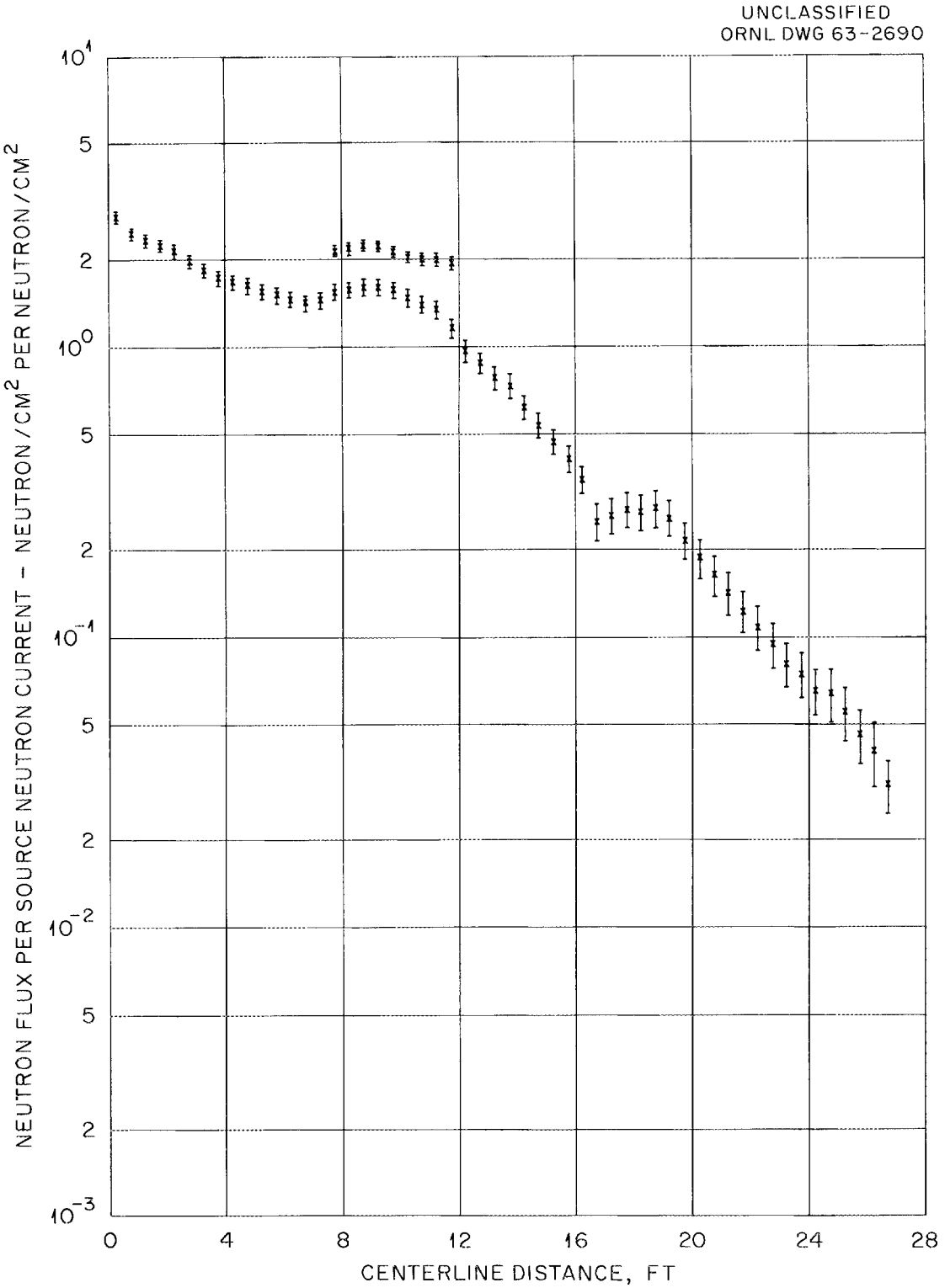

Fig. 46. Total Neutron Flux Calculated for Room (6 by 7.5 by 7.5 ft) and Two-Legged Duct (3 by 6 ft) Configuration (Shown in Fig. 33) Using a Cosine Albedo of 0.80 (4,000 Histories). See text for explanation of geometrical configuration.

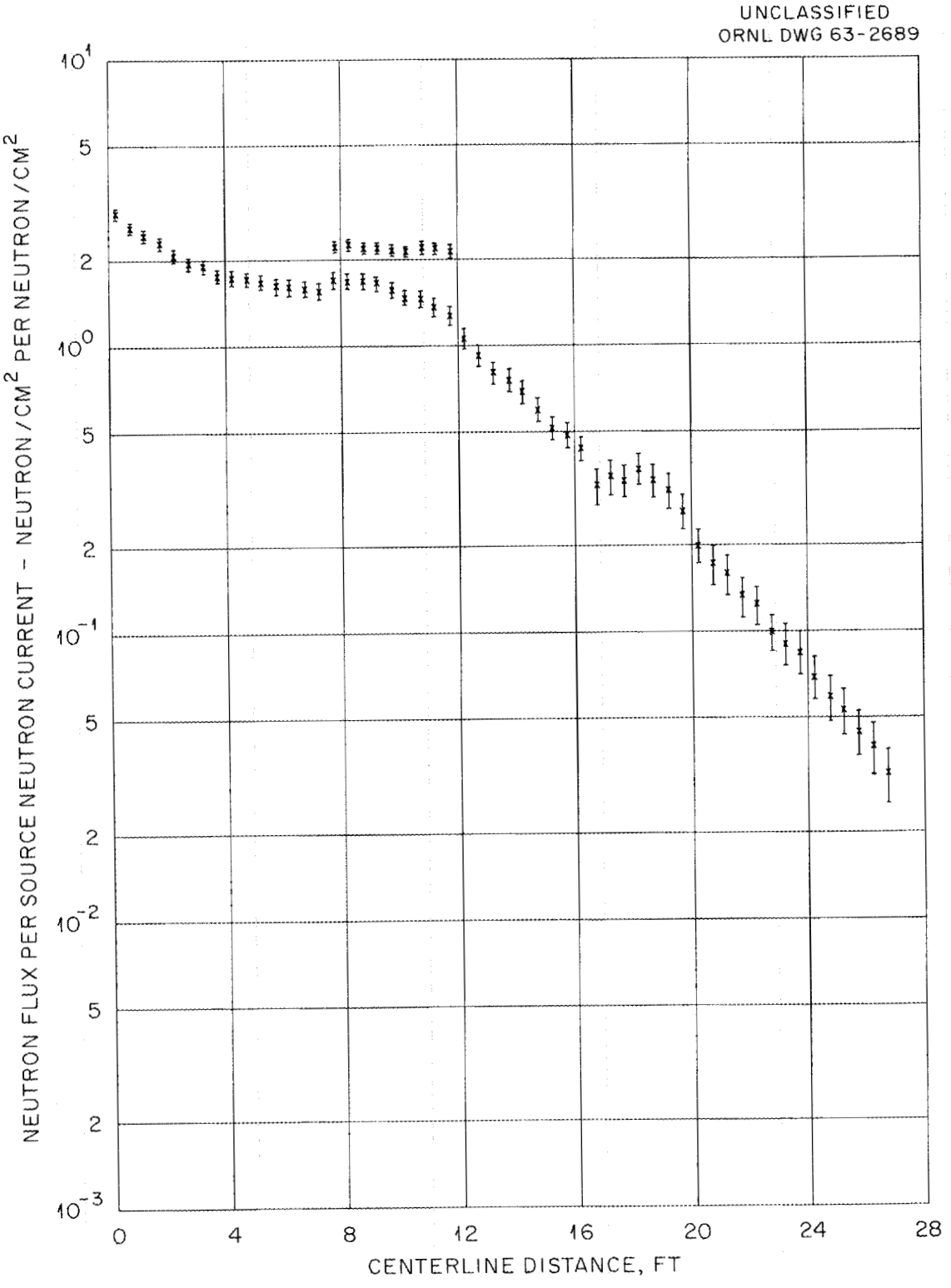

Fig. 47. Total Neutron Flux Calculated for Room (8 by 7.5 by 7.5 ft) and Two-Legged Duct (3 by 8 ft) Configuration (Shown in Fig. 33) Using a Cosine Albedo of 0.80 (4,000 Histories). See text for explanation of geometrical configuration.

Comparison with Experimental Data

In a recent experiment performed at the Tower Shielding Facility measurements of radiation intensities were made in the bunker-tunnel geometry shown in Fig. 48. The two bunkers are 12-ft concrete-walled cubes, each having a variable concrete shield on one face. The Tower Shielding Reactor II, which was used to simulate weapon radiations, was positioned 700 ft away on a line perpendicular to the variable face of the bunker shown at the left of Fig. 48. Measurements of fast-neutron dose rates, gamma-ray dose rates, and thermal-neutron fluxes were made in the two bunkers and in the interconnecting tunnel with various combinations of the concrete shields on the bunker faces.

The measurements which are applicable to the duct problem discussed here are those taken in the interconnecting tunnel. Figure 49 shows data obtained along the center line of the tunnel with the bunker shield facing the reactor open and the other bunker (top bunker) shielded with 20 in. of concrete. It may be noted that the fast-neutron dose rate falls off quite rapidly. The gamma-ray dose rate also falls off rapidly until the neutron-capture gamma rays begin to dominate.

Figure 50 shows corresponding data for an open top bunker and 20 in. concrete on the face of the other bunker. The proportionality of the gamma-ray and thermal-neutron data in this figure again demonstrates the importance of neutron captures in the walls to the gamma-ray dose rates.

UNCLASSIFIED
2-01-056-039-1408

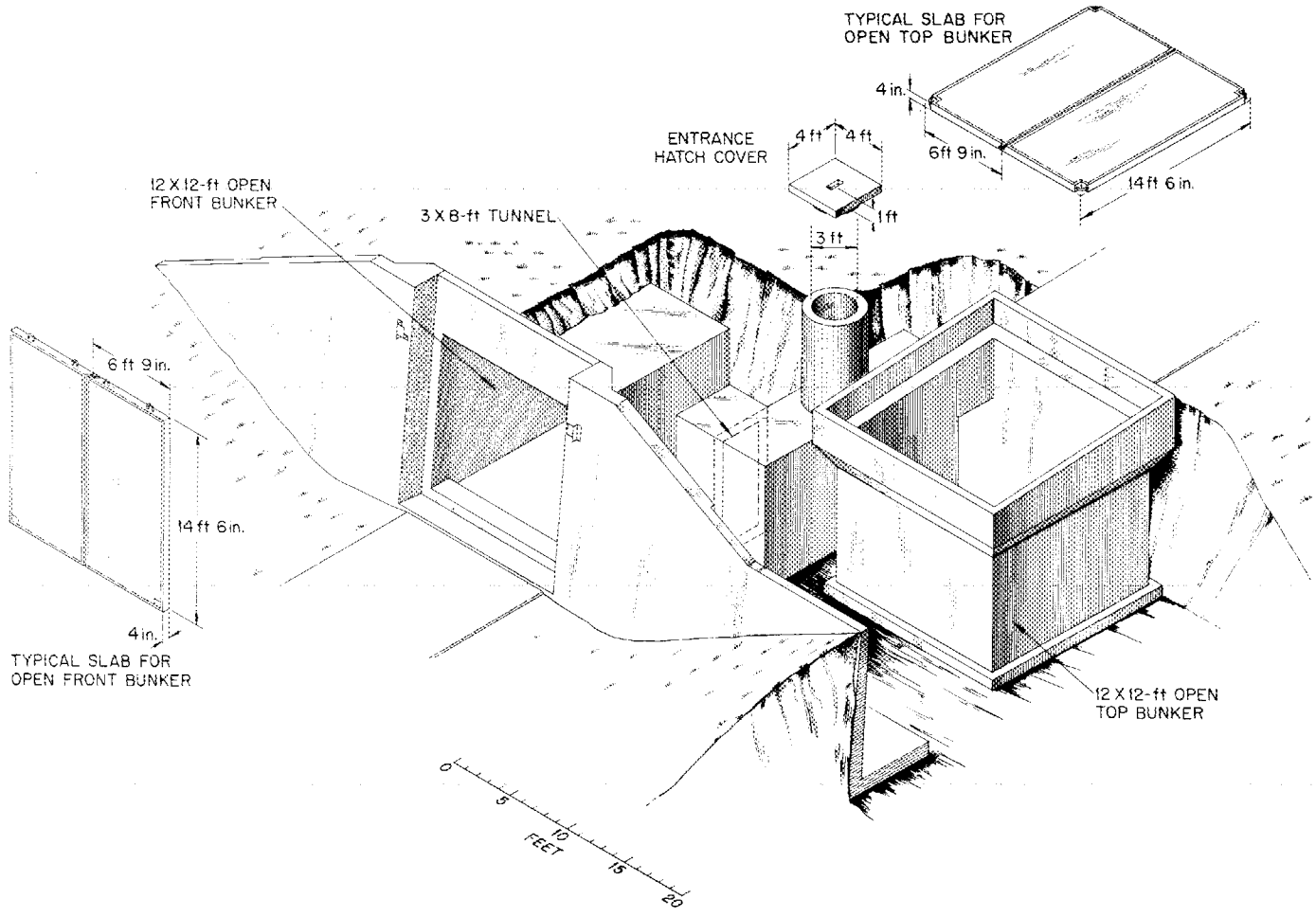

Fig. 48. Bunker-Tunnel Configuration Used in TSF Experiment.

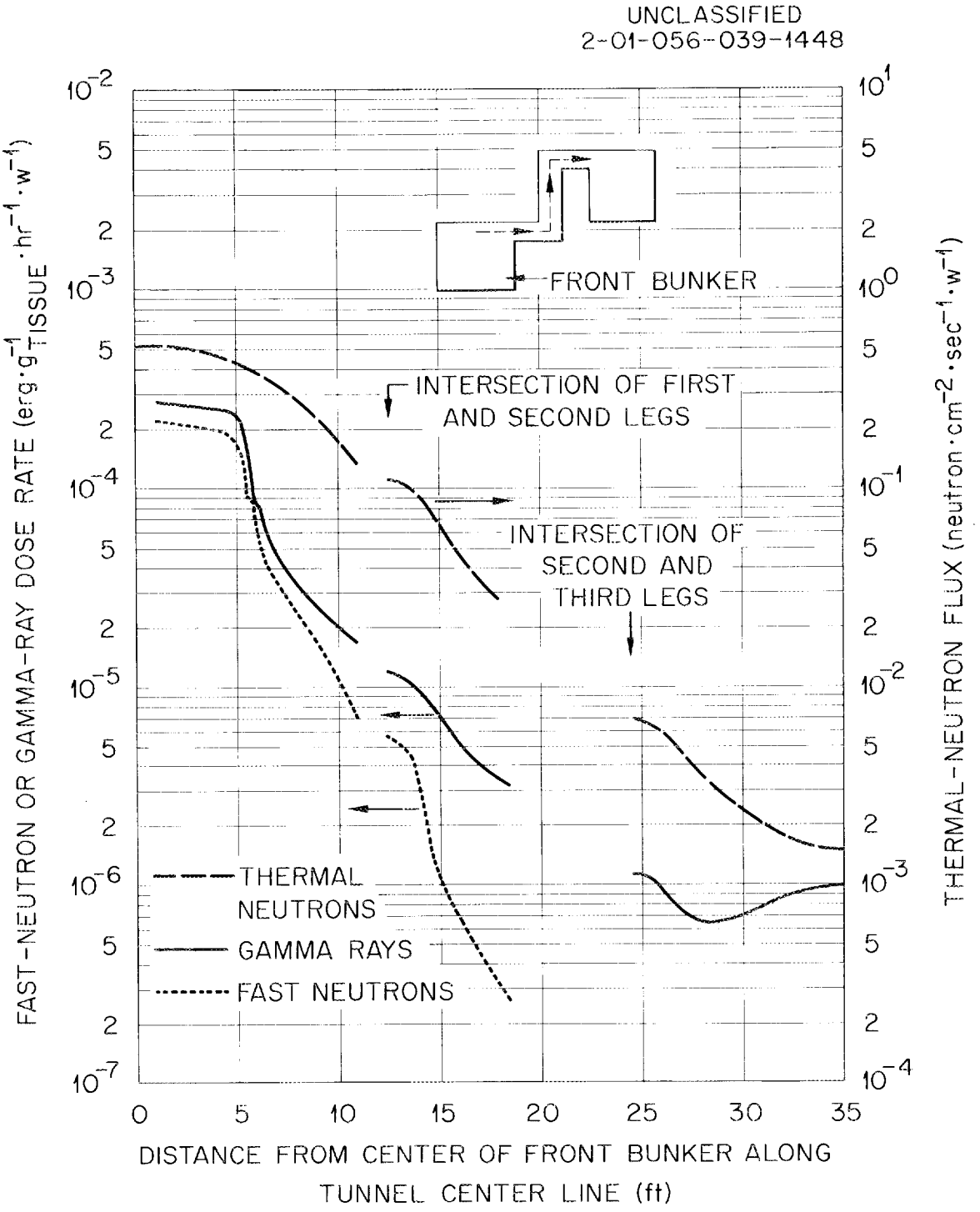

Fig. 49. Fast-Neutron and Gamma-Ray Dose Rates and Thermal-Neutron Fluxes Along Center Line of Interconnecting Tunnel for No Front Shield and 20-in. Top Shield.

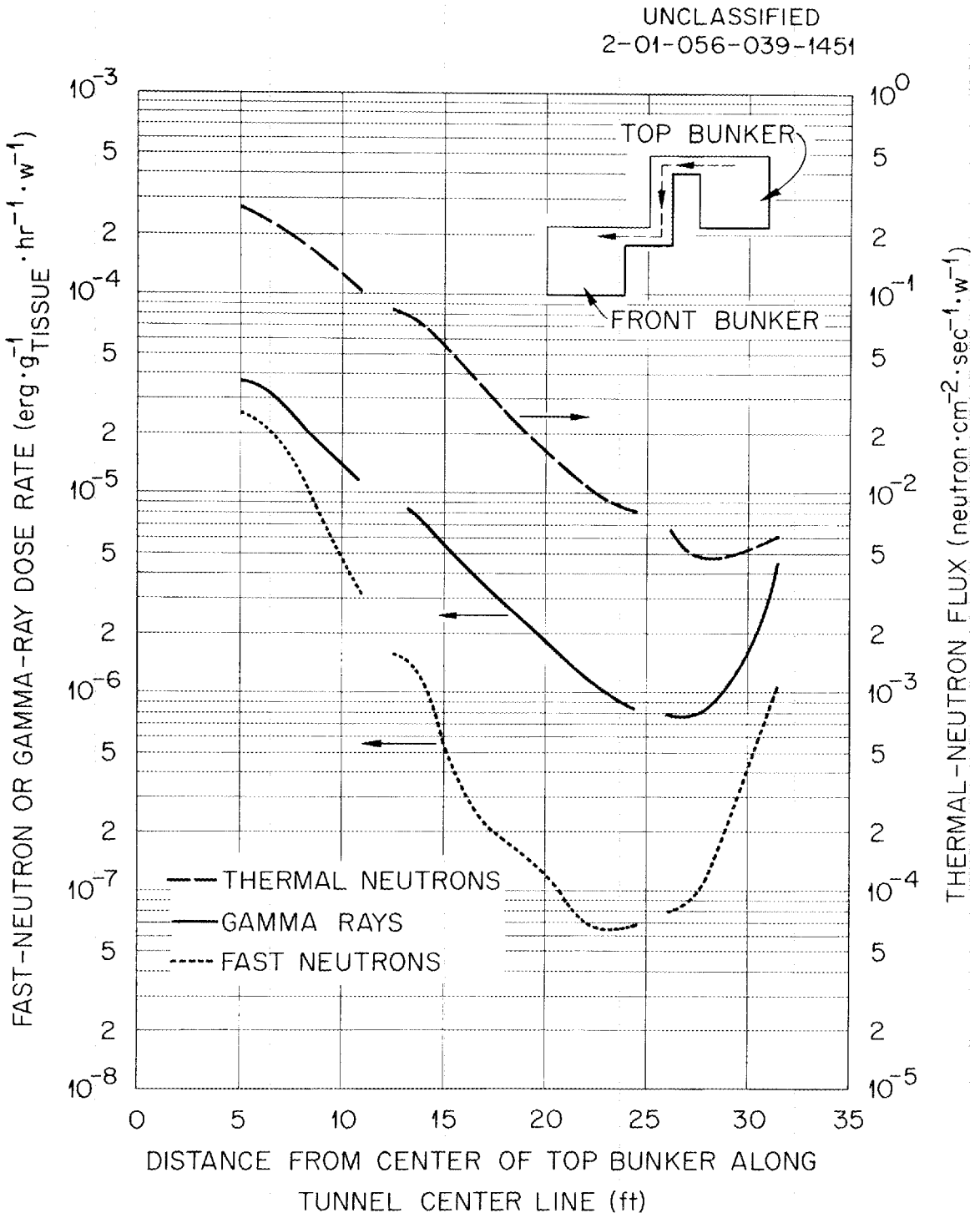

Fig. 50. Fast-Neutron and Gamma-Ray Dose Rates and Thermal-Neutron Fluxes Along Center Line of Interconnecting Tunnel for 20-in. Front Shield and No Top Shield.

The thermal-neutron flux data from Figs. 49 and 50 were corrected for the contributions to the measurements from radiations penetrating the 20-in. concrete shield on the opposite bunker. The corrected data were then compared with calculated results as shown in Fig. 51. The circles on the figure are the results of two of the Monte Carlo calculations (Figs. 43 and 47) arbitrarily normalized. Both of the calculations used an albedo of 0.8 with a cosine distribution. One calculation, plotted from 1.8 to 19.2 ft along the center line, used a geometry mocking up the bunker and two legs of the tunnel. The other calculation, plotted from 6.8 to 32.6 ft along the center line, used a geometry representing the three legs of the tunnel (see page 58 and Fig. 33 for descriptions of these geometries).

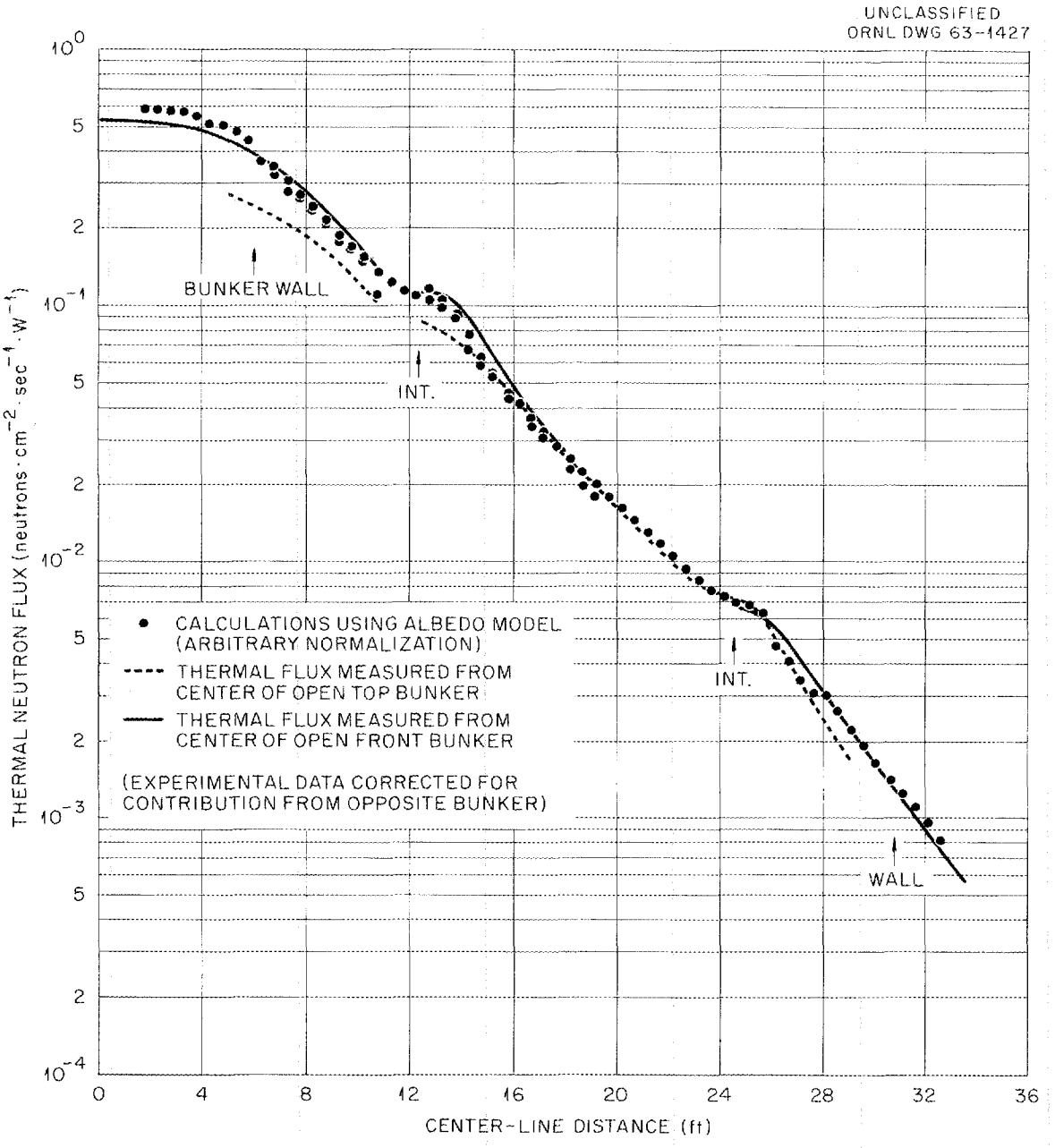

Fig. 51. Comparison of Calculations Using a Cosine Albedo of 0.8 with Thermal-Neutron Flux Measurements Along a Three-Legged Duct.

CHAPTER V

SUMMARY, CONCLUSIONS, RECOMMENDATIONS

Summary

Experimental data obtained at the Tower Shielding Facility in multilegged duct geometries indicate that the gamma rays resulting from the capture of low-energy neutrons in the duct walls can be an important contributor to the total dose. In order to calculate these capture gamma rays, the distribution of the low-energy neutrons must be known.

This study presents calculations of low-energy neutron distributions using a simple albedo, or reflection coefficient, model. Since the albedo for the low-energy neutrons is large, many reflections must be taken into account. The technique chosen to do these calculations is a Monte Carlo procedure, the random-walk technique, which basically consists of random sampling from a statistical analogue of the actual physical process.

A digital computer code was written to perform the calculations. One series of calculations was performed using straight duct geometries, to permit comparison with the Simon-Clifford analytic approximation. Another series of calculations was performed for three-legged rectangular ducts, most of which used a geometry similar to that used in the TSF experiment. Calculations are presented using an albedo similar

to that which would be expected for a pure thermal-neutron source. The calculated results agree fairly well with the experimental data.

Conclusions

The machine program, as written, appears to be operating correctly and to be providing useful information more efficiently than other techniques which can be applied to this problem. This study has not proceeded to the point where completely definitive statements can be made as to the proper albedo to use for an arbitrary problem. It appears that the slowing down and transport of low-energy neutrons, including those at thermal and intermediate energies, in concrete-walled ducts are closely described by an albedo similar to the thermal-neutron albedo. The values of the albedo which gave the best comparisons to the available experimental data were on the order of 0.75 or 0.8 and used a cosine distribution. Since the best estimates of the thermal-neutron albedo are on the order of 0.6 (see Appendix F), it appears that the effective albedo is strongly influenced by the slowing down of the intermediate-energy neutrons.

The comparisons of the straight duct calculations with the formula derived by Simon and Clifford (Eq. 2, page 48) help establish the validity of the Monte Carlo calculations. More importantly, they indicate the areas where the Simon-Clifford analytic approximation is not applicable. A good rule of thumb seems to be that for straight ducts the analytic approximation is adequate for distances greater than 10

source diameters from the source. This is illustrated in Fig. 52, which shows a good agreement between the analytic approximation and a Monte Carlo calculation. In this case, for a 3 by 1 ft duct, agreement is good beyond about six source diameters, assuming that the rectangular duct can be represented by a cylindrical duct of equal cross-sectional area.

Figure 52 also includes results from a calculation with a 3 by 1 ft duct having a right-angle bend 6 ft from the source. The reduction of the flux by the bend is demonstrated quite well. The behavior of the flux in multilegged ducts does not seem amenable to simple analytic representation, as can be seen by reference to the figure. The flux in this and some of the other calculations with multilegged ducts seems to behave approximately as an exponential, but it can be seen that this would not be the case with a duct having longer legs. Even in this case, the agreement with an exponential behavior is not too close and, further, there does not seem to be a simple way to represent the shape of the duct in the exponential.

Recommendations

The technique described in this thesis has offered sufficient promise to justify further investigation. This divides logically into two areas: (1) improvement of the computer program and (2) detailed studies, both experimental and theoretical, of the nature of the albedo for various types of particles.

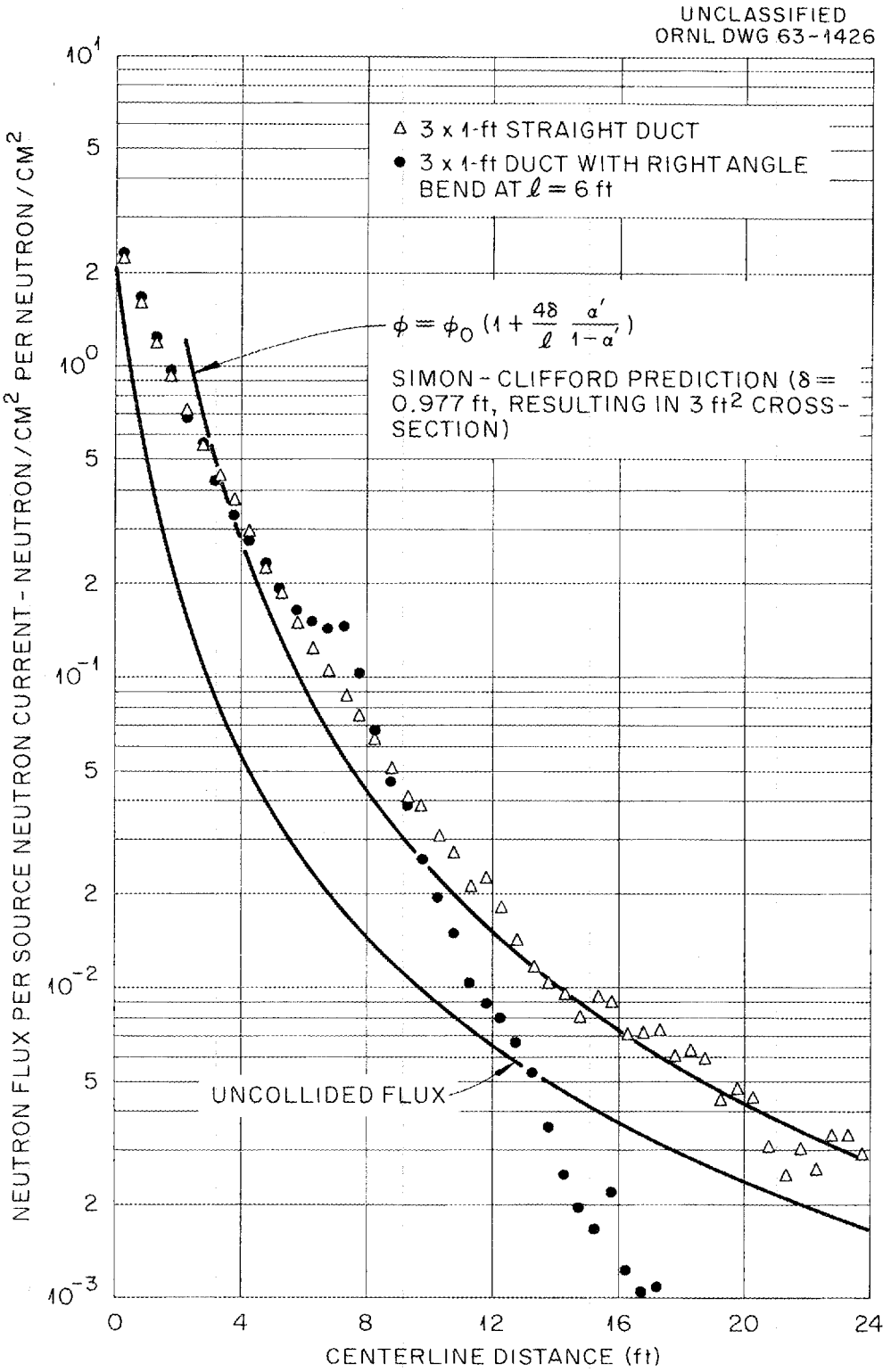

Fig. 52. Comparison of Calculations of Flux Distribution in a 3 by 1-ft Duct Using a Cosine Albedo of 0.80.

Many rather obvious improvements are possible in the computer code, primarily because of the inexperience of the author in this field. Many features were included in the code either to satisfy the curiosity of the author or to gain experience in the use of a certain technique. Some which were included during the development of the code have already been removed and are not shown in the description of the code.

An example of a remaining unneeded feature is the inclusion of a single batch variance and a multiple batch variance. These variances were originally included in the hope that, if one history contributed excessively to a detector score, the batch variance would be significantly larger than the single batch variance. This may be the case, but the information gained is not worth the wasted machine time. Since the batch variance calculation is much faster and usually quite close to the more precise single batch variance, and, furthermore, since it is not really clear what the meaning of the variance is when applied to the skew distributions encountered in radiation penetration problems, the single batch variance calculation should be eliminated. This would enable elimination of the subroutine VARUNS as well.

Another area in which the code could be improved would be the inclusion of several options covering certain features now in the code and others which might be desirable. It was easier for the author to change the code each time than to include options, but this would not

be the case for someone less familiar with the details of the code. For instance, a desirable option would be to allow obtaining the results of the calculation on punched cards. This would allow easy reinsertion of the information into the machine for replotting of the results or for arbitrary manipulations of the data.

A further improvement would be the provision of more versatility in the albedo description. At present it is not clear what form this would take, so changes would have to wait on more detailed albedo information. An additional bit of information which could be useful would be the neutron loss in the duct walls as a function of distance down the duct. This could be done by forming an array, the subscript corresponding to the detector number, which would store the portion of the score subtracted at each scatter point (the difference between the incoming and outgoing particle weights). This quantity could then be used as a source for a gamma-ray dose calculation.

The detailed nature of the albedo should be studied for several cases. The albedos of the intermediate-energy neutrons are of primary concern to this study. There is some information on albedos at thermal and at high energies, but virtually none in between. In general, the neutron albedo can be divided into two primary components: (1) a neutron in -- neutron out albedo, and (2) a neutron in -- secondary gamma ray out albedo. This detailed information could, in principle, be used in a modified version of the machine program to calculate

completely all doses resulting from neutrons entering a duct. This would leave only the gamma-ray problem, which is the simpler and which could also be handled by the code, possibly by using an analytic representation of the gamma-ray albedo.[1]

---

[1]A. B. Chilton and C. M. Huddleston, "A Semi-Empirical Formula for Gamma Rays on Concrete." Transactions of the American Nuclear Society 5, No. 9, p. 220 (1962).

BIBLIOGRAPHY

BIBLIOGRAPHY

1. Blizard, E. P., and L. S. Abbott (eds.), Shielding, Vol. III, Part B, Reactor Handbook. 2nd ed., New York: Interscience Publishers, 1962.

2. Cain, V. R., et al., Measurements of Radiation Intensities in Underground Holes at the TSF. ORNL-TM-285 (unpublished to date).

3. Cain, V. R., A Study of the Radiation Shielding Characteristics of Basic Concrete Structures at the Tower Shielding Facility. ORNL-3464 (1963).

4. Chilton, A. B., and C. M. Huddleston, "A Semi-Empirical Formula for Differential Dose Albedo for Gamma Rays on Concrete." Transactions of the American Nuclear Society 5, No. 1, 220 (1962).

5. Design and Review of Structures for Protection from Fallout Gamma Radiation. Office of Civil Defense, Revised (Oct. 1, 1961).

6. Evans, R. D., The Atomic Nucleus. New York: McGraw-Hill Book Company, Inc., 1955.

7. Fallout Shelter Surveys: Guide for Architects and Engineers. Department of Defense, Office of Civil Defense NP-10-2 (May, 1960).

8. Fermi, Enrico, On the Motion of Neutrons in Hydrogenous Substances. NP-2385 (Oct. 22, 1951). [Translation from Ricerca Scienta. VII-II, 13 (1936)].

9. FORTRAN-62 Reference Manual. Control Data Corporation (June, 1962).

10. Glasstone, S. (ed.), The Effects of Nuclear Weapons. Department of the Army Pamphlet No. 39-3 (April, 1962).

11. Glasstone, S., and M. C. Edlund, The Elements of Nuclear Reactor Theory. D. Van Nostrand Co., Inc., Princeton, 1952.

12. Goertzel, G., and M. H. Kalos, "Monte Carlo Methods in Transport Problems." pp. 315-369, Vol. 2, Physics and Mathematics, Series II, Progress in Nuclear Energy, edited by D. J. Hughes, J. E. Sanders, and J. Horowitz, New York: Pergamon Press, 1958.

13. Halpern, O., R. Lueneburg, and O. Clark, "On Multiple Scattering of Neutrons." Physical Review 53, 173 (Jan. 15, 1938).

14. Hubbell, J. H., R. L. Bach, and J. C. Lamkin, "Radiation Field from a Rectangular Source." NBS Journal of Research, 64C, 2 (April-June, 1960).

15. Irving, D., "Computer Routine for Treating Complex Geometries in Monte Carlo and Other Types of Calculations." ORNL-3360, Neutron Physics Division Annual Progress Report for Period Ending September 1, 1962, p. 230.

16. Kahn, Herman, "Random Sampling (Monte Carlo) Techniques in Neutron Attenuation Problems." Nucleonics 8, 22-33 (May, 1950); and 60-65 (June, 1950).

17. Kahn, Herman, Applications of Monte Carlo. AECU-3259 (April 19, 1954).

18. Kalos, M. H., "On the Estimation of Flux at a Point by Monte Carlo." Nuclear Science and Engineering 16, 111 (1963).

19. Reference Manual 709/7090 FORTRAN Programming System. International Business Machines Corp. (Rev. Jan., 1961).

20. Simon, A., and C. E. Clifford, "The Attenuation of Neutrons in Air Ducts in Shields." Nuclear Science and Engineering 1, 156 (1956).

21. Spencer, L. V., Structure Shielding Against Fallout Radiation from Nuclear Weapons. National Bureau of Standards Monograph 42 (1962).

22. Terrell, C. W., et al., Radiation Streaming in Shelter Entrance-ways. Armour Research Foundation, ARF-1158A01-5 (July, 1961).

23. Trubey, D. K., and M. B. Emmett, An IBM-7090 Subroutine Package for Making Logarithmic and Semilogarithmic Graphs Using the CALCOMP Plotter. ORNL-TM-430 (Dec. 12, 1962).

24. Trubey, D. K., and M. B. Emmett, CDC-1604 Subroutine Package for Making Linear, Logarithmic and Semilogarithmic Graphs Using the CALCOMP Plotter. ORNL-3447 (1963).

25. Zerby, C. D., A Monte Carlo Calculation of Air-Scattered Neutrons. ORNL-2277 (1954).

APPENDIX A

THE ALBEDO MONTE CARLO MACHINE PROGRAM

The albedo Monte Carlo machine program will be described in two versions. One version was written for use on the IBM-7090 computer. Its execution is quite fast (on the order of 15 min for 4,000 particles undergoing up to 50 or 60 collisions) and is relatively simple, but it uses a geometry subroutine (see Appendix C) which is written in machine language (FAP). The other major version of the program was written for the CDC-1604 machine and uses a functionally similar geometry subroutine (see Appendix C) written largely in the FORTRAN language.

Figure 53 is a functional block diagram which applies to either of the programs. The instructions are divided into subroutines in such a way that major logical steps are contained in separate subroutines, shown as boxes in the block diagram. The main program calls the input and output subroutines, and the HISTOR and VARUNS subroutines. HISTOR is called for each particle to be followed and retains control until the death of the particle. This routine calls a series of subroutines which handle certain portions of the calculations required for the determination of the particle history and the related calculations of particle flux. VARUNS calculates an estimate of the variances of each score in two different ways: first, by grouping the particles in an arbitrary

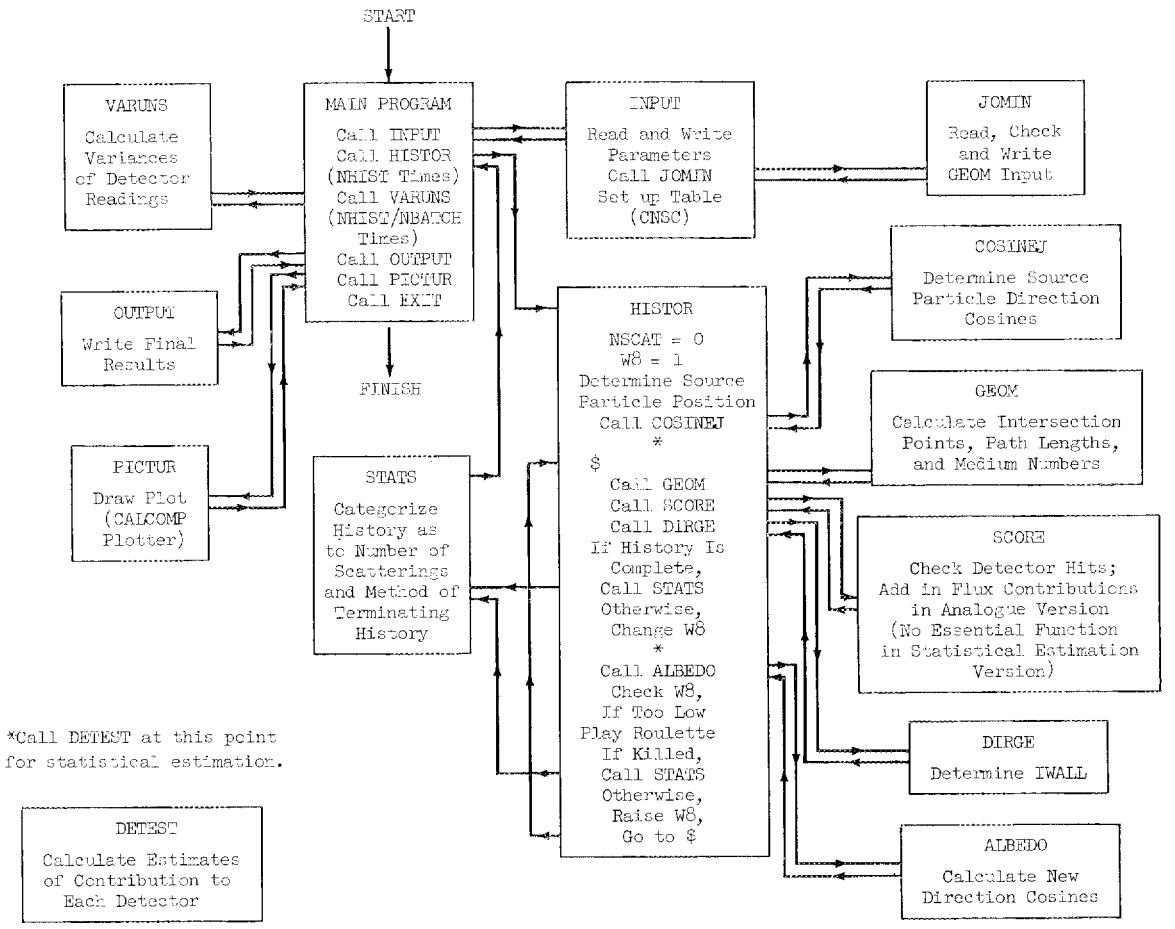

Fig. 53. Block Diagram of Albedo Monte Carlo Machine Program.

number of batches for the calculation, and second, by treating all the histories as a single batch.

FORTRAN listings of the main programs for the two machines are given on the following two pages. They differ primarily in the COMMON and DIMENSION listings[1] and in the PROGRAM and END cards. Functionally, the program is simple. The DO 100 loop calls the HISTOR and VARUNS subroutines, as outlined previously. The DO 120 loop calls VARUNS for the last time (statement 120) to include, in the single batch variance, any histories left over if NHIST was not an integral multiple of NBATCH. This loop also makes the final calculation of the variance calculated in batches. This is done in statement 115, rewritten in more conventional form as follows:

$$\sigma^2_{\overline{x}} = \frac{1}{n(n-1)} \left\{ \sum_{i=1}^{n} (\overline{x}_i)^2 - \frac{1}{n} \left(\sum_{i=1}^{n} \overline{x}_i \right)^2 \right\} ,$$

where

n = number of batches,

$\overline{x}_i$ = mean of scores in the <u>ith</u> batch,

$\sigma^2_{\overline{x}}$ = variance of the overall mean score, $\overline{x}$.

---

[1] Hereinafter COMMON and DIMENSION listings are omitted from the subroutine listings, but, in operation, they must be inserted immediately following the subroutine name.

```
C  ALBEDO MONTE CARLO  VIC CAIN
      COMMON RA,ADDR,XL,YL,ZL,DL,ML,BL,XS,YS,ZS,DCX,DCY,DCZ,SIG,BLZ,
     1NHIST,NSCAT,W,H,W8,SCSOR,SCEND,WSCOR,SCOR,CNSC,SCNSC,PSC,NZONE,
     2NBLOCK,LSNO,SCNSS,SCNSO,SCNSK,SCRSQ,LASNO,AVERJ,VAR,DEDW8,NSKILT,
     3TOH,NBATCH,NUMDET,SUMMSQ,SUMMNS,ALTVAR,NROUL,PSQ,DELW,RELAX,IWALL,
     4XDET,YDET,ZDET,INDX,NHC,LETPAR,TITL,NCY,ITOPY,A5,DELTAX,NOINT,
     5XZERO,XPOS,XW1,XW2,XW3,XW4,YW1,YW2,YW3,YW4,ZW1,ZW2,CONS,NCS,PONCS
      DIMENSION ADDR(1200),XL(50),YL(50),ZL(50),DL(50),ML(50),BL(50),
     1CNSC(40),SCNSC(40),SCNSS(40),SCNSO(40),SCNSK(40),SCOR(100),
     2NZONE(50),NBLOCK(50),SCRSQ(100),LASNO(100),AVERJ(100),VAR(100),
     3TOH(100),SUMMSQ(100),SUMMNS(100),ALTVAR(100),PSQ(100),XDET(100),
     4YDET(100),ZDET(100),XPOS(100),TITL(25),A5(5),PONCS(10)
      CALL INPUT
      KEVIN#0
      DO 100 LEFTY#1,NHIST
      IHIST#LEFTY
      CALL HISTOR
      IF(NBATCH*(IHIST/NBATCH)-IHIST)100,80,100
   80 DO90 KIM#1,NUMDET
   90 CALL VARUNS(NBATCH,KIM)
      KEVIN#KEVIN+1
  100 CONTINUE
      KARL#IHIST-KEVIN*NBATCH
      DO 120 LORI#1,NUMDET
      PAT#KEVIN
      R#PAT-1.0
      IF(R)120,120,115
  115 ALTVAR(LORI)#(SUMMSQ(LORI)-SUMMNS(LORI)/PAT*SUMMNS(LORI))/(PAT*R)
  120 CALL VARUNS(KARL,LORI)
      CALL OUTPUT
      CALL PICTUR
      CALL EXIT
      END
```

```
      PROGRAM ALBEDO MONTE CARLO
      COMMON RA,ADDR(1200),A5(6),ALTVAR(100),AVERJ(100),BL(90),CNSC(40),
     2DCX,DCY,DCZ,DEDW8,DELTAX,DL(90),H,INDX,ITOPY,IWALL,LASNO(100),
     3LSNO,ML(90),NBATCH,NCY,NHC,NHIST,NOINT,NSCAT,NSKILT,NUMDET,PSC,
     4PSQ(100),SCEND,SCNSC(40),SCNSK(40),SCNSO(40),SCNSS(40),SCOR(100),
     5SCRSQ(100),SCSOR,SUMMNS(100),SUMMSQ(100),TITL(20),TOH(100),
     6VAR(100),W,W8,WSCOR,XDET(100),XL(90),XPOS(100),XS,XW1,XW2,XW3,XW4,
     7XZERO,YDET(100),YL(90),YS,YW1,YW2,YW3,YW4,ZDET(100),ZL(90),ZS,ZW1,
     8ZW2,CONS,DELW,RELAX,NCS,PONCS(10)
      CALL INPUT
      KEVIN#0
      DO 100 LEFTY#1,NHIST
      IHIST#LEFTY
      CALL HISTOR
      IF(NBATCH*(IHIST/NBATCH)-IHIST)100,80,100
   80 DO90 KIM#1,NUMDET
   90 CALL VARUNS(NBATCH,KIM)
      KEVIN#KEVIN+1
  100 CONTINUE
      KARL#IHIST-KEVIN*NBATCH
      DO 120 LORI#1,NUMDET
      PAT#KEVIN
      R#PAT-1.0
      IF(R)120,120,115
  115 ALTVAR(LORI)#(SUMMSQ(LORI)-SUMMNS(LORI)/PAT*SUMMNS(LORI))/(PAT*R)
  120 CALL VARUNS(KARL,LORI)
      CALL OUTPUT
      CALL PICTURE
      CALL EXIT
      END ALBEDO MONTE CARLO
```

It should be noted that all variances calculated in this code are variances of the mean, not variances of a single additional measurement. In other words, the standard deviation, or square root of this variance, gives the deviation within which there is a 68% probability of a new mean value falling, if the same number of histories is used again for the new mean. Formal definitions of these quantities are given in Appendix G.

The subroutine INPUT for the IBM-7090 is given on the following page. It is used primarily for bringing the parameters of the calculation into storage, and, for purposes of identification, it is also used for printing some of these parameters. The statements "SUMCØF = 0."[2] through statement 64 reformulate the parameters PØNCS(I). The albedo distribution (in θ, the polar angle of emission) is represented in the input as:

$$\alpha = \alpha_o(\beta_1 + \beta_2 \cos\theta + \ldots + \beta_{n+1} \cos^n\theta),$$

where

α = differential albedo (per unit cosine),

α_o = total albedo (PSC),

β_i = coefficient in series [PØNCS(I)],

n = highest power of $\cos\theta$ (NCS).

---

[2]Definitions of symbols used in the machine programs are given in Appendix B.

```
      SUBROUTINE INPUT
    1 FORMAT(O17,F13.5,4F10.5)
    2 FORMAT(3I5,E20.5,E15.5,2E10.5)
    3 FORMAT(6E12.5)
    4 FORMAT(2I5,2E10.4,2I5,3E10.4)
    5 FORMAT(14F5.2)
      READINPUTTAPE10,2,LSNO,NUMDET,NCS
      READINPUTTAPE10,1,RA,W,H,PSC,RELAX,CONS
      READINPUTTAPE10,2,NHIST,NBATCH,NSKILT,DEDW8
      READINPUTTAPE10,5,XW1,XW2,XW3,XW4,YW1,YW2,YW3,YW4,ZW1,ZW2,DELW
      READINPUTTAPE10,3,(XDET(I),YDET(I),ZDET(I),I#1,NUMDET)
      NCP#NCS+1
      READINPUTTAPE10,3,(PONCS(I),I#1,NCP)
      CALL HOLLER(NHC,LETPAR,TITL,10)
      READINPUTTAPE10,4,NCY,ITOPY,XZERO,DELTAX,NOINT
      READINPUTTAPE10,5,(XPOS(I),I#1,NUMDET)
      CALL JOMIN(LSNO,XL,YL,ZL,DL,ML,BL,ADDR)
      WRITEOUTPUTTAPE9,44,(J,J#2,NCS)
   44 FORMAT(1H2,24X,8I10)
      WRITEOUTPUTTAPE9,43,(PONCS(I),I#1,NCP)
   43 FORMAT(8H ALBEDO#F7.4,8(1H+,F7.4,2HU ))
      WRITEOUTPUTTAPE9,9,NHIST,RA,W,H,PSC,NBATCH,NSKILT,DEDW8
    9 FORMAT(8H  NHIST#I5,7H,   RA#O13,5H,  W#F8.2,5H,  H#F8.2,7H,  PSC#
     1F8.5,10H,  NBATCH#I3,10H,  NSKILT#I3,9H,  DEDW8#E11.4)
      SUMCOF#0.
      DO62I#1,NCP
   62 SUMCOF#SUMCOF+PONCS(I)/FLOATF(I)
      IF(SUMCOF)65,65,63
   63 PONCS(1)#PONCS(1)/SUMCOF
      DO64I#2,NCP
   64 PONCS(I)#PONCS(I)/FLOATF(I)/SUMCOF+PONCS(I-1)
   65 IF(PSC-0.8)31,32,85
   31 IF(PSC-0.7)34,34,32
   85 DO 18 I#1,9
   18 CNSC(I)#I
      DO 19 I#10,14
   19 CNSC(I)#CNSC(I-1)+2.
      DO 21 I#15,19
   21 CNSC(I)#CNSC(I-1)+4.
      DO22I#20,40
   22 CNSC(I)#CNSC(I-1)+5.
      GO TO 96
   32 DO 11 I#1,9
   11 CNSC(I)#I
      DO12I#10,40
   12 CNSC(I)#CNSC(I-1)+2.
      GO TO 96
   34 DO35I#1,40
   35 CNSC(I)#I
   96 RETURN
      END
```

The subroutine assumes that the series is not normalized properly and calculates the following normalizing factor (called SUMCØF in the subroutine):

$$S = \frac{1}{\alpha_0} \int_{\cos\theta=0}^{1} \alpha \, d(\cos\theta) = \int_{\cos\theta=0}^{1} \left\{\beta_1 + \beta_2 \cos\theta + \ldots + \beta_{n+1} \cos^n\theta\right\} d(\cos\theta)$$

$$= \sum_{i=1}^{n+1} \frac{\beta_i}{i} \; .$$

The series is then normalized by dividing by S and multiplying and dividing the i<u>th</u> term by i. Thus,

$$\alpha = \frac{\alpha_0}{S} \left\{\beta_1 + \frac{\beta_2}{2} \; [2 \cos\theta] + \ldots + \frac{\beta_{n+1}}{n+1} \; [(n+1) \cos^n\theta]\right\} \; .$$

The i<u>th</u> term now contains a factor $i \cos^{i-1}\theta$ which is a properly normalized probability density function (p.d.f.). That is,

$$\int_{\cos\theta=0}^{1} i \cos^{i-1}\theta \, d(\cos\theta) = 1 \; .$$

Sampling from the original series may now be done by sampling from a $i \cos^{i-1}\theta$ distribution a fraction β_i/iS of the time. This is done by replacing the original coefficient of the series by the quantities γ_i, where

$$\gamma_1 = \frac{\beta_1}{S} \quad ,$$

$$\gamma_i = \frac{\beta_i}{i\ S} + \gamma_{i-1}, \quad i = 2,3,\ldots n \ .$$

In order to sample from the power series it is now only necessary to pick a random number R ($0 \leq R \leq 1$), determine a j such that $R \leq \gamma_j$, and then select from a distribution $j \cos^{j-1}\theta$. That this is the case may be seen in the following example. Suppose that the desired distribution is

$$\alpha = \alpha_o(1 + 4 \cos\theta + 6 \cos^2\theta) \ .$$

The integral of this series, from $\cos\theta = 0$ to 1, is

$$\int_0^1 \alpha \ d(\cos\theta) = \alpha_o[1 \cos\theta + 2 \cos^2\theta + 2 \cos^3\theta \Big|_0^1 = 5\ \alpha_o \ .$$

The factor multiplying α_o is the variable S (SUMCOF),

$$S = \sum_{i=1}^{n+1} \frac{\beta_i}{i} = \left(\frac{1}{1} + \frac{4}{2} + \frac{6}{3}\right) = 5 \ .$$

The cumulative probabilities γ_i, stored in PØNSC(I), are:

$$\text{PØNCS}(1) = \frac{1}{5} = 0.2,$$

$$\text{PØNCS}(2) = \frac{4}{2 \times 5} + 0.2 = 0.6,$$

$$\text{PØNCS}(3) = \frac{6}{3 \times 5} + 0.6 = 1.0.$$

Note that the new value of the highest coefficient is always 1. When selection from this series is desired, the random number R is selected. Then,

if $R \leq 0.2$	pick from an isotropic distribution;
if $0.2 < R \leq 0.6$	pick from a cosine distribution;
if $0.6 < R \leq 1.0$	pick from a cosine^2 distribution.

(The actual selection process is performed later, in the subroutines ALBEDO and COSJ.)

The INPUT routine also sets up a table of 40 values of CNSC, depending on the value of the albedo, PSC. These values are used as the limits of boxes used to form histograms of the numbers of particles which undergo specified numbers of scatterings. Several of these histograms are formed and printed on the output for all particles (SCNSC), for those particles terminated by re-entering the source plane (SCNSS), for those particles leaving the end of the duct (SCNSO), and for those particles killed (SCNSK).

The minor modifications required in the CDC-1604 version are listed below:

CALL HØLLER(NHC,LETPAR,TITL,10) becomes CALL HØLLER(NHC,TITL,10)

CALL JØMIN(LSNØ,XL,YL,ZL,DL,ML,BL,ADDR) is replaced by

NADD = 1

CALL JØMIN(NADD).

(HØLLER is a subroutine in the package controlling the curve plotting.[3]) A series of statements is inserted which set to zero the following storage cells:

SCSØR,SCEND,WSCØR,

LASNØ(I),AVERJ(I),VAR(I),SCRSQ(I),TØH(I) for I = 1 to NUMDET,

SCNSC(I),SCNSØ(I),SCNSS(I),SCNSK(I) for I = 1 to 40.

(This is not required on the IBM-7090 since its monitor zeros the entire core between separate runs.)

Pages 104 through 106 contain a sample listing of input cards which are read by subroutine INPUT. These cards specify a problem using a three-legged 3 x 8 ft rectangular duct and a cosine albedo of magnitude 0.75. It is a suitable input only for the 54-detector geometry described in Appendix C; the use of statistical estimation would require a modified geometry input.

Pages 107 and 108 are listings of the subroutines HISTOR for the IBM-7090 and the CDC-1604, respectively. The simpler IBM-7090 version

---

[3]D. K. Trubey and M. B. Emmett, An IBM-7090 Subroutine Package for Making Logarithmic and Semilogrithmic Graphs Using the CALCOMP Plotter, ORNL-TM-430 (Dec. 12, 1962).

```
*DATA
   50    54     1
     153245743735        3.0       8.0       0.75      0.131233
 4000  200  100           1.00000E-05
  0.0  4.5  7.5 15.0  0.0  3.0 12.0 15.0  0.0  8.0.0001
 0.5         1.5         3.0         1.0         1.5         3.0
 1.5         1.5         3.0         2.0         1.5         3.0
 2.5         1.5         3.0         3.0         1.5         3.0
 3.5         1.5         3.0         4.0         1.5         3.0
 4.5         1.5         3.0         5.0         1.5         3.0
 5.5         1.5         3.0         6.0         1.5         3.0
 6.0         2.0         3.0         6.0         2.5         3.0
 6.0         3.0         3.0         6.0         3.5         3.0
 6.0         4.0         3.0         6.0         4.5         3.0
 6.0         5.0         3.0         6.0         5.5         3.0
 6.0         6.0         3.0         6.0         6.5         3.0
 6.0         7.0         3.0         6.0         7.5         3.0
 6.0         8.0         3.0         6.0         8.5         3.0
 6.0         9.0         3.0         6.0         9.5         3.0
 6.0         10.0        3.0         6.0         10.5        3.0
 6.0         11.0        3.0         6.0         11.5        3.0
 6.0         12.0        3.0         6.0         12.5        3.0
 6.0         13.0        3.0         6.0         13.5        3.0
 6.5         13.5        3.0         7.0         13.5        3.0
 7.5         13.5        3.0         8.0         13.5        3.0
 8.5         13.5        3.0         9.0         13.5        3.0
 9.5         13.5        3.0         10.0        13.5        3.0
 10.5        13.5        3.0         11.0        13.5        3.0
 11.5        13.5        3.0         12.0        13.5        3.0
 12.5        13.5        3.0         13.0        13.5        3.0
 13.5        13.5        3.0         14.0        13.5        3.0
 14.5        13.5        3.0
 0.0           1.0
   54
   COSINE(0.75) 4000 HISTORIES (3X8 FT 3-LEGGED DUCT)
    4     1  0.0       4.0           7
 0.25 0.75 1.25 1.75 2.25 2.75 3.25 3.75 4.25 4.75 5.25 5.75 6.25 6.75
 7.25 7.75 8.25 8.75 9.25 9.7510.2510.7511.2511.7512.2512.7513.2513.75
14.2514.7515.2515.7516.2516.7517.2517.7518.2518.7519.2519.7520.2520.75
21.2521.7522.2522.7523.2523.7524.2524.7525.2525.7526.2526.7527.2527.75
X ZONE BOUNDARIES 0,45
Y ZONE BOUNDARIES -3,0,3,12,15,60
Z ZONE BOUNDARIES -3,0,8,15
ZONE 1,1,1 X BLOCK 0,45 Y BLOCK -3,0 Z BLOCK -3,0 BLOCK 1,1,1 MEDIA 99
ZONE 1,2,1 X BLOCK 0,45 Y BLOCK 0,3 Z BLOCK -3,0 BLOCK 1,1,1 MEDIA 99
ZONE 1,3,1 X BLOCK 0,45 Y BLOCK 3,12 Z BLOCK -3,0 BLOCK 1,1,1 MEDIA 99
ZONE 1,4,1 X BLOCK 0,45 Y BLOCK 12,15 Z BLOCK -3,0 BLOCK 1,1,1 MEDIA 99
ZONE 1,5,1 X BLOCK 0,45 Y BLOCK 15,60 Z BLOCK -3,0 BLOCK 1,1,1 MEDIA 99
ZONE 1,1,2 X BLOCK 0,45 Y BLOCK -3,0 Z BLOCK 0,8 BLOCK 1,1,1 MEDIA 99
ZONE 1,2,2                                    FIRST HALL
X BLOCK BOUNDARIES 0,0.5,1,1.5,2,2.5,3,3.5,4,4.5,5,5.5,6,6.5,7,7.5,45
Y BLOCK BOUNDARIES 0,3          Z BLOCK BOUNDARIES 0,8
BLOCK 1,1,1  MEDIA  1
BLOCK 2,1,1  MEDIA  2
BLOCK 3,1,1  MEDIA  3
BLOCK 4,1,1  MEDIA  4
BLOCK 5,1,1  MEDIA  5
BLOCK 6,1,1  MEDIA  6
BLOCK 7,1,1  MEDIA  7
BLOCK 8,1,1  MEDIA  8
BLOCK 9,1,1  MEDIA  9
```

```
BLOCK 10,1,1 MEDIA 10
BLOCK 11,1,1 MEDIA 11
BLOCK 12,1,1 MEDIA 12
BLOCK 13,1,1 MEDIA 13
BLOCK 14,1,1 MEDIA 14
BLOCK 15,1,1 MEDIA 15
BLOCK 16,1,1 MEDIA 99
ZONE 1,3,2                                        SECOND HALL
X BLOCK BOUNDARIES 0,4.5,7.5,45
Y BLOCK BOUNDARIES 3,3.5,4,4.5,5,5.5,6,6.5,7,7.5,8,8.5,9,9.5,10,10.5,11,
11.5,12      Z BLOCK BOUNDARIES 0,8
BLOCK 1,1,1   MEDIA 99
BLOCK 2,1,1   MEDIA 16
BLOCK 3,1,1   MEDIA 99
BLOCK 1,2,1   MEDIA 99
BLOCK 2,2,1   MEDIA 17
BLOCK 3,2,1   MEDIA 99
BLOCK 1,3,1   MEDIA 99
BLOCK 2,3,1   MEDIA 18
BLOCK 3,3,1   MEDIA 99
BLOCK 1,4,1   MEDIA 99
BLOCK 2,4,1   MEDIA 19
BLOCK 3,4,1   MEDIA 99
BLOCK 1,5,1   MEDIA 99
BLOCK 2,5,1   MEDIA 20
BLOCK 3,5,1   MEDIA 99
BLOCK 1,6,1   MEDIA 99
BLOCK 2,6,1   MEDIA 21
BLOCK 3,6,1   MEDIA 99
BLOCK 1,7,1   MEDIA 99
BLOCK 2,7,1   MEDIA 22
BLOCK 3,7,1   MEDIA 99
BLOCK 1,8,1   MEDIA 99
BLOCK 2,8,1   MEDIA 23
BLOCK 3,8,1   MEDIA 99
BLOCK 1,9,1   MEDIA 99
BLOCK 2,9,1   MEDIA 24
BLOCK 3,9,1   MEDIA 99
BLOCK 1,10,1  MEDIA 99
BLOCK 2,10,1  MEDIA 25
BLOCK 3,10,1  MEDIA 99
BLOCK 1,11,1  MEDIA 99
BLOCK 2,11,1  MEDIA 26
BLOCK 3,11,1  MEDIA 99
BLOCK 1,12,1  MEDIA 99
BLOCK 2,12,1  MEDIA 27
BLOCK 3,12,1  MEDIA 99
BLOCK 1,13,1  MEDIA 99
BLOCK 2,13,1  MEDIA 28
BLOCK 3,13,1  MEDIA 99
BLOCK 1,14,1  MEDIA 99
BLOCK 2,14,1  MEDIA 29
BLOCK 3,14,1  MEDIA 99
BLOCK 1,15,1  MEDIA 99
BLOCK 2,15,1  MEDIA 30
BLOCK 3,15,1  MEDIA 99
BLOCK 1,16,1  MEDIA 99
BLOCK 2,16,1  MEDIA 31
BLOCK 3,16,1  MEDIA 99
BLOCK 1,17,1  MEDIA 99
BLOCK 2,17,1  MEDIA 32
```

```
BLOCK 3,17,1 MEDIA 99
BLOCK 1,18,1 MEDIA 99
BLOCK 2,18,1 MEDIA 33
BLOCK 3,18,1 MEDIA 99
ZONE 1,4,2                                        THIRD HALL
X BLOCK BOUNDARIES 0,4.5,5,5.5,6,6.5,7,7.5,8,8.5,9,9.5,10,10.5,11,11.5,
12,12.5,13,13.5,14,14.5,15,45  Y BLOCK BOUNDARIES 12,15  Z BLOCK 0,8
BLOCK 1,1,1  MEDIA 99
BLOCK 2,1,1  MEDIA 34
BLOCK 3,1,1  MEDIA 35
BLOCK 4,1,1  MEDIA 36
BLOCK 5,1,1  MEDIA 37
BLOCK 6,1,1  MEDIA 38
BLOCK 7,1,1  MEDIA 39
BLOCK 8,1,1  MEDIA 40
BLOCK 9,1,1  MEDIA 41
BLOCK 10,1,1 MEDIA 42
BLOCK 11,1,1 MEDIA 43
BLOCK 12,1,1 MEDIA 44
BLOCK 13,1,1 MEDIA 45
BLOCK 14,1,1 MEDIA 46
BLOCK 15,1,1 MEDIA 47
BLOCK 16,1,1 MEDIA 48
BLOCK 17,1,1 MEDIA 49
BLOCK 18,1,1 MEDIA 50
BLOCK 19,1,1 MEDIA 51
BLOCK 20,1,1 MEDIA 52
BLOCK 21,1,1 MEDIA 53
BLOCK 22,1,1 MEDIA 54
BLOCK 23,1,1 MEDIA 99
ZONE 1,5,2 X BLOCK 0,45 Y BLOCK 15,60 Z BLOCK 0,8 BLOCK 1,1,1 MEDIA 99
ZONE 1,1,3 X BLOCK 0,45 Y BLOCK -3,0 Z BLOCK 8,15 BLOCK 1,1,1 MEDIA 99
ZONE 1,2,3 X BLOCK 0,45 Y BLOCK 0,3 Z BLOCK 8,15 BLOCK 1,1,1 MEDIA 99
ZONE 1,3,3 X BLOCK 0,45 Y BLOCK 3,12 Z BLOCK 8,15 BLOCK 1,1,1 MEDIA 99
ZONE 1,4,3 X BLOCK 0,45 Y BLOCK 12,15 Z BLOCK 8,15 BLOCK 1,1,1 MEDIA 99
ZONE 1,5,3 X BLOCK 0,45 Y BLOCK 15,60 Z BLOCK 8,15 BLOCK 1,1,1 MEDIA 99
       END
```

```
      SUBROUTINE HISTOR
      NSCAT#0
      W8#1.0/CONS
      XS#0.0
      YS#W*RAN(RA)
      ZS#H*RAN(RA)
      CALL COSJ(DCX,DCY,DCZ,1)
      IWALL#3
   10 LSNO#0
      SIG#1.0
      BLZ#0.0
      CALLGEOM(XS,YS,ZS,DCX,DCY,DCZ,SIG,BLZ)
      CALLSCORE
      CALLDIRGE
      IWALL#IWALL
      IF(IWALL-6)60,60,70
   60 NSCAT#NSCAT+1
      W8#W8*PSC
      CALLALBEDO
   42 IF(W8-DEDW8)80,80,10
   80 IF(RAN(RA)-PSC)82,82,83
   82 W8#W8/PSC
      GO TO 10
   83 IWALL#9
   70 CALLSTATS
      RETURN
      END
```

```
      SUBROUTINE HISTOR
      COMMON /GEOM/MARK,X2,Y2,Z2,X1,Y1,Z1,NMED,NR,Q,DTR,BLZON
      NSCAT#0
      W8#1.0/CONS
      R#64.0
      XS#0.0
      YS#RAN(RA)*W
      ZS#RAN(RA)*H
      CALL COSINEJ(DCX,DCY,DCZ,1)
      IWALL#3
   10 XE#DCX*R+XS
      YE#DCY*R+YS
      ZE#DCZ*R+ZS
      XL(1)#XS
      YL(1)#YS
      ZL(1)#ZS
      X2#XS
      Y2#YS
      Z2#ZS
      MARK#1
      CALL LOOKZ(XS,YS,ZS)
      ML(1)#NMED
      Q#R
      DO 35 NJ#1,90
      LSNO#NJ+1
      X1#X2
      Y1#Y2
      Z1#Z2
      X2#XE
      Y2#YE
      Z2#ZE
      CALL GEOM
      XL(LSNO)#X2
      YL(LSNO)#Y2
      ZL(LSNO)#Z2
      ML(LSNO)#NMED
      IF(MARK)45,20,30
   30 DL(NJ)#Q
      GOTO45
   20 DL(NJ)#DTR
      Q#Q-DTR
   32 IF(NMED-99)35,45,35
   35 CONTINUE
   45 CALL SCORE
      RDEL#6.5E-3
      XS#XS-DCX*RDEL
      YS#YS-DCY*RDEL
      ZS#ZS-DCZ*RDEL
      CALLDIRGE
      IWALL#IWALL
      IF(IWALL-6)60,60,70
   60 NSCAT#NSCAT+1
      W8#W8*PSC
      CALLALBEDO
   42 IF(W8-DEDW8)80,80,10
   80 IF(RAN(RA)-0.5)82,82,83
   82 W8#W8*2.
      GO TO 10
   83 IWALL#9
   70 CALLSTATS
      RETURN
      END
```

will be described first. NSCAT, the number of scatterings experienced by a particle, and W8, its weight, are first initialized. Notice that the weight is not simply set to unity but includes a normalizing factor, which is chosen such that the units of the final answer are flux per unit source current. A source particle position is then selected; in this particular version of HISTOR, it is a uniform source over the rectangle between y = 0 and W, and z = 0 and H, and at x = 0. COSJ (named COSINEJ in the CDC-1604 program) is called to select direction cosines. The last parameter in the calling sequence is the power of cosine of the polar angle from which the selection is to be made. This polar angle is measured from the normal to the surface. The statement "IWALL = 3" is inserted as a marker; it is used only with the statistical estimation version of the code. For statistical estimation, the statement "CALL DETEST" is inserted after the "IWALL = 3" and just before "CALL ALBEDØ" later in the listing. (This is also the case for the CDC-1604 program.) The next three statements initialize parameters for the subroutine GEOM, which is then called. The subroutine GEOM locates all intersection points with system surfaces and stores them in the arrays XL, YL, and ZL. It also determines the distance between each pair of points (stored in array DL), as well as the medium number of the paths (stored in array ML), and packs a storage word specifying the zone and block numbers of each point (stored in array BL).[4] The medium numbers are used to

---

[4]Subroutine GEOM, its function, and use are described more fully in Appendix C.

identify detectors and volumes including the duct walls. Medium numbers from 1 to 89 are reserved for detectors; medium No. 99 is used for duct walls; if regions of void are used, they are designated medium No. 90. No other medium numbers are allowed. The array BL is used only by GEOM itself.

Subroutine SCORE is called to add in flux contributions to the appropriate detectors. It also locates the coordinates of the wall intersection points and stores them in XS, YS, and ZS for GEOM's use on the next flight. Subroutine DIRGE is then called. DIRGE determines which wall has been hit, then sets the variable IWALL appropriately, for later use by other subroutines. (DIRGE allows a maximum of six walls plus the floor and roof.) The cryptic statement "IWALL = IWALL" is necessary because of a peculiarity of the FORTRAN compiler. Suffice it to say that the program will not work correctly without it. The next instruction transfers to statement 60 if IWALL $\leq$ 6 (a normal wall hit) and calls STATS if IWALL > 6. With a normal wall hit, NSCAT is increased by one, the weight is multiplied by the albedo, and the subroutine ALBEDO, which selects new direction cosines, is called. If IWALL is 7, 8, or 9, the history is terminated by calling subroutine STATS. If IWALL is 7, the particle has re-entered the source plane; if IWALL is 8, the particle has left the end of the duct; and if IWALL is 9, the particle must be killed either because its weight has fallen too low, or because the subroutine DIRGE has encountered difficulty locating the wall intersection point. The weight is checked in statement 42. If it is too low

(< DEDW8) a game of Russian Roulette is played (statement 80). This is done by selecting a random number which is compared to PSC, the albedo value. If the random number is smaller, the particle has its weight increased by the factor 1/PSC and continues. Otherwise, the particle is killed. Subroutine STATS then categorizes the particles by the number of scatterings they had and the manner in which their histories were terminated.

The subroutine HISTOR for the CDC-1604 is identical in function to the IBM-7090 HISTOR, differing only in the use of subroutine GEOM. The statement 10 and the next three statements on page 107 are replaced by 33 statements between statements 10 and 35 on page 108. The added complications are caused because: (1) the CDC-1604 GEOM will accept only the end point of the required path, not direction cosines, (2) it follows the track only to the first intersection point with a new medium, and (3) it does not fill in the needed arrays XL, YL, ZL, DL, and ML. The added FORTRAN statements perform these functions. An additional complication is evidenced in the four statements immediately following statement 45. These are required because the CDC-1604 GEOM calculates an intersection point which differs from the true value by 10^{-4} times the original path length (which in this code is always set to 64). The statements mentioned above bring the wall intersection points back along the original path by an amount sufficient to ensure that they lie inside the duct. If this is not done the program occasionally starts paths outside the duct.

Page 113 contains a listing of the subroutine COSJ (named COSINEJ in the CDC-1604 program). This routine selects the direction cosines of a direction distributed uniformly in the azimuthal angle and with the polar angle distributed as $\cos^J\theta$, where θ is the polar angle. The techniques used to do this are explained in Appendix D, along with the results of tests performed with this routine, using the pseudorandom numbers used in the actual machine program.

Page 114 is a listing of subroutine DETEST for the IBM-7090. This routine calculates a statistical estimation of the flux at a series of predetermined detector locations. As written, the routine uses a cosine distribution of the polar angle as the albedo distribution for the estimates. The formula used for the estimation is

$$\phi(r) = \frac{(W8)}{\pi} \frac{\cos\theta}{\ell^2} e^{-d/\lambda} ,$$

where

r = the detector location,

$\phi(r)$ = particle flux at r,

W8 = weight of the particle after scattering,

θ = polar angle of the direction from the scatter point to r,

ℓ = distance from the scatter point to r,

d = portion of path ℓ which consists of duct wall,

λ = relaxation length appropriate for wall penetration.

```
      SUBROUTINE COSJ(DC1,DC2,DC3,J)
      CSTH#0.
      JP#J+1
      DO30I#1,JP
      R#RAN(RA)
      IF(R-CSTH)30,30,20
   20 CSTH#R
   30 CONTINUE
      SITH#SQRTF(1.0-CSTH*CSTH)
   70 FRAN#RAN(RA)
      SRAN#RAN(RA)
      FR2#FRAN*FRAN
      SR2#SRAN*SRAN
      IF(1.0-(FR2+SR2))70,80,80
   80 CSPHI#(FR2-SR2)/(FR2+SR2)
      SIPHI#2.0*FRAN*SRAN/(FR2+SR2)
      IF(RAN(RA)-0.5)90,90,100
   90 SIPHI#-SIPHI
  100 DC1#CSTH
      DC2#SITH*SIPHI
      DC3#SITH*CSPHI
      RETURN
      END
```

```
      SUBROUTINE DETEST
C   NOT SET UP FOR POWER SERIES ALBEDO
      DO100J#1,NUMDET
      LSNO#0
      SIG#0.0
      BLZ#0.0
      WT#0.0
      TD#0.0
      CALL GEOM(XS,YS,ZS,XDET(J),YDET(J),ZDET(J),SIG,BLZ)
      LSM1#LSNO-1
      DO 20 L#1,LSM1
      IF(ML(L)-99)20,10,20
   10 WT#WT+DL(L)
   20 TD#TD+DL(L)
      GO TO (30,30,40,40,50,50),IWALL
   30 D2#ZDET(J)
      D1#ZS
      GOTO60
   40 D2#XDET(J)
      D1#XS
      GOTO60
   50 D2#YDET(J)
      D1#YS
   60 DCP#(D2-D1)/TD
      GO TO (80,70,80,70,80,70),IWALL
   70 DCP#-DCP
   80 IF(DCP)100,100,85
   85 IF(WT/RELAX-50.0)90,100,100
   90 PSQ(J)#PSQ(J)+W8*DCP/TD/TD/EXPF(WT/RELAX)
  100 CONTINUE
      RETURN
      END
```

The factor $1/\pi$ is not included by DETEST but should be included in the normalizing factor CONS included in the initial particle weight. This routine is quite slow in operation partially because it performs an estimate for every detector location, even though the path to the detector may travel through a large thickness of the duct wall. This occurs because subroutine GEOM is called for every path. It would have saved computer time to have written a special geometry routine for this application rather than to have used the extremely general GEOM.

Page 116 lists the corresponding DETEST subroutine for the CDC-1604. It is functionally identical with that for the IBM-7090, differing only because of the different GEOM used. The added complications are because the CDC-1604 GEOM follows the track only to the first intersection point with a new medium and it does not fill in the needed arrays XL, YL, ZL, DL, and ML (see Appendix C).

The listing of subroutine SCORE for the IBM-7090 program is on page 117. In the analogue version of the code, this subroutine checks each medium number in the array ML. If it is between 1 and 89, the volume is a detector and the corresponding track length in that detector, stored in array DL, is multiplied times the weight of the particle and added to the score of that detector. The track is followed until a medium number 99 is encountered, signifying that the particle entered the duct wall.

The corresponding subroutine SCORE for the CDC-1604 is listed

```
      SUBROUTINE DETEST
      COMMON /GEOM/MARK,X2,Y2,Z2,X1,Y1,Z1,NMED,NR,Q,DTR,BLZON
      XL(1)#XS
      YL(1)#YS
      ZL(1)#ZS
      CALL LOOKZ(XS,YS,ZS)
      ML(1)#NM
      DO100J#1,NUMDET
      X2#XS
      Y2#YS
      Z2#ZS
      XE#XDET(J)
      YE#YDET(J)
      ZE#ZDET(J)
      TD#SQRTF((XE-XS)**2+(YE-YS)**2+(ZE-ZS)**2)
      MARK#1
      NMED#NM
      NR#NRE
      BLZON#BLZ
      Q#TD
      JW#0
      WT#0.0
      DO 75 JL#1,90
      LSNO#JL+1
      X1#X2
      Y1#Y2
      Z1#Z2
      X2#XE
      Y2#YE
      Z2#ZE
      CALL GEOM
      XL(LSNO)#X2
      YL(LSNO)#Y2
      ZL(LSNO)#Z2
      ML(LSNO)#NMED
      IF(MARK)100,10,5
    5 DTR#Q
   10 IF(JW)20,20,15
   15 WT#WT+DTR
      IF(WT/RELAX-10.0)20,100,100
   20 IF(MARK)100,25,45
   25 Q#Q-TDR
      IF(NMED-99)55,35,55
   35 JW#1
      GO TO 75
   55 JW#0
   75 CONTINUE
   45 GO TO (30,30,40,40,50,50),IWALL
   30 D2#ZDET(J)
      D1#ZS
      GOTO60
   40 D2#XDET(J)
      D1#XS
      GOTO60
   50 D2#YDET(J)
      D1#YS
   60 DCP#(D2-D1)/TD
      GO TO (80,70,80,70,80,70),IWALL
   70 DCP#-DCP
   80 IF(DCP)100,100,90
   90 PSQ(J)#PSQ(J)+W8*DCP/TD/TD/EXPF(WT/RELAX)
  100 CONTINUE
      RETURN
      END
```

```
      SUBROUTINE SCORE
      DO10K#2,50
      KF#K
      IF(ML(K))20,20,12
   12 IF(ML(K)-99)10,20,10
   10 CONTINUE
      WRITEOUTPUTTAPE9,15
   15 FORMAT(36H  ERROR IN SCORE - NO MEDIUM 0 OR 99)
   20 LEND#KF-1
      DO 40 I#1,LEND
      IF(ML(I))40,40,14
   14 IF(ML(I)-90)16,40,40
   16 IN#ML(I)
      PSQ(IN)#PSQ(IN)+W8*DL(I)
      TOH(IN)#TOH(IN)+1.0
   40 CONTINUE
      XS#XL(KF)
      YS#YL(KF)
      ZS#ZL(KF)
      RETURN
      END
```

```
      SUBROUTINE SCORE
   10 LEND#LSNO-1
      DO 40 I#1,LEND
      IF(ML(I))40,40,14
   14 IF(ML(I)-90)16,40,40
   16 IN#ML(I)
      PSQ(IN)#PSQ(IN)+W8*DL(I)
      TOH(IN)#TOH(IN)+1.0
   40 CONTINUE
   45 XS#XL(LSNO)
      YS#YL(LSNO)
      ZS#ZL(LSNO)
      RETURN
      END
```

near the bottom of page 117. It differs only because subroutine HISTOR has already determined how many of the array entries are valid detector hits (i.e., the point in the array where the particle entered the duct wall).

The next subroutine, DIRGE, is listed on page 119. This routine assigns the parameter IWALL indicating which wall the particle entered. IWALL is used by subroutines ALBEDO and HISTOR to properly handle the collision, depending on which wall was hit. If either no wall was hit or the hit was too close to the intersection of two walls for the routine to be able to decide on one, IWALL is set to 9 and the particle is killed.

When used with straight cylindrical ducts, statement 222 in DIRGE is replaced with:

```
222 IF (ABSF(YS*YS+ZS*ZS-W*W) -DELW)223,223,224
223 IWALL=6
    IW=IW+1
224 IF (IW-1)230,225,230.
```

These statements set IWALL to 6 if the collision point is a normal wall hit. In this case, W is used for the duct radius and the only meaningful rectangular duct parameters are XW1, the position of the source plane , and XW4, the position of the end of the duct. All the others are set to values which will not be achieved by XS, YS, and ZS.

```
      SUBROUTINE DIRGE
      IW#0
      IF(ABSF(ZS-ZW1)-DELW)40,40,50
   40 IWALL#1
      IW#IW+1
   50 IF(ABSF(ZS-ZW2)-DELW)60,60,70
   60 IWALL#2
      IW#IW+1
   70 IF(ABSF(XS-XW2)-DELW)80,80,90
   80 IWALL#3
      IW#IW+1
   90 IF(ABSF(XS-XW3)-DELW)100,100,110
  100 IWALL#4
      IW#IW+1
  110 IF(ABSF(YS-YW1)-DELW)120,120,130
  120 IWALL#5
      IW#IW+1
  130 IF(ABSF(YS-YW2)-DELW)140,140,150
  140 IWALL#6
      IW#IW+1
  150 IF(ABSF(YS-YW3)-DELW)160,160,170
  160 IWALL#5
      IW#IW+1
  170 IF(ABSF(YS-YW4)-DELW)180,180,190
  180 IWALL#6
      IW#IW+1
  190 IF(ABSF(XS-XW1)-DELW)200,200,210
  200 IWALL#7
      IW#IW+1
  210 IF(ABSF(XS-XW4)-DELW)220,220,222
  220 IWALL#8
      IW#IW+1
  222 IF(IW-1)230,225,230
  225 RETURN
  230 WRITEOUTPUTTAPE9,240
  240 FORMAT(54H ERROR IN DIRGE - DID NOT LOCATE SCATTER POINT ON WALL)
      IWALL#9
      W8#0.0
      RETURN
      END
```

Page 121 contains the listing of subroutine ALBEDO used with rectangular ducts. This routine first makes a selection from the power series in $\cos\theta$ representing the albedo distribution, as explained on pages 98 through 102. Then subroutine COSJ (COSINEJ on the CDC-1604) is called to select the direction cosines. These direction cosines (DC1, DC2, and DC3) are then assigned to the actual rectangular coordinate system, depending on which wall the collision occurred.

Also listed on page 121 is an alternate subroutine ALBEDO used for straight cylindrical ducts. The selection from COSJ (or COSINEJ) is identical, but the transformation of the direction cosines to the rectangular coordinate system used by the remainder of the program is different. The direction cosine DC1 supplied by COSJ must be referenced with respect to the normal to the scattering surface and therefore must be directed towards the centerline of the duct. DC2 is taken to be parallel to the duct center line (the x axis). DC3 is tangent to the cylindrical surface and perpendicular to the duct center line.

Subroutine STATS, listed on page 122, is the same in both machine programs. The routine is called at the end of each particle history. Its primary function is to categorize the number of scatterings in the arrays SCNSC, SCNSS, SCNSO, and SCNSK, as outlined previously. It also accumulates the quantities SCOR and SCRSQ for each detector, to be used in the calculation of the single batch variance. SCOR is simply the sum of all scores; SCRSQ is the summation, over the histories, of the squared scores.

```
      SUBROUTINE ALBEDO
C    ALBEDO FOR RECTANGULAR DUCT
      RQ#RAN(RA)
      DO 20 J#1,NCS
      JCOF#J-1
      IF(RQ-PONCS(J))30,30,20
   20 CONTINUE
      JCOF#NCS
   30 CALL COSINEJ(DC1,DC2,DC3,JCOF)
      GO TO (140,150,170,180,200,210,115,115),IWALL
  115 WRITEOUTPUTTAPE9,116,IWALL
  116 FORMAT(26H  ERROR IN ALBEDO - IWALL#I2)
      W8#0.0
      RETURN
  140 DCZ#DC1
      GO TO 160
  150 DCZ#-DC1
  160 DCX#DC2
      DCY#DC3
      RETURN
  170 DCX#DC1
      GO TO 190
  180 DCX#-DC1
  190 DCY#DC2
      DCZ#DC3
      RETURN
  200 DCY#DC1
      GO TO 220
  210 DCY#-DC1
  220 DCZ#DC2
      DCX#DC3
      RETURN
      END
```

```
      SUBROUTINE ALBEDO
C    ALBEDO FOR LONG CYLINDRICAL DUCT
      RQ#RAN(RA)
      DO 20 J#1,NCS
      JCOF#J-1
      IF(RQ-PONCS(J))30,30,20
   20 CONTINUE
      JCOF#NCS
   30 CALL COSINEJ(DC1,DC2,DC3,JCOF)
      DCX#DC2
      DCY#(-DC1*YS+DC3*ZS)/W
      DCZ#(-DC1*ZS-DC3*YS)/W
      RETURN
      END
```

```
      SUBROUTINE STATS
      INDX#IWALL-6
      DO 10 I#1,NUMDET
      SCOR(I)#SCOR(I)+PSQ(I)
      SCRSQ(I)#SCRSQ(I)+PSQ(I)*PSQ(I)
   10 PSQ(I)#0.0
      FN#NSCAT
      DO 20 J#1,40
      JF#J
      IF(FN-CNSC(J))30,30,20
   20 CONTINUE
   30 SCNSC(JF)#SCNSC(JF)+1.0
      GO TO (40,50,60),INDX
   40 SCNSS(JF)#SCNSS(JF)+1.0
      SCSOR#SCSOR+1.0
      RETURN
   50 SCNSO(JF)#SCNSO(JF)+1.0
      SCEND#SCEND+1.0
      WSCOR#WSCOR+W8
      RETURN
   60 SCNSK(JF)#SCNSK(JF)+1.0
      RETURN
      END
```

Subroutine VARUNS, page 124, is also identical in both machine programs. As one of its functions, it accumulates the quantities SUMMNS and SUMMSQ for use in calculating the batch variance for each detector. SUMMNS is simply the sum of the means of all the batches, while SUMMSQ is the sum of the squared means of all the batches. The routine's primary purpose is to combine the means and variances of two independent batches into a mean and variance appropriate to the combined batch. The statements of the subroutine are rewritten below, using more conventional nomenclature on the right-hand sides of the equations. The two batches of events have means $\bar{x}_1$ and $\bar{x}_2$ and variances of their means $\sigma^2_{\bar{x}_1}$ and $\sigma^2_{\bar{x}_2}$, and consist of n_1 and n_2 events. The resultant of the calculation will be a new mean $\bar{x}$ and a new variance $\sigma^2_{\bar{x}}$ for the $n_1 + n_2$ events. All quantities are computed for a particular detector numbered NDET. The statements are:

$$Q = \bar{x}_1$$

$$F = n_1$$

$$F1 = n_1 - 1$$

$$G = n_2$$

$$G1 = n_2 - 1$$

$$AVE = \frac{1}{n_2} \sum_{i=1}^{n_2} x_i = \bar{x}_2$$

$$SUMMNS = \sum_j \bar{x}_j$$

```
      SUBROUTINE VARUNS(NHITS,NDET)
      IF(NHITS-1)10,10,20
   10 RETURN
   20 Q#AVERJ(NDET)
      F#LASNO(NDET)
      F1#F-1.0
      G#NHITS
      G1#G-1.0
      AVE#SCOR(NDET)/G
      SUMMNS(NDET)#SUMMNS(NDET)+AVE
      SUMMSQ(NDET)#SUMMSQ(NDET)+AVE*AVE
      UP#SCOR(NDET)*AVE
      SUMSQ#(SCRSQ(NDET)-UP)/(G1*G)
      AVERJ(NDET)#(AVERJ(NDET)*F+AVE*G)/(F+G)
      P#VAR(NDET)
      R#(AVE-AVERJ(NDET))**2
      T#(Q-AVERJ(NDET))**2
      S#F+G
      S1#S-1.0
      VAR(NDET)#(G*G1*SUMSQ+F*F1*P+G*R+F*T)/(S*S1)
      SCOR(NDET)#0.0
      SCRSQ(NDET)#0.0
      LASNO(NDET)#LASNO(NDET)+NHITS
      RETURN
      END
```

$$\text{SUMMSQ} = \sum_{j} (\overline{x}_j)^2$$

$$\text{UP} = \frac{1}{n_2} \left(\sum_{i=1}^{n_2} x_i \right)^2$$

$$\text{SUMSQ} = \frac{1}{n_2(n_2 - 1)} \left\{ \sum_{i=1}^{n_2} (x_i)^2 - \frac{1}{n_2} \left[\sum_{i=1}^{n_2} x_i \right]^2 \right\} \equiv \sigma^2_{\overline{x}_2}$$

$$\text{AVERJ} = \frac{n_1 \overline{x}_1 + n_2 \overline{x}_2}{n_1 + n_2} \equiv \overline{x}$$

$$P = \sigma^2_{\overline{x}_1}$$

$$R = (\overline{x}_2 - \overline{x})^2$$

$$T = (\overline{x}_1 - \overline{x})^2$$

$$S = n_1 + n_2$$

$$S1 = n_1 + n_2 - 1$$

$$\text{VAR} = \frac{1}{(n_1 + n_2)(n_1 + n_2 - 1)} \left\{ n_2(n_2 - 1)\ \sigma^2_{\overline{x}_2} + n_1(n_1 - 1)\ \sigma^2_{\overline{x}_1} \right.$$

$$\left. + n_2(\overline{x}_2 - \overline{x})^2 + n_1(\overline{x}_1 - \overline{x})^2 \right\} \equiv \sigma^2_{\overline{x}}$$

$$\text{SCOR} = 0$$

$$\text{SCRSQ} = 0$$

$$\text{LASNO} = n_1 + n_2$$

Page 127 is a listing of the subroutine OUTPUT for both machine programs. A sample of the output produced by this routine is given on pages 128 and 129. Both the single batch variance (VAR) and the batch variance (ALTVAR) are listed along with a percentage standard deviation (PV) computed as the square root of VAR divided by the flux, AVERJ, and expressed as a percentage.

Page 130 contains listings of the subroutines PICTUR (IBM-7090) and PICTURE (CDC-1604), which plot the calculated fluxes versus distance along the duct center line, using the CALCOMP plotter at ORNL's Computing Center.[5]

Page 131 contains listings of the function RAN, the pseudorandom number generator, in its IBM-7090 and CDC-1604 versions. The IBM-7090 version, at the top of the page, is written in the assembly language FAP. The starting octal random number is multiplied by $5^{15}(34327724461 5_8)$. The 35 least significant bits of the product are stored for use the next time. This quantity is then converted to a floating point number between 0 and 1 which can be used by the FORTRAN routines. The CDC -1604 version, written in the assembly language CODAP-1, is quite similar in principle. Since the CDC-1604 has 48 bit storage cells rather than 36, slightly different numbers are used. The constant multiplier is 5^{19} (labelled FIV19 and equal to $42543443011047 5_8$). Tests performed on these routines are described in Appendix D.

---

[5]Details of the subroutines which are called to do this plotting are given by D. K. Trubey and M. B. Emmett, An IBM-7090 Subroutine Package for Making Logarithmic and Semilogarithmic Graphs Using the CALCOMP Plotter, ORNL-TM-430 (Dec. 12, 1962).

```
      SUBROUTINE OUTPUT
      WRITEOUTPUTTAPE9,120,SCSOR
  120 FORMAT(F20.1,28H PARTICLES RE-ENTERED SOURCE)
      WRITEOUTPUTTAPE9,130,SCEND
  130 FORMAT(F20.1,25H PARTICLES TRAVERSED DUCT)
      WRITEOUTPUTTAPE9,140,WSCOR
  140 FORMAT(20X23HEXIT WEIGHTED PARTICLESF20.9)
      WRITEOUTPUTTAPE9,150
  150 FORMAT(93H    NO SCATTERINGS       TOTAL PARTICLES       LOST TO SOU
     IRCE         SCORED                KILLED)
      WRITEOUTPUTTAPE9,160,(CNSC(I),SCNSC(I),SCNSS(I),SCNSO(I),SCNSK(I),
     II#1,40)
  160 FORMAT(F11.1,F24.1,F20.1,F18.1,F20.1)
      WRITEOUTPUTTAPE9,101
  101 FORMAT(1H1)
      WRITEOUTPUTTAPE9,190
  190 FORMAT(118H     DETECTOR       AVE SCORE            VARIANCE
     INO HITS       SCORE         PERCENT STANDARD DEVIATION  BATCH VAR)
      DO200N#1,NUMDET
      TOTSCOR#AVERJ(N)*FLOATF(LASNO(N))*CONS
      PV#SQRTF(VAR(N))/AVERJ(N)*100.0
  200 WRITEOUTPUTTAPE9,220,N,AVERJ(N),VAR(N),TOH(N),TOTSCOR,PV,ALTVAR(N)
  220 FORMAT(I10,2F20.9,F10.1,3F20.9)
      RETURN
      END
```

END

2

ALBEDO# 0. + 1.00000 +
NHIST# 4000, RA# 153245743735, W# 3.00, F# 8.00, PSC# 0.75000, NBATCH#200, NSKILT#100, DEDW8# 0.10000E-04
ERROR IN DIRGE - DID NOT LOCATE SCATTER POINT ON WALL
ERROR IN DIRGE - DID NOT LOCATE SCATTER POINT ON WALL
ERROR IN DIRGE - DID NOT LOCATE SCATTER POINT ON WALL
ERROR IN DIRGE - DID NOT LOCATE SCATTER POINT ON WALL
ERROR IN DIRGE - DID NOT LOCATE SCATTER POINT ON WALL
3243.0 PARTICLES RE-ENTERED SOURCE
528.0 PARTICLES TRAVERSED DOOT
EXIT WEIGHTED PARTICLES 11.837659478

NO SCATTERINGS	TOTAL PARTICLES	LOST TO SOURCE	SCORED	KILLED
1.0	943.0	943.0	0.	0.
2.0	460.0	460.0	0.	0.
3.0	326.0	324.0	2.0	0.
4.0	233.0	231.0	2.0	0.
5.0	182.0	177.0	5.0	0.
6.0	145.0	140.0	5.0	0.
7.0	113.0	93.0	17.0	3.0
8.0	100.0	86.0	14.0	0.
9.0	92.0	78.0	14.0	0.
11.0	166.0	139.0	25.0	2.0
13.0	117.0	82.0	35.0	0.
15.0	119.0	82.0	37.0	0.
17.0	106.0	66.0	40.0	0.
19.0	101.0	52.0	49.0	0.
21.0	63.0	37.0	26.0	0.
23.0	74.0	41.0	33.0	0.
25.0	61.0	28.0	33.0	0.
27.0	59.0	33.0	26.0	0.
29.0	52.0	27.0	25.0	0.
31.0	60.0	32.0	28.0	0.
33.0	43.0	20.0	23.0	0.
35.0	39.0	19.0	20.0	0.
37.0	47.0	17.0	30.0	0.
39.0	21.0	10.0	11.0	0.
41.0	83.0	17.0	11.0	55.0
43.0	90.0	4.0	9.0	77.0
45.0	53.0	1.0	4.0	48.0
47.0	28.0	2.0	2.0	24.0
49.0	11.0	0.	1.0	10.0
51.0	3.0	1.0	0.	2.0
53.0	5.0	1.0	1.0	3.0
55.0	3.0	0.	0.	3.0
57.0	1.0	0.	0.	1.0
59.0	1.0	0.	0.	1.0
61.0	0.	0.	0.	0.
63.0	0.	0.	0.	0.
65.0	0.	0.	0.	0.
67.0	0.	0.	0.	0.
69.0	0.	0.	0.	0.
71.0	0.	0.	0.	0.

DETECTOR	AVE SCORE	VARIANCE	NO HITS	SCORE	PERCENT STANDARD DEVIATION	BATCH VAR
1	2.449344993	0.000740498	8785.0	4898.689941406	1.110996962	0.000531085
2	2.050602019	0.000611961	8433.0	4101.203979492	1.206370011	0.000626132
3	1.864286840	0.000718936	8309.0	3728.573669434	1.438247427	0.000716805
4	1.638770863	0.000647143	8089.0	3277.541717529	1.552322894	0.000912279
5	1.385267183	0.000513904	7782.0	2770.534362793	1.636477992	0.000526264
6	1.306166187	0.000593379	7734.0	2612.332366943	1.864954382	0.000329137
7	1.183566943	0.000540100	7610.0	2367.133880615	1.963571146	0.000297949
8	1.060545787	0.000493854	7390.0	2121.091552734	2.095427424	0.000470310
9	0.954884216	0.000430234	7197.0	1909.768417358	2.172210127	0.000359155
10	0.849485047	0.000347406	6995.0	1698.970092773	2.194136798	0.000273205
11	0.780328676	0.000333950	6963.0	1560.657348633	2.341891229	0.000327632
12	0.716677159	0.000314102	6827.0	1433.354309082	2.472952127	0.000145882
13	0.686251283	0.000318654	6783.0	1372.502563477	2.601241887	0.000130355
14	0.670297645	0.000340536	6765.0	1340.595275879	2.753055751	0.000249214
15	0.679918990	0.000339902	6690.0	1359.837966919	2.907903880	0.000339575
16	0.509432256	0.000297673	6015.0	1018.864509583	3.386765718	0.000125580
17	0.421725601	0.000220612	5778.0	843.451202393	3.521976918	0.000185445
18	0.349411741	0.000168934	5613.0	698.823478699	3.719847828	0.000192098
19	0.293804608	0.000115573	5439.0	587.609222412	3.659074455	0.000124328
20	0.264662743	0.000076500	5400.0	529.325485229	3.711818039	0.000100218
21	0.233052663	0.000079609	5213.0	466.105327606	3.828509152	0.000090159
22	0.204302505	0.000066787	4993.0	408.605018616	4.000198603	0.000093721
23	0.192750491	0.000068612	4860.0	385.500991821	4.297535896	0.000118136
24	0.164516084	0.000054404	4664.0	329.032165527	4.483694732	0.000073738
25	0.142258428	0.000042737	4501.0	284.516860962	4.595681727	0.000045732
26	0.128595747	0.000037946	4387.0	257.191501617	4.790268600	0.000057265
27	0.111457743	0.000029914	4081.0	222.915493011	4.907580316	0.000030607
28	0.101169161	0.000024773	3996.0	202.338323593	4.919862509	0.000027426
29	0.099240370	0.000032112	3865.0	198.480745316	5.710438132	0.000032760
30	0.091501638	0.000024304	3741.0	183.003276625	5.388329089	0.000027455
31	0.083752215	0.000021301	3619.0	167.504403108	5.510749221	0.000025168
32	0.078866862	0.000019252	3523.0	157.733726501	5.563967586	0.000024721
33	0.077621914	0.000020646	3422.0	155.243837357	5.853895426	0.000020504
34	0.066694595	0.000026137	2875.0	133.389196396	7.666294456	0.000021987
35	0.066054873	0.000028864	2880.0	132.109748840	8.133619547	0.000030935
36	0.059953168	0.000021845	2786.0	119.906342506	7.796062887	0.000026844
37	0.060104743	0.000023119	2745.0	120.209486008	8.000094056	0.000020199
38	0.060312919	0.000021428	2683.0	120.625849724	7.675824821	0.000028238
39	0.055919312	0.000020921	2601.0	111.838636398	8.179875970	0.000031106
40	0.039570116	0.000012070	2398.0	79.140239716	8.779857159	0.000010282
41	0.029026955	0.000006057	2213.0	58.053916454	8.480365276	0.000006542
42	0.024198495	0.000004694	2080.0	48.396994114	8.955998421	0.000004522
43	0.020263933	0.000002794	1967.0	40.527878761	8.257939816	0.000003248
44	0.017811514	0.000002518	1865.0	35.623032570	8.918631673	0.000003286
45	0.016143896	0.000002891	1715.0	32.287804127	10.532115698	0.000003234
46	0.013526328	0.000001639	1597.0	27.052656174	9.485372066	0.000002146
47	0.011718709	0.000001080	1490.0	23.437421799	8.873281360	0.000001833
48	0.010732949	0.000001028	1397.0	21.465899706	9.471399426	0.000001520
49	0.009606481	0.000001147	1230.0	19.212964296	11.178197026	0.000001840
50	0.009185858	0.000001073	1113.0	18.371716499	11.281479239	0.000001527
51	0.008671433	0.000001311	1063.0	17.342878819	13.223006487	0.000001699
52	0.007020511	0.000000767	934.0	14.041028380	12.508560657	0.000000864
53	0.006081872	0.000000499	809.0	12.163761483	11.696847081	0.000000790
54	0.005519964	0.000000827	692.0	11.039929628	16.532338858	0.000001028

```
      SUBROUTINE PICTUR
      CALL SEMLOG(NCY,ITOPY,XZERO,DELTAX,NOINT,A5)
      CALL LETTER(0,NHC,TITL(LETPAR),A5)
      CALL LETTER(1,23,23HCENTERLINE DISTANCE, FT,A5)
      CALL LETTER(2,68,68HNEUTRON FLUX PER SOURCE NEUTRON CURRENT - NEUT
     1RON/CM  PER NEUTRON/CM,A5)
      CALL EXPON(2,68,52,1H2,A5)
      CALL EXPON(2,68,68,1H2,A5)
      DO 10 JL#1,NUMDET
      R#AVERJ(JL)
      S#2.0*SQRTF(VAR(JL))
      T#R+S
      CALL CURVE(JL,XPLOT,U,A5)
      U#R-S
      XPLOT#XPOS(JL)
      CALL POINT(XPLOT,R,4,0.04,A5)
      IF(U)10,10,5
    5 CALL POINT(XPLOT,U,5,0.02,A5)
   10 CALL POINT(XPLOT,T,5,0.02,A5)
      CALL ADVANC
      RETURN
      END
```

```
      SUBROUTINE PICTURE
      CALL SEMLOG(NCY,ITOPY,XZERO,DELTAX,NOINT,8.0,6,A5)
      CALL LETTER(0,NHC,TITL,A5)
      CALL LETTER(1,23,23HCENTERLINE DISTANCE, FT,A5)
      CALL LETTER(2,68,68HNEUTRON FLUX PER SOURCE NEUTRON CURRENT - NEUT
     1RON/CM  PER NEUTRON/CM,A5)
      CALL EXPON(2,68,52,1H2,A5)
      CALL EXPON(2,68,68,1H2,A5)
      DO 10 JL#1,NUMDET
      R#AVERJ(JL)
      S#2.0*SQRTF(VAR(JL))
      T#R+S
      U#R-S
      CALL CURVE(JL,XPOS(JL),R,A5)
      CALL POINT(JL,XPOS(JL),T,13,0.04,90.0,1,A5)
    5 CALL POINT(JL,XPOS(JL),U,13,0.04,90.0,1,A5)
   10 CALL POINT(JL,XPOS(JL),R,4,0.04,90.0,1,A5)
      CALL ADVANCE(A5)
      RETURN
      END
```

```
        COUNT   11
        ENTRY   RAN
RAN     SXD     *-2,4
        LDQ     #0343277244615
        MPY*    1,4
        STQ*    1,4
        CLA     FLOAT
        LLS     27
        FAD     FLOAT
        TRA     2,4
FLOAT   OCT     170000000200
        END
```

```
        IDENT       RAN
        ENTRY       RAN
RAN     SLJ         **
        STA         DUMMY
        LDA         RAN
        ARS         24
        INA         1
        SAU         RAN
        LDA         FIV19
        MUI     7   DUMMY
        STA     7   DUMMY
        LDQ         LOG1
        LLS         84
        FAD         LOG1
        SLJ         RAN
FIV19   OCT         0425434430110475
LOG1    OCT         0176400000002000
DUMMY   50
        END
```

APPENDIX B

IDENTIFICATION OF IMPORTANT SYMBOLS USED IN MACHINE PROGRAMS

A5 - A 5-cell array set aside for the plotting routines (6-cell on CDC-1604).

ADDR - Array set aside for GEOM input (JOMIN) storage.

ALTVAR - Variance of the overall mean, calculated using batches of particles.

AVERJ - Total accumulated score for each detector, divided by the number of source particles (upon output, normalized to give particle flux per particle current leaving source plane).

BL - Array used by GEOM, containing a packed word describing the zone and block location of a point.

BLZ - Same as BL(1); set to zero when GEOM is called.

CNSC - Array giving values of the number of scatterings used in calculating histograms of particles versus their number of scatterings.

CONS - Constant which normalizes scores to particle flux per source particle current.

DCX - Direction cosine in the x-direction.

DCY - Same as DCX for y.

DCZ - Same as DCX for z.

DEDW8 - Weight below which particles are killed.

DELTAX - Spacing of abscissa labels in plots.

DELW - Maximum spacing of intersection point from wall position to be considered an intersection.

DL - Array filled in by GEOM, DL(I) contains distance from X(I), Y(I), Z(I) to next intersection point.

H - Height of rectangular duct.

INDX - Index used by STATS to categorize scatterings of particles which re-entered source (=1), left the end of duct (=2), or were killed (=3).

ITOPY - Exponent of 10 which is maximum ordinate value to be plotted.

IWALL - Index calculated by DIRGE to indicate which wall a collision occurred on.

LASNO - Accumulated number of histories.

LETPAR - Parameter calculated by HOLLER in input and used by LETTER in PICTUR to draw title of plot.

LSNO - Parameter in GEOM.

ML - Array filled by GEOM with medium numbers of intersection points.

NADD - Used in CDC-1604 GEOM to designate first address to be used for storage of GEOM input.

NBATCH - Number of histories accumulated for each batch score to be used to calculate batch variance.

NCS - Largest exponent of cosine of polar angle to be used in albedo distribution function.

NCY - Number of cycles on ordinate of plot.

NHC - Number of Hollerith characters read in by HOLLER (title of plot).

NHIST - Number of histories to be run.

NOINT - Number of intervals on abscissa of plot.

NSCAT - Number of scatterings undergone by a particle.

NSKILT - Number of scatterings above which a particle is killed.

NUMDET - Number of detectors.

PONCS - Coefficients of power series (in the cosine of the polar angle) which represents the albedo distribution.

PSC - Integral value of albedo (probability of re-emission from wall).

PSQ - Array of accumulated scores in detectors during a history.

RA - Octal random number.

RELAX - Relaxation length for exponential corner penetration probability.

SCEND - Number of particles traversing duct.

SCNSC - Array giving histogram of particles having undergone a number of scatterings within limits specified by CNSC.

SCNSK - Similar to SCNSC for particles which were killed.

SCNSO - Similar to SCNSC for particles completely traversing duct.

SCNSS - Similar to SCNSC for particles re-entering source.

SCOR - Array of accumulated detector scores (cleared by VARUNS every NBATCH histories).

SCRSQ - Array of accumulated squares of detector hits (accumulated each history and cleared every NBATCH histories).

SCSOR - Number of particles which re-entered source.

SIG - Signal given GEOM specifying whether direction cosines (=1) or an end point (=0) was given.

SUMCOF - Integral of power series representing differential albedo, used to renormalize the series properly.

SUMMNS - Sum of batch means.

SUMMSQ - Sum of squares of batch means.

TITL - Hollerith array for title of plot.

TOH - Array giving total number of hits for each detector.

VAR - Variance of overall mean, for each detector.

W - Width of rectangular duct; also used as radius of cylindrical duct.

W8 - Weight of particle.

WSCOR - Sum of weights of particles completely traversing duct.

XDET - Array of x-coordinates of detectors.

XL - Array of x-coordinates of intersection points (from GEOM).

XPOS - Array of center-line coordinates of detectors (used in plotting).

XS - X-coordinate of scattering point.

XW1 - X-coordinate of source plane.

XW2 - X-coordinate of second leg wall.

XW3 - X-coordinate of second leg wall (XW3 > XW2).

XW4 - X-coordinate of end of duct.

XZERO - Smallest abscissa value used in plot.

YDET - Array of y-coordinates of detectors.

YL - Array of y-coordinates of intersection points (calculated by GEOM).

YS - Y-coordinate of scattering point.

YW1 - Y-coordinates of duct walls.

YW2 - Y-coordinates of duct walls.

YW3 - Y-coordinates of duct walls.

YW4 - Y-coordinates of duct walls.

ZDET - Array of z-coordinates of detectors.

ZL - Array of z-coordinates of intersection points (calculated by GEOM).

ZS - Z-coordinate of scattering point.

ZW1 - Z-coordinates of floor and roof of duct.

ZW2 - Z-coordinates of floor and roof of duct.

APPENDIX C

DESCRIPTIONS OF THE GEOMETRY SUBROUTINES AND INPUTS

The general-purpose geometry routine, GEOM,[1] is available in two principal versions. One version is written in the IBM assembly language FAP and is intended for use on the IBM-7090. It was written as a general routine for treating complex geometries in Monte Carlo and other types of calculations. The other version is written largely in the FORTRAN language and was used in the CDC-1604 version of the Albedo Monte Carlo machine program. It was written specifically for the 05R Monte Carlo system, but is quite similar in use to the FAP version. Only the features of the routines which were used in this study will be described.

The basic purpose of both routines is to take any straight-line path through the configuration and determine the media through which it passes and the length of the path segment in each medium.

The geometry specification is quite general, permitting very complex geometries. The entire system of interest must be enclosed in a parallelepiped whose faces are parallel to the coordinate planes. This system may then be divided into one or more parallelepipeds, called "zones," by planes which are parallel to the coordinate planes and extend completely across the system. Similarly each zone may be divided,

---

[1]Descriptions of the use of GEOM and the routines themselves were obtained from D. Irving, Neutron Physics Division, Oak Ridge National Laboratory.

independently, into smaller parallelepipeds, called "blocks." Each block or zone boundary may be a medium boundary, if desired. In addition, medium boundaries may be specified by surfaces defined by the zeros of general quadratic functions. Two examples of geometries and their inputs are given later in this appendix.

The FAP version of GEOM will accept a path specification either by the coordinates of the starting and ending points of the path or by the coordinates of the starting point and the direction cosines of the path. It then follows the entire path (to the system boundary, if direction cosines are given), filling in six arrays which are provided in the main program. These arrays will contain the coordinates of each point where the path changes media, the medium numbers along the path, the distances between the intersection points, and an array of packed words giving the block and zone locations of each point. For each path GEOM is called with the FORTRAN statement

```
CALL GEOM(X1,Y1,Z1,X2,Y2,Z2,SIGNAL,BLZON).
```

X1, Y1, Z1 are the starting-point coordinates. If SIGNAL = 0, then X2, Y2, and Z2 are the endpoint coordinates. If SIGNAL $\neq$ 0, then X2, Y2, and Z2 are the direction cosines of the path. BLZON, the packed word containing the block and zone of X1, Y1, Z1, is set to zero initially if it is not known.

The FORTRAN version of O5R-GEOM will only accept the starting and ending points of a path, and it only follows the path until it reaches a

boundary where a medium change occurs. It then returns with the coordinates of the intersection point, its medium number, and the distance travelled. The routine is called by the sequence:[2]

```
CALL GEOM(MARK,X2,Y2,Z2,X1,Y1,Z1,NMED,NREG,R,RUSED,BLZON)
```

where MARK signals the type of collision upon return and

MARK = 1 for completed flight,

= 0 for normal medium boundary crossing,

= -1 for escape from system,

X2,Y2,Z2 = initially endpoint coordinates and upon return give the intersection point,

X1,Y1,Z1 = starting point coordinates,

NMED = medium number of X1, Y1, Z1 initially and medium number of X2, Y2, Z2 upon return,

NREG = region[3] number of X2, Y2, Z2 (given only when MARK = 1),

R = length of the path given GEOM,

RUSED = actual path length (not given if MARK = 1),

BLZON = packed word giving block and zone locations of X1, Y1, Z1 upon entry, and X2, Y2, Z2 upon exit.

---

[2]The GEOM used in the CDC-1604 program described in Appendix A has a slightly different calling sequence being a later FORTRAN version using the labelled COMMON feature of CDC's FORTRAN-62 (see Ref. 9 in Bibliography).

[3]Region descriptions are a feature used in O5R which are not used in the albedo Monte Carlo program.

To obtain NMED, NREG, and BLZON initially, the subroutine LOOKZ must be called, as follows:

```
CALL LOOKZ(X1,Y1,Z1,NMED,NREG,BLZON,1).
```

Special input routines are contained in both GEOM packages which read the necessary geometry input cards and, in the case of the FAP version, perform several checks and then print out the input data. The FAP version input is called by the following statement:

```
CALL JOMIN(LISTNO,XL,YL,ZL,DL,ML,BL,ADDR).
```

LISTNO is the dimension of the arrays XL, YL, ZL, DL, ML, and BL, which are used by GEOM to store the path descriptions. ADDR, as used in this program, is the name of the FORTRAN variable which sets aside room in the COMMON storage for geometry input storage.

The FORTRAN GEOM input is called by the following statement:

```
CALL JOMIN(NADD),
```

where NADD is the difference between the first location in the COMMON storage and the first location which is available for geometry input storage.

Two examples of GEOM inputs will be given. The first will be a three-legged rectangular duct configuration containing 54 parallelepiped detectors, written in the free-field format used by the FAP GEOM.

The second configuration will be the same three-legged duct with no detectors, using the FORTRAN input format.

Figure 54 shows the zone configuration of a three-legged duct with a 3 x 6 ft cross section. System boundaries are at x = 0 and 45 ft, y = -3 and 60 ft, and z = -3 and 15 ft. Zone boundaries are located at y = 0, 3, 12, and 15 ft, and z = 0 and 6 ft. This divides the system into 15 zones shown in the figure, all extending from x = 0 to 45 ft. The duct system is contained in zones 7, 8, and 9, shown cross-hatched in the figure. The surrounding 12 zones are included to ensure that points on the duct walls are well inside the system. (In some cases, if a starting point that is slightly outside the system is given to GEOM, errors will occur.)

Figure 55 is a cross section of the essential portions of zones 7, 8, and 9; it shows the block configuration in these zones and the various medium numbers that are assigned. Zone 7 is divided by planes from x = 0.5 to 7.5 ft in 0.5-ft steps. The first 15 blocks thus formed are assigned medium Nos. 1 to 15 for use as detectors. Note that this forms a set of 15 detectors, each 0.5 ft thick and covering the full 3 x 6 ft cross section of the duct. The 16th block is assigned medium No. 99, labelling it as a duct wall. Zone 8 is divided into 54 blocks by planes at x = 4.5 and 7.5 ft and, in steps of 0.5 ft, from y = 3.5 to 11.5 ft. The 36 blocks thus formed which are located from x = 0 to 4.5 ft and x > 7.5 ft are all assigned medium number 99. The 18 blocks

UNCLASSIFIED
ORNL DWG 63-3057

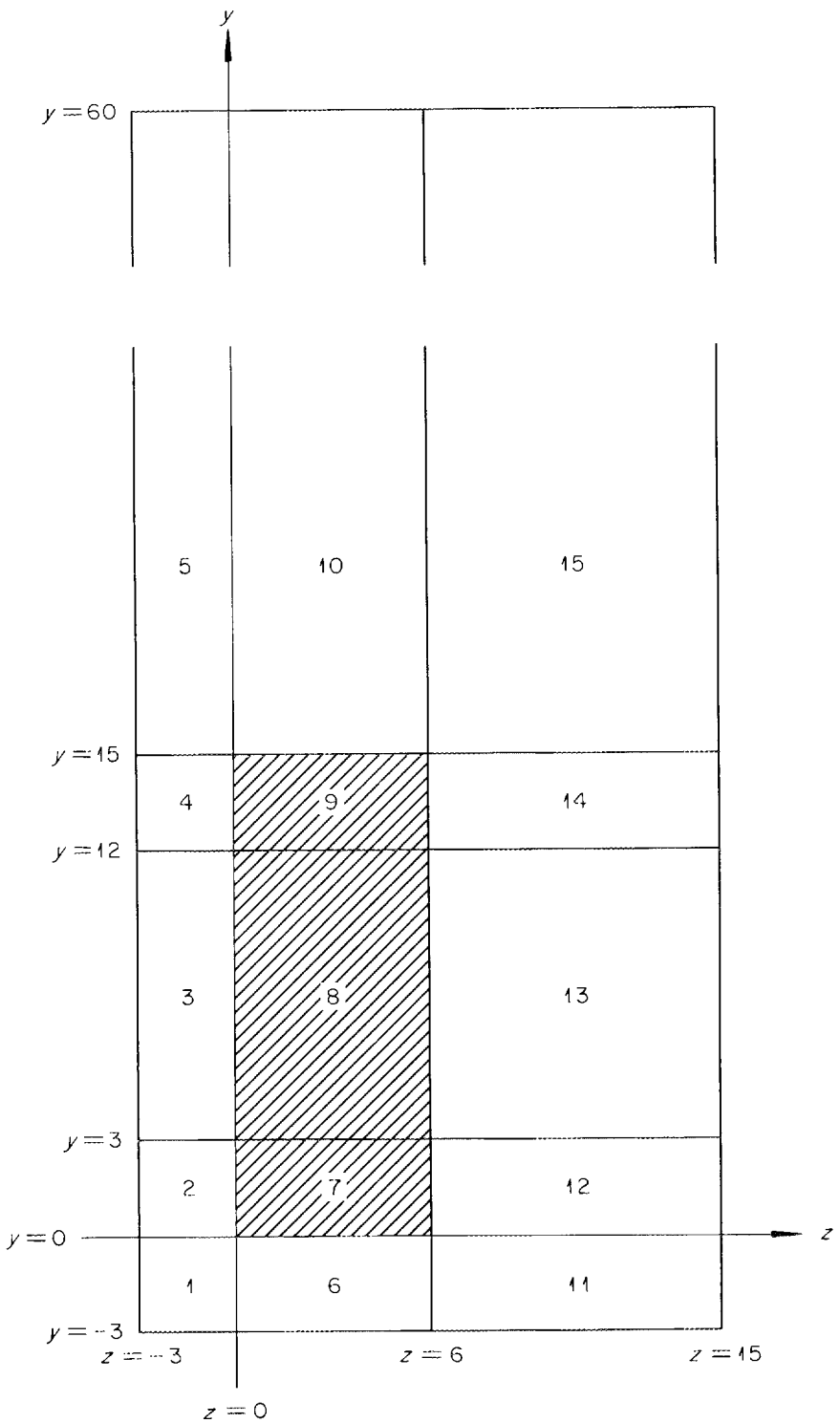

Fig. 54. Zone Configuration of Three-Legged Duct Geometry.

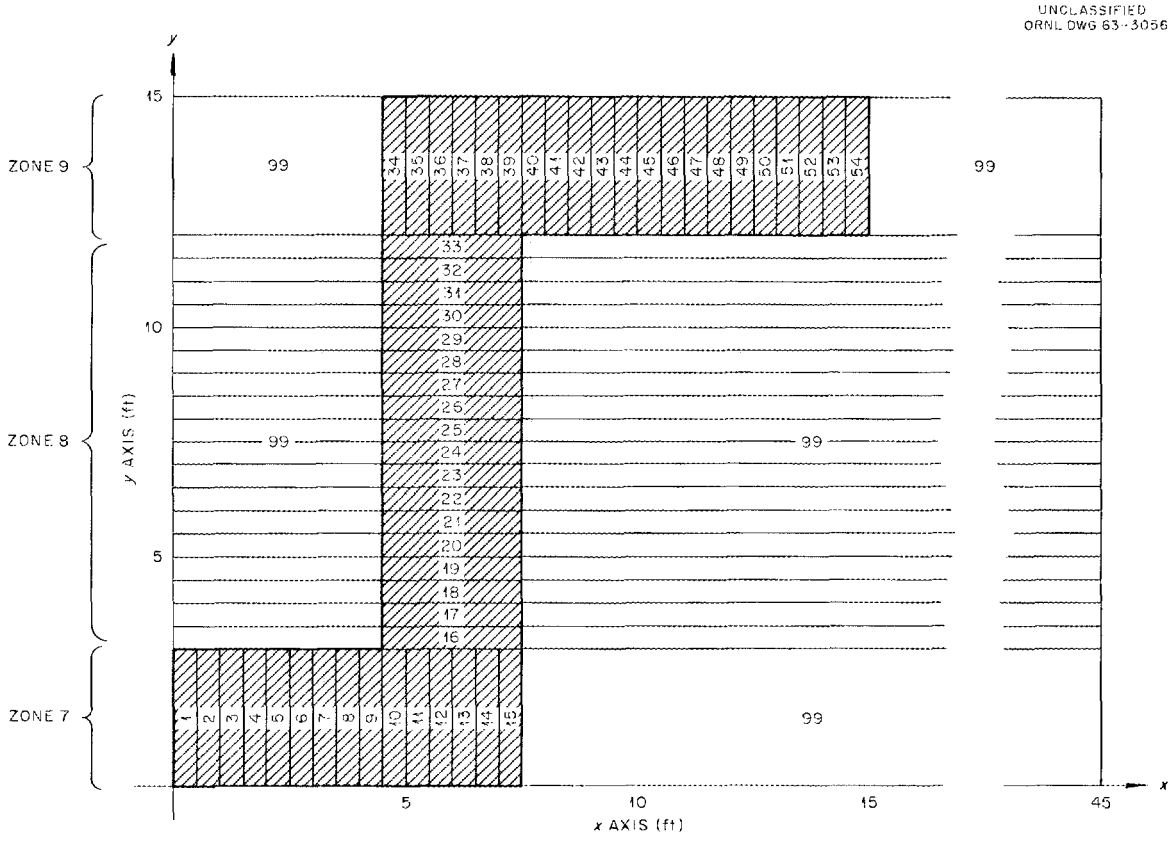

Fig. 55. Block Configuration of Zones 7, 8, and 9 of Three-Legged Duct Geometry.

between x = 4.5 and 7.5 ft are assigned medium numbers between 16 and 33 for use as detectors. Zone 9 is divided into blocks by planes running from x = 4.5 to 15 ft in 0.5-ft steps. The first block (x = 0 to 4.5 ft) and the last block (x > 15 ft) are assigned medium No. 99. The blocks between x = 4.5 and x = 15 ft are assigned medium numbers from 34 to 54. A listing of the input cards for this geometry, as they are reproduced on the output listing, is given on the next three pages. This geometry uses 1085_{10} storage locations.

The second geometry to be described is similar except that no detectors are used. The duct volume is assigned medium No. 90, indicating void. The zone configuration is the same as that shown in Fig. 54. Zone 7 has two blocks divided by the plane x = 7.5 ft with the volume x < 7.5 having medium number 90 and x > 7.5 having medium number 99. Similarly, zone 8 is divided into three blocks by planes at x = 4.5 and 7.5 ft. These three blocks have medium numbers 99, 90, and 99, respectively. Zone 9 is also divided into three blocks having medium numbers 99, 90, and 99 by planes at x = 4.5 and 15 ft. The listing of this input is given on the last three pages of this appendix.

```
X ZONE BOUNDARIES 0,45
Y ZONE BOUNDARIES -3,0,3,12,15,60
Z ZONE BOUNDARIES -3,0,6,15
ZONE 1,1,1
X BLOCK  0,45   Y BLOCK  -3,0   Z BLOCK  -3,0
BLOCK 1,1,1   MEDIA 99
ZONE 1,2,1
X BLOCK  0,45   Y BLOCK   0,3   Z BLOCK  -3,0
BLOCK 1,1,1   MEDIA 99
ZONE 1,3,1
X BLOCK  0,45   Y BLOCK   3,12  Z BLOCK  -3,0
BLOCK 1,1,1   MEDIA 99
ZONE 1,4,1
X BLOCK  0,45   Y BLOCK  12,15  Z BLOCK  -3,0
BLOCK 1,1,1   MEDIA 99
ZONE 1,5,1
X BLOCK  0,45   Y BLOCK  15,60  Z BLOCK  -3,0
BLOCK 1,1,1   MEDIA 99
ZONE 1,1,2
X BLOCK  0,45   Y BLOCK  -3,0   Z BLOCK   0,6
BLOCK 1,1,1   MEDIA 99
ZONE 1,2,2
X BLOCK BOUNDARIES 0,2.25,3.75,5.25,7.5,45
Y BLOCK BOUNDARIES 0,3
Z BLOCK BOUNDARIES 0,6
BLOCK 1,1,1
MEDIA 90,1
SURFACE 1
SECTOR +1
SECTOR -1
BLOCK 2,1,1
MEDIA 90,2
SURFACE 2
SECTOR +1
SECTOR -1
BLOCK 3,1,1
MEDIA 90,3
SURFACE 3
SECTOR +1
SECTOR -1
BLOCK 4,1,1
MEDIA 90,4
SURFACE 4
SECTOR +1
SECTOR -1
BLOCK 5,1,1
MEDIA 99
ZONE 1,3,2
X BLOCK BOUNDARIES 0,4.5,7.5,45
Y BLOCK BOUNDARIES 3,4.5,6,7.5,9,10.5,12
Z BLOCK BOUNDARIES 0,6
BLOCK 1,1,1
MEDIA 99
BLOCK 2,1,1
MEDIA 90,5
SURFACE 5
SECTOR +1
SECTOR -1
BLOCK 3,1,1
MEDIA 99
BLOCK 1,2,1
```

```
MEDIA 99
BLOCK 2,2,1
MEDIA 90,6
SURFACE 6
SECTOR +1
SECTOR -1
BLOCK 3,2,1
MEDIA 99
BLOCK 1,3,1
MEDIA 99
BLOCK 2,3,1
MEDIA 90,7
SURFACE 7
SECTOR +1
SECTOR -1
BLOCK 3,3,1
MEDIA 99
BLOCK 1,4,1
MEDIA 99
BLOCK 2,4,1
MEDIA 90,8
SURFACE 8
SECTOR +1
SECTOR -1
BLOCK 3,4,1
MEDIA 99
BLOCK 1,5,1
MEDIA 99
BLOCK 2,5,1
MEDIA 90,9
SURFACE 9
SECTOR +1
SECTOR -1
BLOCK 3,5,1
MEDIA 99
BLOCK 1,6,1
MEDIA 99
BLOCK 2,6,1
MEDIA 90,10
SURFACE 10
SECTOR +1
SECTOR -1
BLOCK 3,6,1
MEDIA 99
ZONE 1,4,2
X BLOCK BOUNDARIES 0,4.5,6.75,8.25,9.75,11.25,12.75,15,45
Y BLOCK BOUNDARIES 12,15
Z BLOCK BOUNDARIES 0,6
BLOCK 1,1,1
MEDIA 99
BLOCK 2,1,1
MEDIA 90,11
SURFACE 11
SECTOR +1
SECTOR -1
BLOCK 3,1,1
MEDIA 90,12
SURFACE 12
SECTOR +1
SECTOR -1
BLOCK 4,1,1
```

```
MEDIA 90,13
SURFACE 13
SECTOR +1
SECTOR -1
BLOCK 5,1,1
MEDIA 90,14
SURFACE 14
SECTOR +1
SECTOR -1
BLOCK 6,1,1
MEDIA 90,15
SURFACE 15
SECTOR +1
SECTOR -1
BLOCK 7,1,1
MEDIA 90,16
SURFACE 16
SECTOR +1
SECTOR -1
BLOCK 8,1,1
MEDIA 99
ZONE 1,5,2
X BLOCK  0,45   Y BLOCK  15,60  Z BLOCK   0,6
BLOCK 1,1,1   MEDIA 99
ZONE 1,1,3
X BLOCK  0,45   Y BLOCK  -3,0   Z BLOCK   6,15
BLOCK 1,1,1   MEDIA 99
ZONE 1,2,3
X BLOCK  0,45   Y BLOCK   0,3   Z BLOCK   6,15
BLOCK 1,1,1   MEDIA 99
ZONE 1,3,3
X BLOCK  0,45   Y BLOCK   3,12  Z BLOCK   6,15
BLOCK 1,1,1   MEDIA 99
ZONE 1,4,3
X BLOCK  0,45   Y BLOCK  12,15  Z BLOCK   6,15
BLOCK 1,1,1   MEDIA 99
ZONE 1,5,3
X BLOCK  0,45   Y BLOCK  15,60  Z BLOCK   6,15
BLOCK 1,1,1   MEDIA 99
QUADRATIC FUNCTIONS 16,
(X-1.5)SQ+(Y-1.5)SQ+(Z-3)SQ-.25,
(X-3)SQ+(Y-1.5)SQ+(Z-3)SQ-.25,
(X-4.5)SQ+(Y-1.5)SQ+(Z-3)SQ-.25,
(X-6)SQ+(Y-1.5)SQ+(Z-3)SQ-.25,
(X-6)SQ+(Y-3.75)SQ+(Z-3)SQ-.25,
(X-6)SQ+(Y-5.25)SQ+(Z-3)SQ-.25,
(X-6)SQ+(Y-6.75)SQ+(Z-3)SQ-.25,
(X-6)SQ+(Y-8.25)SQ+(Z-3)SQ-.25,
(X-6)SQ+(Y-9.75)SQ+(Z-3)SQ-.25,
(X-6)SQ+(Y-11.25)SQ+(Z-3)SQ-.25,
(X-6)SQ+(Y-13.5)SQ+(Z-3)SQ-.25,
(X-7.5)SQ+(Y-13.5)SQ+(Z-3)SQ-.25,
(X-9)SQ+(Y-13.5)SQ+(Z-3)SQ-.25,
(X-10.5)SQ+(Y-13.5)SQ+(Z-3)SQ-.25,
(X-12)SQ+(Y-13.5)SQ+(Z-3)SQ-.25,
(X-13.5)SQ+(Y-13.5)SQ+(Z-3)SQ-.25
      END
```

```
   2
   2
0.0        45.0
   6
-3.0       0.0        3.0        12.0       15.0       60.0
   4
-3.0       0.0        6.0        15.0
   1     1     1
   2
0.0        45.0
   2
-3.0       0.0
   2
-3.0       0.0
   1     1     1
   1
  99
   1     2     1
   2
0.0        45.0
   2
0.0        3.0
   2
-3.0       0.0
   1     1     1
   1
  99
   1     3     1
   2
0.0        45.0
   2
3.0        12.0
   2
-3.0       0.0
   1     1     1
   1
  99
   1     4     1
   2
0.0        45.0
   2
12.0       15.0
   2
-3.0       0.0
   1     1     1
   1
  99
   1     5     1
   2
0.0        45.0
   2
15.0       60.0
   2
-3.0       0.0
   1     1     1
   1
  99
   1     1     2
   2
0.0        45.0
   2
```

```
-3.0        0.0
   2
0.0         6.0
   1     1     1
   1
  99
   1     2     2
   3
0.0         7.5         45.0
   2
0.0         3.0
   2
0.0         6.0
   1     1     1
   1
  90
   2     1     1
   1
  99
   1     3     2
   4
0.0         4.5         7.5         45.0
   2
3.0         12.0
   2
0.0         6.0
   1     1     1
   1
  99
   2     1     1
   1
  90
   3     1     1
   1
  99
   1     4     2
   4
0.0         4.5         15.0        45.0
   2
12.0        15.0
   2
0.0         6.0
   1     1     1
   1
  99
   2     1     1
   1
  90
   3     1     1
   1
  99
   1     5     2
   2
0.0         45.0
   2
15.0        60.0
   2
0.0         6.0
   1     1     1
   1
  99
```

```
   1     1     3
   2
0.0        45.0
   2
-3.0       0.0
   2
6.0        15.0
   1     1     1
   1
  99
   1     2     3
   2
0.0        45.0
   2
0.0        3.0
   2
6.0        15.0
   1     1     1
   1
  99
   1     3     3
   2
0.0        45.0
   2
3.0        12.0
   2
6.0        15.0
   1     1     1
   1
  99
   1     4     3
   2
0.0        45.0
   2
12.0       15.0
   2
6.0        15.0
   1     1     1
   1
  99
   1     5     3
   2
0.0        45.0
   2
15.0       60.0
   2
6.0        15.0
   1     1     1
   1
  99
   0
```

APPENDIX D

INDIVIDUAL SUBROUTINE CHECKS

Two of the subroutines used in this program are unique to Monte Carlo type of calculations because they involve the random-sampling technique and therefore necessitated the operational checks described here. The two subroutines are the pseudorandom number generator RAN and COSJ (or COSINEJ), which selects a set of direction cosines from the desired distribution.

Versions of the FORTRAN functions RAN for the IBM-7090 and the CDC-1604 are similar in operation and are described in Appendix A. A starting random number is given the routine. When called, the function multiplies it by a large number (5^{15} on the IBM-7090, 5^{19} on the CDC-1604). The least significant portion of the answer is retained as an octal integer to be used to generate the next number and is also converted to a floating point number between 0 and 1 which can be used by the FORTRAN routines. The test program, which was used on each machine, printed a list of the first 50 numbers and then ran through a series of checks on 10,000 numbers. Each number was categorized in two histograms of ten boxes each as to the value of its first and second digits. In other words, the number 0.2563.... was scored in SCOR1(3) and SCOR2(6), indicating that its first digit was 2 and the second 5. Four other quantities calculated were SUM1, SUM2, SUM3, and SUM4. SUM1 was simply the mean of all 10,000 numbers, having an expected value of 0.5:

$$E(\text{SUM1}) = \int_0^1 x\,dx = \frac{x^2}{2}\Big|_0^1 = \frac{1}{2}\,,$$

where x is a random variable uniformly distributed between 0 and 1. SUM2 was the mean of the squared numbers, which has the expected value

$$E(\text{SUM2}) = \int_0^1 x^2\,dx = \frac{1}{3}\,.$$

The quantity SUM3 was the mean of the product xy, where x is one of the 10,000 random numbers and y is another random number, with the expected value

$$E(\text{SUM3}) = \int_0^1 x \int_0^1 y\,dy = \int_0^1 \frac{x}{2} = \frac{1}{4}\,.$$

The last quantity was the mean of the product D_1D_2, where D_1 and D_2 are the first and second digits of each of the random numbers, with the following expected value:

$$E(\text{SUM4}) = \frac{1}{10} \sum_{i=1}^{10} D_1(i) \left[\frac{1}{10} \sum_{i=1}^{10} D_1(i) \right].$$

Since D_1 and D_2 have equal probabilities of attaining any integral value between 0 and 9,

$$E(SUM4) = \left[\frac{1}{10} \ (0 + 1 + 2 + \ldots + 9) \right]^2 = (4.5)^2 = 20.25 \ .$$

The following tabulation gives the results of the test run on the IBM-7090:

SCOR1	SCOR2	
991	1019	SUM1 0.4979875
1031	1001	
960	1034	SUM2 = 0.3306696
1012	1039	
1003	1010	SUM3 = 0.2483983
1043	1015	
1025	975	SUM4 = 19.9859
976	944	
975	973	
984	990	

The tabulation below gives the corresponding results for the test on the CDC-1604:

SCOR1	SCOR2	
1033	972	SUM1 = 0.5017188
992	965	
965	964	SUM2 = 0.3360349
1005	1009	
995	1001	SUM3 = 0.2510409
969	1003	
979	1032	SUM4 = 20.5333
1029	1035	
1018	1017	
1015	1002	

It was concluded from the above results that the sequences generated by the two routines are sufficiently random for the purposes of a Monte Carlo calculation.

The listing of the subroutine COSJ (or COSINEJ in the CDC-1604 program) is shown on the following page. This routine selects from a polar angle distribution equal to $\cos^J\theta$ by using the largest of J + 1 random numbers as the value of $\cos\theta$. This technique is justified in the following paragraphs, first by showing that selection may be performed by taking the J + 1 root of a random number and then by demonstrating the equivalent (and faster) procedure of selecting the largest of J + 1 random numbers.

It is given that a particle has a probability proportional to

```
      SUBROUTINE COSJ(DC1,DC2,DC3,J)
      CSTH#0.
      JP#J+1
      DO30I#1,JP
      R#RAN(RA)
      IF(R-CSTH)30,30,20
   20 CSTH#R
   30 CONTINUE
      SITH#SQRTF(1.0-CSTH*CSTH)
   70 FRAN#RAN(RA)
      SRAN#RAN(RA)
      FR2#FRAN*FRAN
      SR2#SRAN*SRAN
      IF(1.0-(FR2+SR2))70,80,80
   80 CSPHI#(FR2-SR2)/(FR2+SR2)
      SIPHI#2.0*FRAN*SRAN/(FR2+SR2)
      IF(RAN(RA)-0.5)90,90,100
   90 SIPHI#-SIPHI
  100 DC1#CSTH
      DC2#SITH*SIPHI
      DC3#SITH*CSPHI
      RETURN
      END
```

$\cos^n\theta \, d\Omega$ of being emitted into the solid angle element $d\Omega$ about θ. Since $d\Omega = 2\pi \sin\theta \, d\theta$, the probability of the particle being emitted into $d\theta$ about θ is proportional to

$$2\pi \cos^n\theta \sin\theta \, d\theta = - 2\pi \mu^n \, d\mu \ ,$$

where $\mu = \cos\theta$. If this probability is normalized so that the probability of θ being between 0 and $\pi/2$ is 1, it becomes

$$(n + 1) \mu^n \, d\mu \ .$$

If $g(\mu)$ is the probability density function (p.d.f.) of μ and x is a uniformly distributed variable ($0 \leq x \leq 1$), it is desired to find a monotonically increasing function of x, $\mu = f(x)$, which will satisfy $g(\mu)$. Then, for a specific value R of the random variable x,

$$\text{prob}[x < R] = \text{prob}[\mu < f(R)] \ ,$$

$$\int_0^R dx = \int_0^{f(R)} g(\mu) \, d\mu,$$

$$R = \int_0^{f(R)} g(\mu) \, d\mu = (n + 1) \int_0^{f(R)} \mu^n \, d\mu = [f(R)]^{n+1} \ ,$$

$$\mu = f(R) = R^{\frac{1}{n+1}} \ .$$

The alternate technique consists of the following. It is first necessary to find the p.d.f. of a random number Z, which is the larger of two random numbers X and Y which have p.d.f.'s f(x) and g(y). The two random numbers X and Y also have associated with them cumulative distribution functions (c.d.f.) F(x) and G(y) defined by:

$$F(x) = \int_0^x f(x')\, dx' ,$$

$$G(y) = \int_0^y g(y')\, dy' .$$

The probability that X is in Δx is $f(x)\ \Delta x$, and the probability that Y is smaller than x is G(x); therefore the probability of getting X in the region Δx and accepting it is $f(x)\ \Delta x\ G(X)$. Similarly, the probability of getting Y in Δy and accepting it is $g(y)\ \Delta y\ F(y)$. The probability of one or the other of the two mutually exclusive events is the sum of the separate probabilities; therefore

$$h(z) = f(z)\ G(z) + g(z)\ F(z) .$$

The p.d.f. of the largest of n random numbers can be found by induction. Let X be the largest of n - 1 random numbers and assume that its p.d.f. is $(n - 1)\ x^{n-2}$, where $0 \leq x \leq 1$. Let Y equal another random number and let Z be larger than X or Y. Then, the p.d.f. of Z (the largest of n random numbers) is:

$$h(z) = f(z)\ G(z) + g(z)\ F(z)$$

$$= (n - 1)\ z^{n-2}\ z + z^{n-1}$$

$$= n\ z^{n-1}\ .$$

The two techniques are therefore seen to be equivalent. The FORTRAN statements down through statement 30 in subroutine COSJ pick the largest of the J + 1 random numbers. After the cosine of the polar angle is determined, the triangle is solved to determine the corresponding sine.

The selection of the sine and cosine of the azimuthal angle, which is assumed to be uniformly distributed, uses a rejection technique. A point is selected uniformly from a square with sides of unit length by selecting two random numbers which then represent the coordinates of a point. This point is rejected if it lies outside an arc of unit length drawn from one corner of the square, and another point is selected. This results in a series of points that are uniformly distributed on one quadrant of a circle of unit radius. This determines an angle α, distributed uniformly between 0 and $\pi/2$ with

$$\sin\alpha = \frac{R_2}{\sqrt{R_1^2 + R_2^2}}\ ,$$

and

$$\cos\alpha = \frac{R_1}{\sqrt{R_1^2 + R_2^2}}\ ,$$

where the two random numbers R_1 and R_2 represent the coordinates of the point. From this the sine and cosine of 2α, an angle distributed uniformly from 0 to π, may be determined from the following trigonometric identities:

$$\sin 2\alpha = 2 \sin\alpha \cos\alpha$$

$$= \frac{2 R_1 R_2}{R_1^2 + R_2^2},$$

$$\cos 2\alpha = \cos^2\alpha - \sin^2\alpha$$

$$= \frac{R_1^2 - R_2^2}{R_1^2 + R_2^2}.$$

From this the distribution of an angle between 0 and 2π is obtained by attaching a random sign to sine 2α.

Having obtained the sines and cosines of the polar and azimuthal angles (θ and ϕ), the direction cosines in the rectangular coordinate system are calculated by:

$$\ell_z = \cos\theta$$

$$\ell_x = \sin\theta \sin\phi$$

$$\ell_y = \sin\theta \cos\phi.$$

The test routine for subroutine COSJ calls COSJ to generate a direction

(COSJ was modified slightly to produce the sines and cosines of θ and ϕ for the use of the test routine rather than the direction cosines). The test routine then calls the arcsin routine in order to determine the azimuthal angle which is then sorted into one of ten equal angle boxes running from 0 to 360 degrees. The cosine of the polar angle, θ, is categorized into a set of ten boxes having limits

$$0, \quad \sqrt[J+1]{0.1}, \quad \sqrt[J+1]{0.2}, \quad \ldots, \quad \sqrt[J+1]{0.9}, \quad 1$$

when a $\cos^J\theta$ distribution has been requested. These are the limits which should produce a uniform distribution in the boxes. Tests were run with 10,000 tries for isotropic, cosine, and cosine^2 distributions ($J = 0$, 1, and 2, respectively). Results of the calculations are tabulated on the following page.

	cosθ Interval	Number in cosθ Interval	ϕ Interval (deg)	Number in ϕ Interval
Isotropic Distribution	0 to 0.1	1029	0 to 36	965
	0.1 to 0.2	966	36 to 72	1041
	0.2 to 0.3	1022	72 to 108	1023
	0.3 to 0.4	1006	108 to 144	986
	0.4 to 0.5	992	144 to 180	1023
	0.5 to 0.6	985	180 to 216	996
	0.6 to 0.7	952	216 to 252	966
	0.7 to 0.8	1023	252 to 288	981
	0.8 to 0.9	1007	288 to 324	1010
	0.9 to 1.0	1018	324 to 360	1009
Cosine Distribution	0 to 0.3162	1005	0 to 36	1001
	0.3162 to 0.4472	985	36 to 72	1025
	0.4472 to 0.5477	1039	72 to 108	985
	0.5477 to 0.6325	998	108 to 144	992
	0.6325 to 0.7071	1022	144 to 180	1017
	0.7071 to 0.7746	1009	180 to 216	1000
	0.7746 to 0.8367	978	216 to 252	1008
	0.8367 to 0.8944	974	252 to 288	1008
	0.8944 to 0.9487	978	288 to 324	1026
	0.9487 to 1.0	1012	324 to 360	938
Cosine^2 Distribution	0 to 0.4642	1018	0 to 36	929
	0.4642 to 0.5848	998	36 to 72	1049
	0.5848 to 0.6694	1041	72 to 108	960
	0.6694 to 0.7368	959	108 to 144	1039
	0.7368 to 0.7937	993	144 to 180	1020
	0.7937 to 0.8434	1067	180 to 216	955
	0.8434 to 0.8879	959	216 to 252	1033
	0.8879 to 0.9283	1022	252 to 288	972
	0.9283 to 0.9655	996	288 to 324	1019
	0.9655 to 1.0	947	324 to 360	1024

APPENDIX E

CALCULATIONS OF UNCOLLIDED FLUX AND CURRENT IN STRAIGHT DUCTS

The calculation of the uncollided particle flux in straight ducts was necessary for use with the analytical approximation derived by Simon and Clifford.[1] Equations are given below for the uncollided particle flux and current along the center lines of both rectangular and cylindrical ducts from a cosine current source uniformly distributed over the duct mouth.

The assumed geometry for the cylindrical duct is shown below. To

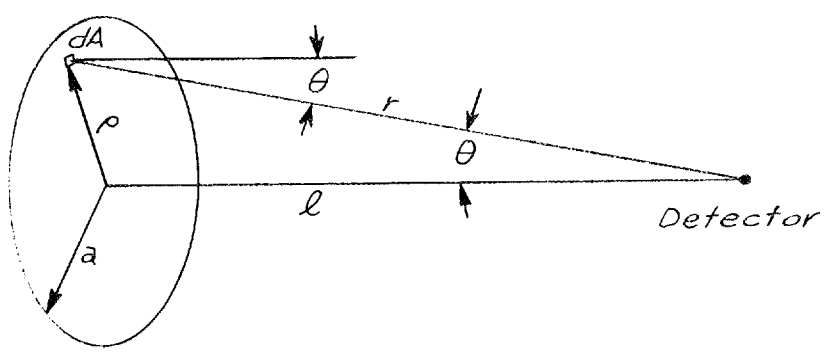

the left of the source plane, space is filled uniformly with sources of magnitude such that $(1/\pi)\cos\theta$ particles arrive per unit solid angle per cm^2 of source area (i.e., the flux is isotropic in the left half-space). The particle current, to the right, through the source plane then is

$$J = \int_{2\pi} \frac{\cos\theta}{\pi}\, d\Omega = \frac{2\pi}{\pi} \int_0^1 \cos\theta \; d(\cos\theta) = 1 \; .$$

[1]Simon and Clifford, op. cit., Eq. 2, p. 48.

Similarly, the particle flux at the source plane due to the source particles, is

$$\phi = \int_{2\pi} \frac{\cos\theta}{\pi} \left(\frac{1}{\cos\theta}\right) d\Omega = \frac{2\pi}{\pi} \int_0^1 d(\cos\theta) = 2 \ .$$

The current of uncollided particles on the duct center line at distance ℓ is

$$J(\ell) = \int_{\rho=0}^{a} \frac{\cos\theta}{\pi} \ \frac{dA \cos\theta}{r^2} \ ,$$

since $dA \cos\theta/r^2$ is the solid angle subtended by the differential source area, as seen from the detector. Because $r^2 = \rho^2 + \ell^2$ and therefore $rdr = \rho d\rho$, dA may be expressed as $dA = 2\pi\rho d\rho = 2\pi r dr$. Now, since $\cos\theta = \ell/r$, the integral becomes

$$J(\ell) = \frac{1}{\pi} \int_{r=1}^{\sqrt{\ell^2+a^2}} \frac{\ell}{r} \ \frac{\ell}{r} \ \frac{2\pi r dr}{r^2} = 2\ell^2 \int_{\ell}^{\sqrt{\ell^2+a^2}} \frac{dr}{r^3} = - \frac{\ell^2}{r^2}\Bigg|_{\ell}^{\sqrt{\ell^2+a^2}}$$

$$= \ell^2 \left(\frac{1}{\ell^2} - \frac{1}{\ell^2 + a^2} \right) = \frac{a^2}{\ell^2 + a^2} \ .$$

This expression approaches 1 at the source plane, as it should, and approaches a^2/ℓ^2 for $\ell \gg a$.

In a similar manner, the flux from the uncollided particles is

$$\phi(\ell) = \frac{1}{\pi} \int_{r=\ell}^{\sqrt{\ell^2+a^2}} \frac{2\pi\ell\, dr}{r^2} = 2\ell \int_{\ell}^{\sqrt{\ell^2+a^2}} \frac{dr}{r^2} = -\left.\frac{2\ell}{r}\right|_{\ell}^{\sqrt{\ell^2+a^2}}$$

$$= 2\left[1 - \frac{\ell}{\sqrt{\ell^2 + a^2}}\right] ,$$

which also can be expressed as

$$\phi(\ell) = 2(1 - \cos\theta_s) ,$$

where $\theta_s = \tan^{-1}\frac{a}{\ell} = \cos^{-1}\frac{\ell}{\sqrt{\ell^2 + a^2}}$. Note that these expressions properly approach the value 2 at the source plane. They also must approach a^2/ℓ^2 for $\ell \gg a$, as did the expression for particle current. That they do can be shown as follows:

$$\frac{\ell}{\sqrt{\ell^2 + a^2}} = \frac{\ell}{\ell\sqrt{1 + \left(\frac{a}{\ell}\right)^2}} = \frac{1}{1 + \frac{1}{2}\left(\frac{a}{\ell}\right)^2 + 0\left[\left(\frac{a}{\ell}\right)^4\right]} ,$$

where 0 [ ] represents the higher order terms. Neglecting these, the particle flux is

$$\phi(\ell) \simeq 2 \left[1 - \frac{1}{1 + \frac{1}{2} \left(\frac{a}{\ell}\right)^2} \right]$$

$$\simeq 2 \left[1 - \left\{ 1 - \frac{1}{2} \left(\frac{a}{\ell}\right)^2 \right\} \right]$$

$$\simeq \frac{a^2}{\ell^2} \quad .$$

The expressions for the uncollided flux and current from a rectangular source are taken from the work by J. H. Hubbell _et al._,[2] which allows for the angular distribution of the source particles to be expressed as a sum of Legendre polynomials. Since this case is restricted to a cosine distribution, it is only necessary to use one term to describe the source, and analytic expressions are available for the results. For a rectangular source of width 2w and height 2h the current at a point located a distance ℓ from the surface and on a line normal to the center of the surface is

$$\phi(\ell) = \frac{4}{\pi} \tan^{-1} \left(\frac{a\ b}{\sqrt{a^2 + b^2 + 1}} \right)$$

$$J(\ell) = \frac{2}{\pi} \left\{ \frac{b}{\sqrt{b^2 + 1}} \tan^{-1} \frac{a}{\sqrt{b^2 + 1}} + \frac{a}{\sqrt{a^2 + 1}} \tan^{-1} \frac{b}{\sqrt{a^2 + 1}} \right\} ,$$

---

[2] J. H. Hubbell, R. L. Bach, and J. C. Lamkin, "Radiation Field from a Rectangular Source," _NBS Journal of Research_, 64C, 2 (April-June 1960).

where $a = w/\ell$ and $b = h/\ell$. The factor π arises from the source normalization to a unit particle current at the source plane.

It is of interest to show that at large distances the rectangular and circular sources of equal area produce the same uncollided flux. As was shown previously, the uncollided flux from a circular source of radius a approaches $(a/\ell)^2$ as $\ell \gg a$.

The flux at a point located a distance ℓ from the rectangular source surface and on a line normal to the center of the surface is

$$\phi = \frac{4}{\pi} \tan^{-1} \frac{a\ b}{\sqrt{a^2 + b^2 + 1}}$$

$$= \frac{4}{\pi} \tan^{-1} \frac{w\ h}{\ell^2 \sqrt{\frac{w^2}{\ell^2} + \frac{h^2}{\ell^2} + \frac{\ell^2}{\ell^2}}}$$

$$= \frac{4}{\pi} \tan^{-1} \frac{w\ h}{\ell \sqrt{w^2 + h^2 + \ell^2}} \quad .$$

As $\ell^2 \gg w^2 + h^2$, this becomes

$$\phi \simeq \frac{4}{\pi} \tan^{-1} \frac{wh}{\ell^2}$$

$$\simeq \frac{4}{\pi} \frac{wh}{\ell^2} \quad .$$

For the two expressions to be equal, one of the following conditions must exist:

$$a^2 = 4wh/\pi \ ,$$

or

$$\pi a^2 = 4wh \ .$$

Therefore, the source areas must be equal.

APPENDIX F

CALCULATIONS OF THE THERMAL-NEUTRON ALBEDO

Several methods for calculating the albedo, or reflection coefficient, of thermal neutrons are presented in this appendix in approximately historical order. The resulting values of the albedo for concrete compositions used in the TSF experiments[1] are also given.

Probably the first definitive calculation of the thermal-neutron albedo was performed by Fermi.[2] A brief description of Fermi's derivation will be given. The albedo of a neutron incident on a slab of thickness a at an angle θ may be written as an integral of the products of the probability that the neutron suffers a first collision at a depth between x and x + dx but does not get captured there, multiplied by the probability p(x) that the neutron, having suffered this first collision, leaves the slab across the face through which it entered. That is,

$$\left[\frac{N - 1}{N} e^{-(x/\lambda \cos\theta)} \frac{dx}{\lambda \cos\theta} \right] p(x) ,$$

where

N = average number of free paths traversed by a neutron before capture

---

[1]V. R. Cain, A Study of the Radiation Shielding Characteristics of Basic Concrete Structures at the Tower Shielding Facility, ORNL-3464 (1963).

[2]E. Fermi, On the Motion of Neutrons in Hydrogenous Substances, NP-2385 (Oct. 22, 1951). (Translation from Ricerca Scienta VII-II, 13, 1936).

$= \Sigma_t/\Sigma_a$, the ratio of total to absorption cross section,

λ = mean free path of a neutron,

$$\alpha = \frac{1}{\lambda\sqrt{N}} ,$$

$$p(x) = Ae^{\alpha x} + Be^{-\alpha x}.$$

The albedo is then

$$\beta(a,\theta) = \frac{N-1}{N} \int_0^a e^{-(x/\lambda \cos\theta)} \frac{p(x)}{\lambda \cos\theta} dx .$$

For $a = \infty$, $A = 0$ and $B = \frac{\sqrt{N}}{\sqrt{N}+1}$, so that

$$p(x) = \frac{\sqrt{N}}{\sqrt{N}+1} e^{-(x/\lambda\sqrt{N})} ,$$

and the albedo becomes

$$\beta(\infty,\theta) = \frac{\sqrt{N}-1}{\sqrt{N}+\sqrt{3}\cos\theta} .$$

For large N, for which $\sqrt{N} \gg \sqrt{3}\cos\theta$, this can be approximated as

$$\beta(\infty,\theta) \simeq 1 - \frac{(1+\sqrt{3}\cos\theta)}{\sqrt{N}} .$$

For the concrete used in the TSF experiments,[1] $\Sigma_s/\Sigma_a = 34.6$ so that $N = 35.6$ and $\sqrt{N} = 5.97$. The Fermi method for calculating the albedo

then yields a value of $\beta(\infty,\theta) = 4.97/(5.97 + 1.732 \cos\theta)$, which varies from 0.645 at $\theta = 0$ to 0.832 at $\theta = \pi/2$. The average of these two extremes is 0.74.

More exact calculations were carried out by Halpern, Lueneburg, and Clark[3] for three different angular distributions of the incident neutrons. Their formulas, together with the values obtained for $N = 35.6$, are as follows:

$$\text{for normal incidence:} \quad \beta = 1 - \frac{2.91}{\sqrt{N+1}} = 0.52,$$

$$\text{for an isotropic distribution:} \quad \beta = 1 - \frac{2.31}{\sqrt{N+1}} = 0.62,$$

$$\text{for a cosine distribution:} \quad \beta = 1 - \frac{2.48}{\sqrt{N+1}} = 0.59.$$

Glasstone and Edlund[4] derived a formula for diffusion theory, given below

$$\beta = \frac{1 - 2KD}{1 + 2KD} ,$$

where

K = the reciprocal of the diffusion length,

---

[3]O. Halpern, R. Lueneburg, and O. Clark, "On Multiple Scattering of Neutrons." Physical Review 53, 173 (1938).

[4]S. Glasstone and M. C. Edlund, The Elements of Nuclear Reactor Theory (Princeton: D. Van Nostrand Co., Inc., 1952).

D = the diffusion coefficient.

Inserting values of K and D for concretes 1a and 3a on pages 94 and 95 of the Reactor Handbook,[5] both concretes being similar to that used in the TSF experiments, results in values for the albedo of 0.74 and 0.75, respectively.

---

[5]E. P. Blizard and L. S. Abbott, eds., Shielding, Vol. III, Part B, Reactor Handbook, 2nd ed. (New York: Interscience Publishers, 1962).

APPENDIX G

DERIVATION OF STATISTICAL FORMULAE

The probability density function (p.d.f.) on which the statistical theory of errors is ordinarily based is called the "normal distribution." It is an analytic approximation to the binomial distribution for a large number of samples and is defined such that the probability $dP(x)$ that x will lie between x and $x + dx$ is

$$dP(x) = \frac{1}{\sigma\sqrt{2\pi}} e^{-\frac{(x-m)^2}{2\sigma^2}} dx ,$$

where m is the true value of the quantity whose measured values are x, and σ is the standard deviation, a measure of the breadth of the distribution. There is a 31.7% probability that a single measurement of x will lie outside $m \pm \sigma$ and a 68.3% probability that it will fall inside $m \pm \sigma$.

The mean value $\overline{x}$ of a series of n measurements is an approximation to the true value m and is given by

$$m \simeq \overline{x} = \frac{1}{n} \sum_{i=1}^{n} x_i .$$

For a general distribution, the standard deviation (S.D.) of a large number of observations is defined by

$$\sigma^2 \equiv \sum_{x=-\infty}^{x=\infty} (x - m)^2 \, P(x) \; ;$$

that is, the S.D. is the square root of the average of the squared deviations. For a large series of n measurements of x, the S.D. is defined by

$$\sigma^2 \equiv \frac{1}{n} \sum_{i=1}^{n} (x_i - m)^2 \; .$$

The square of the S.D., σ^2, is usually called the "variance."

In a finite series of n observations m is not known. An estimate of the S.D. can be obtained as follows. The "sample variance" s^2 is defined as

$$s^2 \equiv \frac{1}{n} \sum_{i=1}^{n} (x_i - \overline{x})^2 \; .$$

It can be shown that the expected value of s^2 is

$$E(s^2) = \frac{n - 1}{n} \sigma^2 \; ,$$

and therefore the estimate of σ^2 is

$$\sigma^2 \simeq \frac{n}{n - 1} \left[\frac{1}{n} \sum_{i=1}^{n} (x_i - \overline{x})^2 \right] = \frac{1}{n - 1} \sum_{i=1}^{n} (x_i - \overline{x})^2 \; .$$

It should be remembered that the square root of this variance is the S.D. of the distribution, or the S.D. of a single observation, since it represents the limits within which 68% of the n observations should lie. Therefore the probability of a single additional measurement lying within $\bar{x} \pm \sigma$ is 68%.

This is not, however, the quantity which is usually required. The desired quantity is the S.D. of the mean value $\sigma_{\bar{x}}$ such that there is a 68% probability of a new mean value $\bar{x}'$ (obtained from an additional n measurement) lying within $\bar{x} \pm \sigma_{\bar{x}}$

The value of this variance of the mean can be calculated by using the result from the statistical theory of errors that the variance of a sum of independent random variables is the sum of their variances. That is, if $x = x_1 + x_2$, then $\sigma_x^2 = \sigma_{x_1}^2 + \sigma_{x_2}^2$. In addition, it is also necessary to use the result that

$$\mathrm{var}\left(\frac{x}{n}\right) = \frac{1}{n^2}\,\mathrm{var}(x) \ ,$$

where var(x) represents the variance of x and n is any constant. This is easily proven from the basic definition of variance, that is, that the variance is the expected value of the squared deviations from the true mean:

$$\mathrm{var}(x) \equiv E\left\{(x - m)^2\right\} \ .$$

Then,

$$\operatorname{var}\left(\frac{x}{n}\right) = E\left\{\left(\frac{x}{n} - \frac{m}{n}\right)^2\right\}$$

$$= E\left\{\frac{1}{n^2}(x - m)^2\right\}$$

$$= \frac{1}{n^2} E\left\{(x - m)^2\right\}$$

$$= \frac{1}{n^2} \operatorname{var}(x) \ .$$

Now, since $\overline{x} = \frac{1}{n}(x_1 + x_2 + \ldots + x_n)$,

$$\operatorname{var}(\overline{x}) = \frac{1}{n^2} \operatorname{var}\left(\sum_{i=1}^{n} x_i\right)$$

$$= \frac{1}{n^2} \sum_{i=1}^{n} \operatorname{var}(x_i) = \frac{1}{n^2}\left[n \operatorname{var}(x)\right]$$

$$= \frac{1}{n}\sigma^2 \ .$$

For a single series of n, measurements of the mean and variance of the mean are obtained by

$$\overline{x} = \frac{1}{n} \sum_{i=1}^{n} x_i$$

$$\sigma^2_{\bar{x}} = \frac{1}{n(n-1)} \sum_{i=1}^{n} (x_i - \bar{x})^2 .$$

A more useful form of the above expression for the variance for use on a digital computer can be obtained by expanding the squared term:

$$\sum_{i=1}^{n} (x_i - \bar{x})^2 = \sum_{i=1}^{n} \left[(x_i)^2 - 2x_i \bar{x} + (\bar{x})^2 \right] .$$

Combining terms and substituting the definition of $\bar{x}$ into the above expression gives

$$\sum_{i=1}^{n} (x_i - \bar{x})^2 = \sum_{i=1}^{n} (x_i)^2 - 2\bar{x} \sum_{i=1}^{n} x_i + n(\bar{x})^2$$

$$= \sum_{i=1}^{n} (x_i)^2 - 2n(\bar{x})^2 + n(\bar{x})^2$$

$$= \sum_{i=1}^{n} (x_i)^2 - n \left\{ \frac{1}{n} \sum_{i=1}^{n} x_i \right\}^2$$

$$= \sum_{i=1}^{n} (x_i)^2 - \frac{1}{n} \left\{ \sum_{i=1}^{n} x_i \right\}^2 .$$

The variance of the mean becomes

$$\sigma^2_{\bar{x}} = \frac{1}{n(n-1)} \left\{ \sum_{i=1}^{n} (x_i)^2 - \frac{1}{n} \left(\sum_{i=1}^{n} x_i \right)^2 \right\} .$$

In the computer code, the variance of the mean is calculated by two methods, one by using the equation above, where n represents the total number of measurements (called the single batch variance), and the other by dividing the histories into batches. Suppose that the n measurements are divided into k batches, each containing ℓ measurements ($n = k\ell$). A mean may be calculated for the jth batch by

$$\bar{x}_j = \frac{1}{\ell} \sum_{i=1}^{\ell} x_{ij} .$$

These batch means may now be treated as independent measurements. As before, the variance of a single batch mean may be calculated by

$$\sigma^2_{\bar{x}_j} = \frac{1}{(k - 1)} \sum_{j=1}^{k} (\bar{x}_j - \bar{x})^2 .$$

The variance of the overall mean is then

$$\sigma^2_{\bar{x}} = \frac{1}{k(k - 1)} \sum_{j=1}^{k} (\bar{x}_j - \bar{x})^2 ,$$

where

$$\bar{x} = \frac{1}{k} \sum_{j=1}^{k} \bar{x}_j , \quad \bar{x}_j = \frac{1}{n} \sum_{i=1}^{n} x_i .$$

A formula to combine the variances, $\sigma_{\overline{x}_1}$ and $\sigma_{\overline{x}_2}$, of two means $\overline{x}_1$ and $\overline{x}_2$, obtained with n_1 and n_2 measurements, into a grand mean $\overline{x}$ and variance $\sigma_{\overline{x}}$ will now be derived. The mean of the two batches is

$$\overline{x} = \frac{1}{n_1 + n_2} \left\{ \sum_{i=1}^{n_1} x_i + \sum_{j=1}^{n_2} x_j \right\} = \frac{n_1\overline{x}_1 + n_2\overline{x}_2}{n_1 + n_2} .$$

The variance of $\overline{x}$ is

$$\sigma^2_{\overline{x}} = \frac{1}{(n_1 + n_2)(n_1 + n_2 - 1)} \sum_{i=1}^{n_1+n_2} (x_i - \overline{x})^2$$

$$= \frac{1}{(n_1 + n_2)(n_1 + n_2 - 1)} \left\{ \sum_{i=1}^{n_1} (x_i - \overline{x})^2 + \sum_{j=1}^{n_2} (x_j - \overline{x})^2 \right\} .$$

Expanding one of the sums,

$$\sum_{i=1}^{n_1} (x_i - \overline{x})^2 = \sum_{i=1}^{n_1} \left\{(x_i - \overline{x}_1) + (\overline{x}_1 - \overline{x})\right\}^2$$

$$= \sum_{i=1}^{n_1} \left\{(x_i - \overline{x}_1)^2 + (\overline{x}_1 - \overline{x})^2 + 2(x_i - \overline{x}_1)(\overline{x}_1 - \overline{x})\right\}$$

$$= \sum_{i=1}^{n_1} (x_i - \overline{x}_1)^2 + \sum_{i=1}^{n_1} (\overline{x}_1 - \overline{x})^2$$

since $\sum_{i=1}^{n_1} (x_i - \bar{x}_1) = 0.$

The variance of $\bar{x}$ now becomes

$$\sigma^2_{\bar{x}} = \frac{1}{(n_1 + n_2)(n_1 + n_2 - 1)} \left\{ \sum_{i=1}^{n_1} (x_i - \bar{x}_1)^2 + \sum_{i=1}^{n_1} (\bar{x}_1 - \bar{x})^2 + \right.$$

$$\left. + \sum_{j=1}^{n_2} (x_j - \bar{x}_2)^2 + \sum_{j=1}^{n_2} (\bar{x}_2 - \bar{x})^2 \right\}$$

$$= \frac{n_1(n_1 - 1)\ \sigma^2_{\bar{x}_1} + n_2(n_2 - 1)\ \sigma^2_{\bar{x}_2} + n_1(\bar{x}_1 - \bar{x})^2 + n_2(\bar{x}_2 - \bar{x})^2}{(n_1 + n_2)(n_1 + n_2 - 1)} .$$

ACKNOWLEDGMENTS

The author thanks Dr. P. N. Stevens and Mr. C. E. Clifford for their suggestions and criticisms guiding this work. Appreciation is also extended to Mr. D. Irving for the use of his geometry subroutine, to Mr. D. K. Trubey and Mrs. M. B. Emmett for the use of their plotting routines, and to the many others who made valuable criticisms and who assisted in the presentation. Messrs. Clifford, Irving, and Trubey and Mrs. Emmett are employed at the Oak Ridge National Laboratory.

Facilities at the Oak Ridge National Laboratory were used in this study through the courtesy of Union Carbide Nuclear Company, the operating company, and the United States Atomic Energy Commission.

ORNL-3507
UC-34 — Physics
TID-4500 (24th ed.)

INTERNAL DISTRIBUTION

1. Biology Library
2-4. Central Research Library
5. Reactor Division Library
6-7. ORNL — Y-12 Technical Library Document Reference Section
8-57. Laboratory Records Department
58. Laboratory Records, ORNL R.C.
59. J. A. Auxier
60. E. P. Blizard
61. H. R. Brashear
62. H. C. Claiborne
63. E. L. Compere
64. G. A. Cristy
65. L. C. Emerson
66. C. B. Fulmer
67. L. B. Holland
68. F. T. Howard
69. W. H. Jordan
70. C. E. Larson
71. R. E. Maerker
72. J. A. Martin
73. S. K. Penny
74. J. J. Pinajian
75. C. A. Preskitt
76. M. J. Skinner
77. J. A. Swartout
78. D. K. Trubey
79. A. M. Weinberg
80. R. A. Charpie (consultant)
81. P. F. Gast (consultant)
82. M. L. Goldberger (consultant)
83. R. F. Taschek (consultant)
84. T. J. Thompson (consultant)

EXTERNAL DISTRIBUTION

85. Chief of Naval Operations, Navy Department, Attn: OP-754, Washington, D.C. 20350
86-88. HQ USAF (AFRNEA), Attn: Major Edward C. Lowry, Washington, D.C. 20330, Assistant Secretary of Defense (Civil Defense), Attn: Director of Research (1 copy each to W. E. Strope and J. O. Buchanan, Washington, D.C. 20301
89. Commanding Officer, U.S. Army Combat Developments Command, Nuclear Group, Attn: Major Joseph T. Gibson, Fort Bliss, Texas 79906
90. Chief of Research and Development, Department of the Army, Attn: Lt. Col. D. Baker, Washington, D.C. 20310
91. Chief, Bureau of Ships, Navy Department, Attn: Code 362, Lorenz E. Sieffert, Washington, D.C. 20360
92. Chief, Bureau of Yards and Docks, Navy Department, Attn: Code 74, Washington, D.C. 20390
93. Commanding Officer and Director, Naval Civil Engineering Laboratory, Attn: C. Huddleston, Port Hueneme, California
94-95. Director, U.S. Army Ballistic Research Laboratories, Attn: N. Ethridge and F. Allen, Aberdeen Proving Ground, Maryland 21005
96. Commanding Officer, U.S. Army Chemical Center Nuclear Defense Laboratory, Attn: H. Donnert, Edgewood Arsenal, Maryland 21040
97. Commanding Officer and Director, U.S. Naval Radiological Defense Laboratory, Attn: W. Kreger, San Francisco, California

98. Director, National Bureau of Standards, Washington, D.C., Attn: Lewis V. Spencer
99. Technical Operations, Inc., South Avenue, Burlington, Massachusetts, Attn: E. Clarke
100. United Nuclear Corporation, Development Division, 5 New Street, White Plaines, New York, Attn: M. N. Kalos
101-105. Chief, Defense Atomic Support Agency, Department of Defense, Washington, D.C. (1 copy to DASARA, Major Verser, 2 copies to DASATP, 1 copy each to DASACT and DASAST)
106. H. E. Hungerford, Nuclear Engineering Department, Purdue University, Lafayette, Indiana
107. A. B. Chilton, Associate Professor, Nuclear Engineering Program, 264 Mechanical Engineering Building, University of Illinois, Urbana, Illinois
108. H. Goldstein, Division of Nuclear Science and Engineering, Columbia University, New York City, New York
109. R. Aronson, Radioptics, Inc., 28 Pilgrim Avenue, Yonkers, New York
110. R. L. French, Radiation Research Associates, Fort Worth, Texas
111. M. B. Wells, Radiation Research Associates, Fort Worth, Texas
112. W. R. Kimel, Department of Nuclear Engineering, Kansas State University, Manhattan, Kansas
113. B. B. Baschkin, Atomic Energy Documentation Center at the Gmelin Institute, U.S. Atomic Energy Commission Depository Library, 7 Woodland Avenue, Larchmont, New York
114. W. P. Neuendorf, Bechtel Corporation, San Francisco, California
115. S. T. Friedman, Nuclear Physicist, Department 8899, Plant 8, Allison Division, General Motors Corp., Indianapolis, Indiana
116. G. G. Biro, Gibbs and Hill, Inc., 393 Seventh Avenue, New York, New York
117. V. B. Bhanot, Physics Department, Panjab University, Chandigarh-3, India
118. University of Chile, Box 2777, Institute of Science, Santiago, Chile
119. Research and Development Division, AEC, ORO
120-763. Given distribution as shown in TID-4500 (24th ed.) under Physics category (75 copies – OTS)